Heavy Quark Production at a $\mu^+\mu^-$-Collider

Diplomarbeit
von
Thorsten Ratzka

Institut für Theoretische Physik
und Astrophysik
Julius-Maximilians-Universität Würzburg

6. August 2001

Für Meine Mutter

[...] "O Boß, ich habe nicht die Symmetrie zerstört. Ich habe lediglich bewirkt, daß sie durch die List des Energieverbrauchs verborgen wird. Und damit habe ich die Welt in der Tat zu einer komplizierten Welt gemacht.

Wer hätte vorhersehen können, daß aus dieser eintönigen Ansammlung identischer Objekte einmal Atomkerne und Atome und Moleküle und Planeten und Sterne hervorgehen würden?

Und wer hätte vorherzusagen vermocht die Sonnenuntergänge und die Ozeane und die organische Brühe, in der all diese schrecklichen Moleküle durch Blitze und durch Wärme in Bewegung versetzt werden? Und wer hätte rechnen können mit der Evolution und mit diesen Physikern, die stochern und bohren und suchen nach dem, was ich - in deinem Dienste - so sorgfältig verborgen habe?"

Und Gott, die Ihr Lachen kaum noch zu unterdrücken vermochte, machte eine Geste, daß Sie Higgs verziehen hatte, und gewährte ihm eine nette Gehaltserhöhung.

Das Ganz Neue Testament 3,1

aus dem Buch "Das schöpferische Teilchen"
von Leon Lederman und Dick Teresi

Contents

1 Introduction **1**
- 1.1 Motivation . . . 1
- 1.2 Overview . . . 3

2 The process $\mu^+\mu^- \to f\bar{f}$ within the Standard Model **4**
- 2.1 Kinematics . . . 4
- 2.2 Higgs Boson Decay . . . 6
  - 2.2.1 Decay into Fermions . . . 7
  - 2.2.2 Decay into W Bosons . . . 8
  - 2.2.3 Decay into Z^0 Bosons . . . 9
  - 2.2.4 Constraints on the Higgs Boson Mass . . . 10
  - 2.2.5 Numerical Results . . . 11
- 2.3 Cross Section . . . 13
  - 2.3.1 Feynman amplitudes . . . 14
  - 2.3.2 Squared Matrix Elements . . . 19
  - 2.3.3 Differential Cross Section . . . 23
  - 2.3.4 Total Cross Section . . . 25
- 2.4 Higgs Boson Effects in $t\bar{t}$-Production . . . 25
- 2.5 Higgs Boson Effects in $b\bar{b}$-Production . . . 27
  - 2.5.1 Total Cross Section . . . 27
  - 2.5.2 Angular Distribution . . . 30
  - 2.5.3 Forward-Backward-Asymmetry . . . 30
- 2.6 Influence of the Energy Resolution of the Collider . . . 31

3 The MSSM with Additional CP Violation **34**
- 3.1 Motivation . . . 34
- 3.2 Supersymmetry Transformations . . . 36
- 3.3 Supermultiplets . . . 36
  - 3.3.1 Matter Supermultiplets of the MSSM . . . 37
  - 3.3.2 Gauge Supermultiplets of the MSSM . . . 37
  - 3.3.3 Remarks and Nomenclature . . . 38

3.4 The Superpotential 39
3.5 Supersymmetry Breaking 39
3.6 CP Violation 40
3.6.1 Complex Parameters 41
3.6.2 One-Loop Effective Potential 42
3.6.3 The Neutral Higgs Boson Mass Matrix 44
3.6.4 The Charged Higgs Boson Mass Matrix 45
3.6.5 Fermion Couplings 45
3.6.6 Gauge Boson Couplings 46
3.7 Higgs Boson Masses and Couplings 47
3.7.1 Heavy Charged Higgs Scenario 47
3.7.2 Light Charged Higgs Scenario 51

4 Signatures of a CP-Violating Higgs Sector in $\mu^+\mu^- \longrightarrow b\bar{b}$ 55
4.1 Higgs Boson Decay 55
4.1.1 Decay into Fermions 55
4.1.2 Decay into Gauge Bosons 56
4.1.3 Numerical Results 57
4.2 Cross Section 61
4.2.1 Squared amplitudes 61
4.2.2 Differential Cross Section 63
4.2.3 Numerical Results 65

5 Longitudinal Polarized $\mu^\pm$-beams 71
5.1 Bouchiat-Michel-Formulae 71
5.2 Squared Amplitudes 72
5.3 Differential Cross Section 75
5.4 Numerical Results 76

6 Conclusion 81

A Useful Formulae 83
A.1 Relativistic Notation 83
A.2 Pauli Matrices 84
A.3 Dirac Matrices 84
A.4 Epsilon Tensor 86
A.5 Spinors 86

B Feynman Rules 88
B.1 Propagators 88
B.2 Vertices 89

B.3 Electroweak Charges 91
B.4 Constants 92

C The Scalar and Pseudoscalar Higgs-Couplings to Fermions 93
C.1 Low-tan β-Scenario 94
C.2 High-tan β-Scenario 96

Chapter 1

Introduction

1.1 Motivation

In the last decades the experiments at the accelerator facilities have been able to verify very precisely the predictions derived from the *Standard Model* (SM) [1, 2, 3]. But there is just a spot of bother: even today there is no evidence how the massless particles become massive in a quantum gauge theory. The only one compelling way of achieving that goal is the so-called "Higgs mechanism". This mechanism of spontaneous symmetry breaking was first postulated 1964 by P. W. Higgs [4, 5, 6, 7, 8]. The Higgs mechanism is based on the idea that the a-priori massless particles acquire an "effective mass" by interaction with a background medium, the Higgs field [9].

The Higgs mechanism was used 1967 by S. Weinberg [2] and 1968 by A. Salam [3] to explain the masses of the gauge bosons $W^{\pm}$ and Z^0 in the electroweak theory. To break the local $SU(2)_L \times U(1)_Y$ symmetry spontaneously down to a $U(1)_{EM}$ symmetry one introduces a Higgs doublet that consists of two complex scalar Higgs fields. The now available four extra degrees of freedom allow one to generate masses for three of the gauge bosons (three degrees of freedom). The remaining one degree of freedom leads to a new massive spin zero particle, the physical Higgs boson H. The mass of H is not determined by the theory and is considered a free parameter. After the proof that spontaneous symmetry breaking of a theory maintains renormalizability in 1971 by G. 't Hofft [10, 11] there was no longer a handicap to solve the problem of the 50's and 60's: the creation of a renormalizable electroweak theory with massive gauge bosons that is called the *Glashow-Weinberg-Salam* (GWS) Model [1, 2, 3].

To finish this short historic description, it is important to note that the massive gauge bosons called $W^{\pm}$ and Z^0 have been detected by measurements made at the *Centre Européen de la Recherche Nucléaire* (CERN) at Geneva, Switzerland in 1983 [12, 13, 14, 15]. In the last year even a successful detection of the Higgs boson seemed to become true. Shortly before the shutdown of the *Large Electron Positron* collider (LEP) at CERN, the four detector collaborations *ALEPH*, *DELPHI*, *L3* and *OPAL* reported a $2.9\,\sigma$ excess of events beyond the expected SM background in the combination of the data from their Higgs boson searches [16, 17, 18, 19, 20]. This excess is consistent with the production of a SM like Higgs boson with a mass $m_H = 115^{+1.3}_{-0.9}$ GeV [21]. Due to the lack of time the results could neither be verified nor confuted. So the search for the Higgs boson as the last undetected elementary particle of the Standard Model has not been successful up to the present.

Nevertheless the experimentalists have been able to raise the lower bound of the Standard Model Higgs mass. Direct searches for the Higgs boson at LEP yield a lower bound of $m_H \geq 113.5$ GeV at the 95% confidendce level [16, 17, 18, 22, 21]. This experimental mass limit is consistent to the upper bound given by supersymmetric theories. In the *Minimal Supersymmetric Standard Model* (MSSM), that includes three neutral and two charged Higgs bosons, the lightest neutral Higgs boson is predicted to have a mass lower than 135 GeV [21]. The five Higgs bosons are a consequence of the two $SU(2)_L$ Higgs doublets that are necessary in a supersymmetric theory to give masses to the charged fermions [23]. Compared to the Standard Model the four extra degrees of freedom yield four additional scalar Higgs particles.

The search for the Higgs boson is the most exciting task of future colliders: one will be able to prove if the Higgs mechanism is responsible for the electroweak symmetry breaking. On the other hand testing the properties of the Higgs boson may reveal its origin in a supersymmetric world and shed light on the other heavy particles in the Higgs spectrum which may lie outside the range covered by the accelerators directly [21]. However, if the other SUSY Higgs bosons are within the accelerators mass reach then one will be able to measure and identify the SUSY scenario. Furthermore the search for Higgs bosons will also reveal possible CP-violating effects.

What circumstances will be helpful to find signals of a Higgs boson within or beyond the Standard Model and why is the process $\mu^+\mu^- \to f\bar{f}$ $(f = b, t)$ chosen?

The coupling strength g_{Hff} of the Higgs boson to a fermion is proportional to the mass of the fermion m_f. This implies that the heaviest fermions should be produced to get as large as possible cross sections. So the top-quark is a good candidate. Otherwise due to the large mass of the top-quark a resonant Higgs boson exchange is impossible for light Higgs particles. It can only be realized in bottom-quark production.

The concept of a muon-collider as a "Higgs factory" is more than 30 years old [24] and has been discussed very intensively in the recent years [25, 26, 27, 28, 29, 30], because it has many advantages compared to an e^+e^--collider that arise mainly from the greater mass of the muons [31]:

- the coupling to the Higgs boson is $\frac{m_\mu}{m_e} \approx 200$ times stronger;
- there is essentially no beamstrahlung;
- there is substantially reduced bremsstrahlung;
- as required for detailed Higgs studies in the s-channel, an excellent beam energy resolution of 0.01% is possible [30].

1.2 Overview

In the next chapter, the process $\mu^+\mu^- \to f\bar{f}$ $(f = b, t)$ as it appears in the Standard Model will be considered. All aspects of calculating a cross section, like kinematics, decay widths, Feynman amplitudes and their squaring will be discussed. In chapter 3 the Minimal Supersymmetric Standard Model with additional CP violation will be introduced and in chapter 4 the differences between this model and the SM are presented. In chapter 5 the advantages of a longitudinal polarization of the muons are discussed. Since all masses are taken into account for the calculations, also a study of the "mass effect", i.e. the neglection of all muon masses except for those responsible for the coupling of the fermions to the Higgs bosons, is possible. A short conclusion in chapter 6 summarizes the previous chapters and will give motivation for further studies.

To complete this diploma thesis some useful informations are collected in the appendices. In appendix A a collection of formulae is presented, while in appendix B the used Feynman rules are listed to get a quick overview. Finally appendix C presents the squared fermion couplings within the scenarios described in chapter 3.

Chapter 2

The process $\mu^+\mu^- \to f\bar{f}$ within the Standard Model

2.1 Kinematics

First the kinematics of a $1,2 \to 3,4$ process with $m_1 = m_2$ and $m_3 = m_4$ are introduced. It is convenient to choose the *C*enter-of-*M*ass (CM) frame [32]. In this frame the particle four-momenta indicated in (Fig. 2.1) are given by

$$
\begin{aligned}
p_1 &= \left(E_1^p, \vec{p_1}\right), \qquad p_2 = \left(E_2^p, \vec{p_2}\right) \overset{CM}{=} \left(E_1^p, -\vec{p_1}\right), \\
k_1 &= \left(E_1^k, \vec{k_1}\right), \qquad k_2 = \left(E_2^k, \vec{k_2}\right) \overset{CM}{=} \left(E_1^k, -\vec{k_1}\right),
\end{aligned}
\tag{2.1}
$$

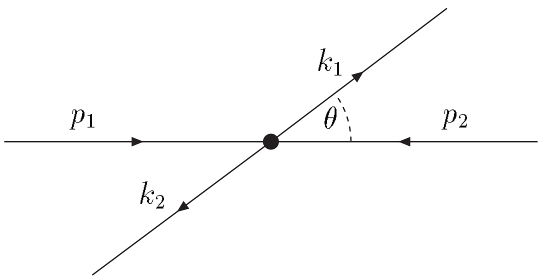

Figure 2.1: Definition of four-momenta and scattering angle θ

with

$$p_1 + p_2 = k_1 + k_2 \stackrel{CM}{=} \left(2E_1^p, \vec{0}\right) = \left(2E_1^k, \vec{0}\right) = \left(\sqrt{s}, \vec{0}\right). \tag{2.2}$$

In (2.2) the *squared center of mass energy*

$$\begin{aligned} s &\equiv (p_1 + p_2)^2 = (k_1 + k_2)^2 \\ &\stackrel{CM}{=} 4\left(E_1^p\right)^2 = 4\left(E_1^k\right)^2 \end{aligned} \tag{2.3}$$

has been used. Furthermore, one has

$$|\vec{p_1}| = |\vec{p_2}| = |\vec{p}| = \sqrt{\frac{s}{4} - m_\mu^2}\ , \tag{2.4}$$

$$|\vec{k_1}| = |\vec{k_2}| = |\vec{k}| = \sqrt{\frac{s}{4} - m_f^2}\ , \tag{2.5}$$

$$(p_1 p_2) = \frac{s}{2} - m_\mu^2\ , \tag{2.6}$$

$$(k_1 k_2) = \frac{s}{2} - m_f^2\ , \tag{2.7}$$

$$(p_i k_j) = \frac{s}{4} - (-1)^{\delta_{ij}} |\vec{p}||\vec{k}|\ \cos\theta\ . \tag{2.8}$$

Another convenient kinematic function is defined by

$$\begin{aligned} \lambda(x,y,z) &= x^2 + y^2 + z^2 - 2xy - 2xy - 2yz \\ &= \left(x - \left(\sqrt{y} + \sqrt{z}\right)^2\right)\left(x - \left(\sqrt{y} - \sqrt{z}\right)^2\right). \end{aligned} \tag{2.9}$$

Using (2.9) the equations (2.4) and (2.5) can be rewritten:

$$|\vec{p}| = \frac{1}{2\sqrt{s}}\sqrt{\lambda(s, m_\mu^2, m_\mu^2)} = \frac{1}{2\sqrt{s}}\sqrt{\lambda_\mu}\ , \tag{2.10}$$

$$|\vec{k}| = \frac{1}{2\sqrt{s}}\sqrt{\lambda(s, m_f^2, m_f^2)} = \frac{1}{2\sqrt{s}}\sqrt{\lambda_f}\ . \tag{2.11}$$

2.2 Higgs Boson Decay

A way to write the decay rate of an elementary particle into n particles, i.e.

$$1 \to 2,\ 3,\ \ldots,\ n\ , \tag{2.12}$$

is [33]

$$\begin{aligned} d\Gamma = |\mathcal{M}|^2 \quad & \cdot \quad \frac{w}{2m_1}\left[\left(\frac{d^3p_2}{(2\pi)^3\, 2E_2}\right)\left(\frac{d^3p_3}{(2\pi)^3\, 2E_3}\right)\cdots\left(\frac{d^3p_n}{(2\pi)^3\, 2E_n}\right)\right] \\ & \cdot \quad (2\pi)^4\ \delta^{(4)}\left(p_1 - p_2 - p_3 - \ldots - p_n\right), \end{aligned} \tag{2.13}$$

where

$$w = \frac{1}{j!} \tag{2.14}$$

is a statistical factor describing the number j of identical particles in the final state. If there is more than one group of identical particles, every group produces a separate factor. In the case of a two-particle decay, i.e.

$$1 \to 2,\ 3\ , \tag{2.15}$$

(2.13) reduces to

$$d\Gamma \quad = \quad |\mathcal{M}|^2\ \frac{w}{2m_1}\,\frac{d^3p_2 d^3p_3}{(2\pi)^6\, 4E_2E_3}\ (2\pi)^4\ \delta^{(4)}\left(p_1 - p_2 - p_3\right). \tag{2.16}$$

Going to the rest frame of the decaying particle ($\vec{p}_1 \stackrel{!}{=} 0$), integrating over $\vec{p}_3$ ($\vec{p}_3 \to -\vec{p}_2$) and using $d^3p_2 = |\vec{p}_2|^2\, d\,|\vec{p}_2|\, d\Omega$ yields

$$\frac{d\Gamma}{d\Omega} \quad = \quad \frac{w}{32\pi^2 m_1^2}\ |\vec{p}_2|\ |\mathcal{M}|^2\,. \tag{2.17}$$

After integration over the whole phase space, the total decay width can be written as

$$\Gamma = \frac{w}{8\pi m_1^2}\ |\vec{p}_2|\ |\mathcal{M}|^2\,. \tag{2.18}$$

2.2.1 Decay into Fermions

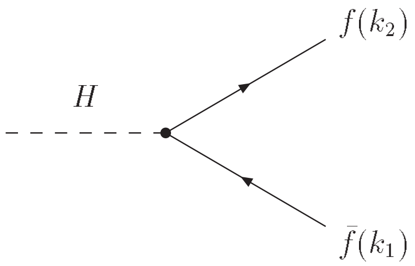

Figure 2.2: Higgs boson decay into fermions

The Feynman amplitude corresponding to Fig. 2.2 is

$$\mathcal{M} = \bar{u}(k_2)\left(-\frac{1}{2}ig\frac{m_f}{m_W}\right)v(k_1) \tag{2.19}$$

with the Feynman rules given in appendix B. Squaring (2.19) yields

$$|\mathcal{M}|^2 = \frac{e^2}{\sin^2\theta_W}\left(\frac{m_f}{m_W}\right)^2\left(k_1k_2 - m_f^2\right) , \tag{2.20}$$

where the fundamental relation

$$g = \frac{e}{\sin\theta_W} \tag{2.21}$$

has been used. Inserting the squared Feynman amplitude into (2.18) and introducing a colour factor

$$N_c^f = \begin{cases} 1 , & \text{if H decays into leptons} \\ 3 , & \text{if H decays into quarks} \end{cases} \tag{2.22}$$

results in

$$\begin{aligned} \Gamma\left(H \to f\bar{f}\right) &= N_c^f \frac{\left|\vec{k}_f\right|}{8\pi m_H^2}\frac{e^2}{\sin^2\theta_W}\left(\frac{m_f}{m_W}\right)^2\left(k_1k_2 - m_f^2\right) \\ &= \frac{N_c^f\cdot\alpha}{8\sin^2\theta_W}m_H\left(\frac{m_f}{m_W}\right)^2\left(1-\frac{4m_f^2}{m_H^2}\right)^{\frac{3}{2}} . \end{aligned} \tag{2.23}$$

For the last line the fact that a particle decays in its rest frame has been taken into account. Furthermore the definition of the *fine structure constant*

$$\alpha = \frac{e^2}{4\pi} \tag{2.24}$$

was inserted.

2.2.2 Decay into W Bosons

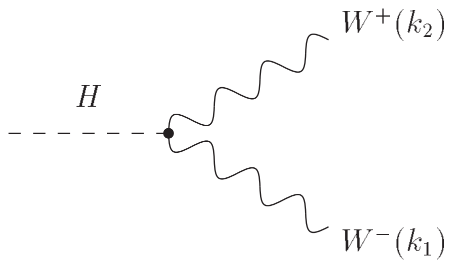

Figure 2.3: Higgs boson decay into W bosons

The Feynman rules given in appendix B lead to

$$\mathcal{M} = \epsilon^\mu(k_2, \lambda)\, ig\, m_W\, g_{\mu\nu}\, \epsilon^\nu(k_1, \lambda) \tag{2.25}$$

resulting in

$$|\mathcal{M}|^2 \;=\; g^2\, m_W^2 \sum_{pol} |\epsilon^\mu(k_2)\, \epsilon_\mu(k_1)|^2 \tag{2.26}$$

with the polarization vectors satisfying

$$\epsilon^\mu(p) \cdot p_\mu = 0\ . \tag{2.27}$$

For a vector particle with mass m and momentum p one has

$$\sum_{pol} \epsilon_\mu^*(p)\, \epsilon_\nu(p) = -g_{\mu\nu} + \frac{p_\mu p_\nu}{m^2}\ , \tag{2.28}$$

where the sum is over the three polarization states. Using (2.26) and (2.28) yields

$$|\mathcal{M}|^2 = \frac{e^2}{\sin^2\theta_W}\, m_W^2 \left(3 - \frac{m_H^2}{m_W^2} + \frac{m_H^4}{m_W^4}\right). \tag{2.29}$$

Together with (2.18) one gets

$$\Gamma\left(H \to W^+W^-\right) = \frac{\alpha}{16\sin^2\theta_W}\, m_H \left(\frac{m_H}{m_W}\right)^2 \sqrt{1-\frac{4m_W^2}{m_H^2}} \cdot \left(1-4\frac{m_W^2}{m_H^2}+12\frac{m_W^4}{m_H^4}\right). \tag{2.30}$$

2.2.3 Decay into Z^0 Bosons

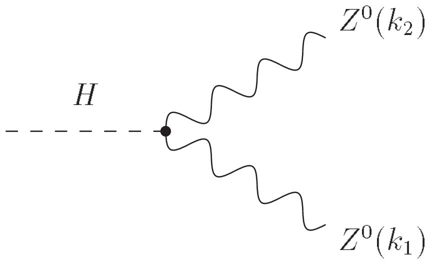

Figure 2.4: Higgs boson decay into Z^0 bosons

The Feynman amplitude describing Fig. 2.4 is according to appendix B

$$\mathcal{M} = \epsilon^\mu(k_2,\lambda)\, ig\, \frac{m_Z^2}{m_W}\, g_{\mu\nu}\, \epsilon^\nu(k_1,\lambda)\ . \tag{2.31}$$

With the calculations in the last section it is easy to write the squared Feynman amplitude:

$$|\mathcal{M}|^2 = \frac{e^2}{\sin^2\theta_W}\, \frac{m_Z^4}{m_W^2} \left(3-\frac{m_H^2}{m_Z^2}+\frac{m_H^4}{4m_Z^4}\right). \tag{2.32}$$

Here the Higgs boson decays into two identical particles. Therefore one has to apply the statistical factor

$$w = \frac{1}{2!}\ . \tag{2.33}$$

Inserting (2.32) and (2.33) into (2.18) results in

$$\Gamma\left(H \to Z^0Z^0\right) = \frac{\alpha}{32\sin^2\theta_W}\, m_H \left(\frac{m_H}{m_W}\right)^2 \sqrt{1-\frac{4m_Z^2}{m_H^2}} \cdot \left(1-4\frac{m_Z^2}{m_H^2}+12\frac{m_Z^4}{m_H^4}\right). \tag{2.34}$$

2.2.4 Constraints on the Higgs Boson Mass

It is important to determine which of the above decay channels exist. Obviously a particle of mass m decays only into a pair of particles whose masses m_1 and m_2 satisfy the relation

$$m_1 + m_2 < m_H \ . \tag{2.35}$$

Therefore a Higgs particle with a mass around the present experimental lower limit [16, 17, 18]

$$m_H^{min} \approx 113.5 \text{ GeV} \ , \tag{2.36}$$

neither decays into gauge bosons nor into top quarks. But a heavier Higgs boson may be possible. A theoretical upper limit can be determined at [34]

$$m_H^{max} \approx 700 \text{ GeV} \ . \tag{2.37}$$

This limit do not apply to the model in general but only to its perturbative realization. It avoids a large self-interaction and the running of the quartic Higgs coupling [34].

If, however, the Higgs particle is much heavier than the gauge bosons and the top-quark

$$m_H \gg m_W, \, m_Z, \, m_t \tag{2.38}$$

all decay channels are open and an approximation of the decay rates can be made by using the following relations

$$\Gamma\left(H \to f\bar{f}\right) \approx \frac{N_c^f \alpha}{8 \sin^2\theta_W} \, m_H \left(\frac{m_f^2}{m_W^2}\right), \tag{2.39}$$

$$\Gamma\left(H \to W^+W^-\right) \approx \frac{\alpha}{16 \sin^2\theta_W} \, m_H \left(\frac{m_H^2}{m_W^2}\right), \tag{2.40}$$

$$\Gamma\left(H \to Z^0Z^0\right) \approx \frac{\alpha}{32 \sin^2\theta_W} \, m_H \left(\frac{m_H^2}{m_W^2}\right). \tag{2.41}$$

In this case the Higgs decay width into fermions is proportional to the square of the mass of the fermions. This means that the decay into fermions is dominated by the channel with the heaviest quark. Otherwise it is important that the decay of a heavy Higgs particle into gauge bosons depends on m_H^3.

Since a large decay width means a very short lifetime, it is reasonable to require for a particle that its decay width is smaller than its mass [34]:

$$m_H > \Gamma_H \ . \tag{2.42}$$

Summing (2.39), (2.40) and (2.41) gives

$$\begin{aligned}\Gamma_H &= \Gamma_{t\bar{t}} + \Gamma_{WW} + \Gamma_{ZZ} \\ &\approx \frac{\alpha}{8\sin^2\theta_W}\frac{m_H}{m_W^2}\left(3m_t^2 + \frac{m_H^2}{2} + \frac{m_H^2}{4}\right) \\ &\overset{(2.38)}{\approx} \frac{3\alpha}{32\sin^2\theta_W}\frac{m_H^3}{m_W^2}\,. \end{aligned} \tag{2.43}$$

Inserting the largest possible Higgs boson mass m_H^{max} discussed above and the parameters given in appendix B.4 into (2.43) yields

$$\Gamma_H^{max} \approx 167 \text{ GeV}. \tag{2.44}$$

So (2.42) is satisfied in the whole possible mass range:

$$113.5 \text{ GeV} \leq m_H \lesssim 700 \text{ GeV}. \tag{2.45}$$

2.2.5 Numerical Results

The following plots are made with the formulae calculated above and the physical constants listed in appendix B.4.

In Fig. 2.5 the decay width Γ_H of a Higgs boson is plotted against its mass m_H. The steep increase of the decay width at a value of $m_H \approx 160$ GeV results from the opening of the decay channel into W-bosons. A similar but less significant rise can be noticed at $m_H \approx 180$ GeV, where the decay into Z^0-bosons becomes possible.

In Fig. 2.6 the main components of the decay width are plotted. The decay into fermions scales with m_H for large Higgs boson masses, while the decay into gauge bosons is proportional to m_H^3. This corresponds to the approximations given in (2.39) - (2.41).

The branching ratios are given in Fig. 2.7. The channel into W-bosons dominates for $m_H > 160$ GeV with $> 55\%$. According to (2.33) this is twice the value of the branching ratio for the decay into Z^0-bosons. If the decay channel into top-quarks is open it contributes less than 20%.

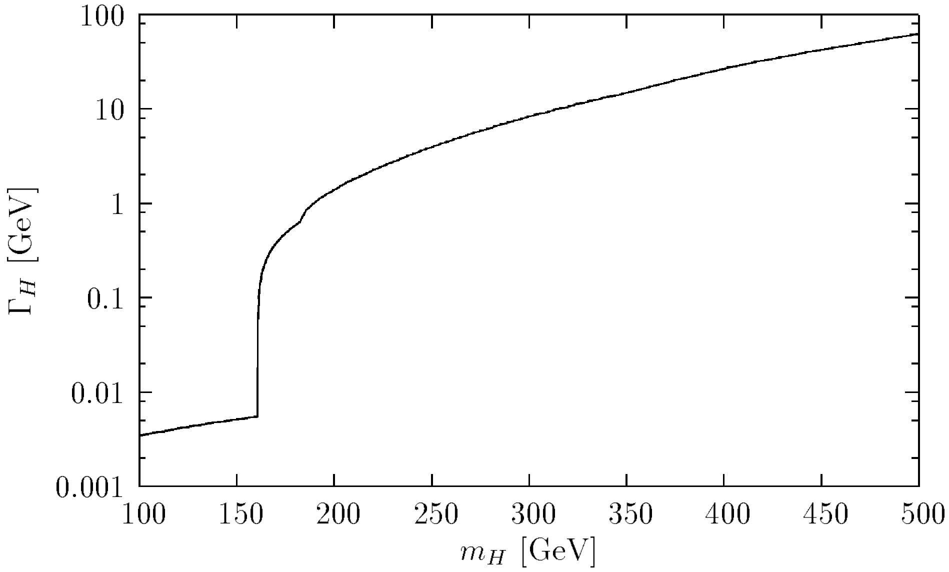

Figure 2.5: Decay width Γ_H versus Higgs boson mass m_H

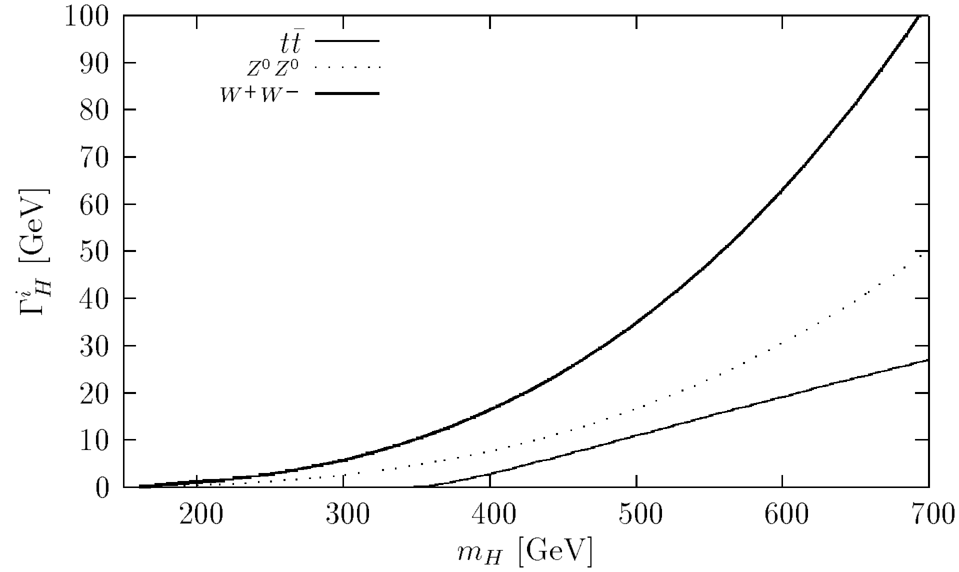

Figure 2.6: Main contributions of the decay width Γ^i_H versus Higgs boson mass m_H

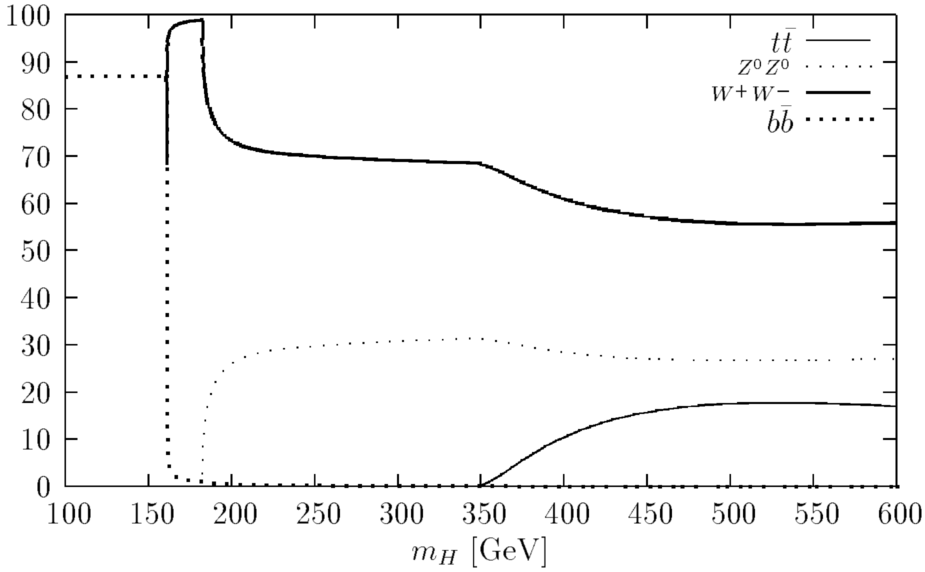

Figure 2.7: Branching ratios in % of the different Higgs decay channels versus Higgs boson mass m_H

2.3 Cross Section

The differential cross section for the scattering process

$$1, 2 \to 3, 4, \ldots, n \tag{2.46}$$

can be calculated from the general expression [33]

$$\begin{aligned} d\sigma = |\mathcal{M}|^2 \quad & \cdot \quad \frac{w}{4\sqrt{(p_1p_2)^2 - (m_1m_2)^2}} \\ & \cdot \quad \left[\left(\frac{d^3p_3}{(2\pi)^3\, 2E_3}\right)\left(\frac{d^3p_4}{(2\pi)^3\, 2E_4}\right)\cdots\left(\frac{d^3p_n}{(2\pi)^3\, 2E_n}\right)\right] \\ & \cdot \quad (2\pi)^4\, \delta^{(4)}\left(p_1 + p_2 - p_3 - p_4 - \ldots - p_n\right), \end{aligned} \tag{2.47}$$

with the statistical factor w defined in (2.14). For the scattering process

$$1, 2 \to 3, 4 \tag{2.48}$$

equation (2.47) reduces to

$$d\sigma = |\mathcal{M}|^2 \cdot \frac{1}{4\sqrt{(p_1 p_2)^2 - (m_1 m_2)^2}} \cdot \left[\left(\frac{d^3 p_3}{(2\pi)^3\, 2E_3}\right)\left(\frac{d^3 p_4}{(2\pi)^3\, 2E_4}\right)\right] \cdot (2\pi)^4\, \delta^{(4)}(p_1 + p_2 - p_3 - p_4)\,. \tag{2.49}$$

Going to the CM, i.e. $\vec{p_1} = -\vec{p_2}$, and using the relativistic energy-momentum-relation, equation (2.49) becomes

$$\begin{aligned} d\sigma &= \frac{|\mathcal{M}|^2}{(8\pi)^2} \cdot \frac{1}{(E_1 + E_2)\,|\vec{p_1}|} \cdot \frac{d^3 p_3 d^3 p_4}{\sqrt{m_3^2 + \vec{p_3}^{\,2}}\sqrt{m_4^2 + \vec{p_4}^{\,2}}} \\ &\cdot \delta\left(E_1 + E_2 - \sqrt{m_3^2 + \vec{p_3}^{\,2}} - \sqrt{m_4^2 + \vec{p_4}^{\,2}}\right) \\ &\cdot \delta^{(3)}(-\vec{p_3} - \vec{p_4})\,. \end{aligned} \tag{2.50}$$

Integrating over $\vec{p_4}$ ($\vec{p_4} \to -\vec{p_3}$) and inserting $d^3 p_3 = |p_3|^2\, d\,|p_3|\, d\Omega$ results in

$$\frac{d\sigma}{d\Omega} = \frac{1}{(8\pi)^2}\,\frac{1}{(E_1 + E_2)^2}\,\frac{|\vec{p_3}|}{|\vec{p_1}|}\,|\mathcal{M}|^2\,. \tag{2.51}$$

After renaming the momenta and using (2.3), (2.10) and (2.11) one finds

$$\frac{d\sigma}{d\Omega} = \frac{N_c^f}{(8\pi)^2}\,\frac{1}{s}\,\sqrt{\frac{\lambda_f}{\lambda_\mu}}\,|\mathcal{M}|^2\,, \tag{2.52}$$

where again the colour factor N_c^f defined in (2.22) has been included.

2.3.1 Feynman amplitudes

In this diploma thesis, the process $\mu^-\mu^+ \to f\bar{f}$ ($f = b, t$) will be studied. Therefore the Feynman graphs below are relevant. The corresponding Feynman amplitudes $\mathcal{M}$ are created with the help of the Feynman rules given in appendix B. The spinors u and v represent fermions and anti-fermions. The Feynman amplitudes are written in the R_ξ gauge. In this case Feynman graphs involving a Goldstone boson appear, that vanish when the unitary gauge ($\xi = \infty$) is used.

Photon Exchange

First the $\mu^+\mu^-$-annihilation via a virtual photon shown in Fig. 2.8 is considered.

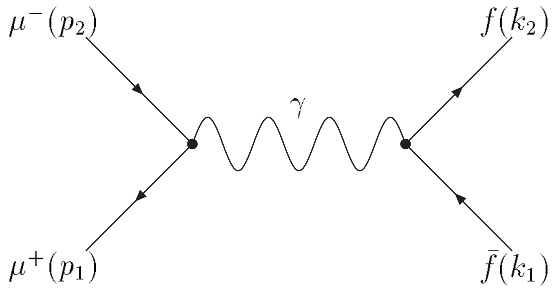

Figure 2.8: Feynman graph of the photon exchange

With the Feynman rules given in appendix B one finds

$$\begin{aligned} \mathcal{M}_\gamma &= \bar{v}(p_1)\,(-ie\gamma_\alpha Q_\mu)\,u(p_2)\left(i\,\frac{-g^{\alpha\beta}+(1-\xi)\,\frac{q^\alpha q^\beta}{q^2}}{q^2+i\epsilon}\right) \\ &\qquad \cdot\bar{u}(k_2)\,(-ie\gamma_\beta Q_f)\,v(k_1)\;. \end{aligned} \tag{2.53}$$

To show the gauge invariance of this amplitude, one has to verify that the second term of the propagator that depends on the gauge factor ξ vanishes:

$$\begin{aligned} \mathcal{M}_\gamma^{II} &\propto \bar{v}(p_1)\;\not{q}\;u(p_2)\cdot\bar{u}(k_2)\;\not{q}\;v(k_1) \\ &= \bar{v}(p_1)\,(\not{p}_1+\not{p}_2)\,u(p_2)\cdot\bar{u}(k_2)\,(\not{k}_1+\not{k}_2)\,v(k_1) \\ &\overset{(A.50)}{=} (m_\mu-m_\mu)\,\bar{v}(p_1)u(p_2)+(m_f-m_f)\,\bar{u}(k_2)v(k_1) \\ &= 0\;. \end{aligned} \tag{2.54}$$

So the Feynman amplitude is gauge invariant, which is a manifestation of current conservation in QED.

Z^0 Boson and Goldstone Boson Exchange

If the energy of the colliding beams is high enough the exchange of a neutral Z^0 boson (Fig. 2.9) has to be taken into account.

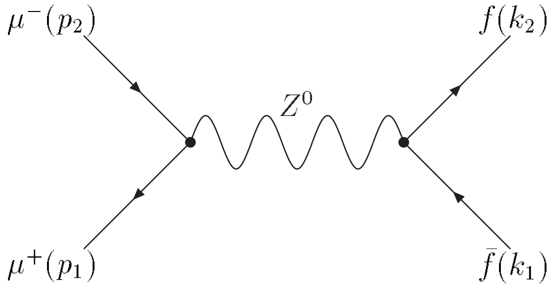

Figure 2.9: Feynman graph of the Z^0-boson exchange

The Feynman amplitude is

$$\begin{aligned}\mathcal{M}_{Z^0} &= \bar{v}(p_2)\left[\frac{ig}{2\cos\theta_W}\gamma_\alpha\,(g_V^\mu - g_A^\mu\gamma_5)\right]u(p_1) \\ &\quad\cdot\left[i\,\frac{-g^{\alpha\beta}+(1-\xi)\,\frac{q^\alpha q^\beta}{q^2-\xi m_Z^2}}{q^2-m_Z^2+i\epsilon}\right] \\ &\quad\cdot\,\bar{u}(k_2)\left[\frac{ig}{2\cos\theta_W}\gamma_\beta\,(g_V^f - g_A^f\gamma_5)\right]v(k_1)\,. \end{aligned} \tag{2.55}$$

To show the ξ-independence of this Feynman amplitude it is necessary to rewrite the propagator:

$$\begin{aligned}\Delta_{Z^0} &= \frac{i}{q^2-m_Z^2}\left[-g^{\alpha\beta}+(1-\xi)\,\frac{q^\alpha q^\beta}{q^2-\xi m_Z^2}\right] \\ &= \frac{i}{q^2-m_Z^2}\left[-g^{\alpha\beta}+\frac{q^\alpha q^\beta}{m_Z^2}-\frac{q^\alpha q^\beta}{m_Z^2}+(1-\xi)\,\frac{q^\alpha q^\beta}{q^2-\xi m_Z^2}\right] \\ &= i\,\frac{\left(-g^{\alpha\beta}+\frac{q^\alpha q^\beta}{m_Z^2}\right)}{q^2-m_Z^2}-i\,\frac{q^\alpha q^\beta}{m_Z^2\,(q^2-\xi m_Z^2)}\,. \end{aligned} \tag{2.56}$$

For the second term of (2.56) one gets

$$\begin{aligned}\mathcal{M}_{Z^0}^{II} &= \frac{ig^2}{4\cos^2\theta_W}\,\frac{1}{m_Z^2\,(q^2-\xi m_Z^2)} \\ &\quad\cdot\left[\bar{v}(p_1)\;\not{q}\,(g_V^\mu - g_A^\mu\gamma_5)\,u(p_2)\,\bar{u}(k_2)\;\not{q}(g_V^f - g_A^f\gamma_5)v(k_1)\right].\end{aligned} \tag{2.57}$$

With the Dirac equations (A.50) one finds

$$\begin{aligned}
\bar{v}(p_1)\, \not{q}\,(g_V^\mu - g_A^\mu\gamma_5)\, u(p_2) &= +2g_A^\mu m_\mu\, \bar{v}(p_1)\gamma_5 u(p_2)\;, && (2.58)\\
\bar{u}(k_2)\, \not{q}\,(g_V^f - g_A^f\gamma_5)\, v(k_1) &= -2g_A^f m_f\, \bar{u}(k_2)\gamma_5 v(k_1)\;. && (2.59)
\end{aligned}$$

Using the above relations and

$$\begin{aligned}
g_A^\mu g_A^f &= T_Z^\mu T_Z^f\;, && (2.60)\\
m_Z \cdot \cos\theta_W &= m_W && (2.61)
\end{aligned}$$

(see appendix B) equation (2.57) can be rewritten:

$$\mathcal{M}_{Z^0}^{II} = -ig^2 T_Z^\mu T_Z^f \cdot \frac{m_\mu m_f}{m_W^2\,(q^2-\xi m_Z^2)} \cdot \left[\bar{v}(p_1)\gamma_5 u(p_2)\,\bar{u}(k_2)\gamma_5 v(k_1)\right]. \quad (2.62)$$

This term is cancelled by the contribution of the would-be Goldstone boson. The corresponding diagram is shown in Fig. 2.10.

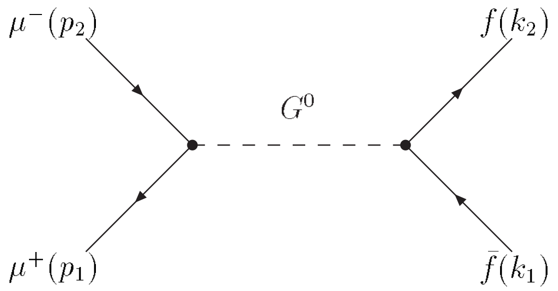

Figure 2.10: Feynman graph of the Goldstone boson exchange

The Feynman rules of appendix B lead to the amplitude

$$\begin{aligned}
\mathcal{M}_{G^0} &= \bar{v}(p_1)\left(-gT_Z^\mu \frac{m_\mu}{m_W}\gamma_5\right) u(p_2) \left(\frac{i}{q^2-\xi m_Z^2+i\epsilon}\right)\\
&\qquad\qquad \cdot \bar{u}(k_2)\left(-gT_Z^f \frac{m_f}{m_W}\gamma_5\right) v(k_1) && (2.63)
\end{aligned}$$

that is identical up to the sign with (2.62):

$$\mathcal{M}_{Z^0}^{II} = -\mathcal{M}_{G^0}. \quad (2.64)$$

The Goldstone boson cancels the contribution of the unphysical timelike polarization state of the gauge boson [35]. Thus, the sum of the Feynman amplitudes is independent of ξ.

Higgs Boson Exchange

Finally, at $s \approx m_H^2$ the Feynman graph of the Higgs boson exchange (Fig. 2.11) has to be taken into account. The amplitude following from the Feynman rules of appendix B is given by

$$\begin{aligned}\mathcal{M}_H &= \bar{v}(p_1)\left(-\frac{1}{2}ig\frac{m_\mu}{m_W}\right)u(p_2)\left(\frac{i}{q^2 - m_H^2 + i\epsilon}\right) \\ &\qquad \cdot\bar{u}(k_2)\left(-\frac{1}{2}ig\frac{m_f}{m_W}\right)v(k_1)\ . \qquad (2.65)\end{aligned}$$

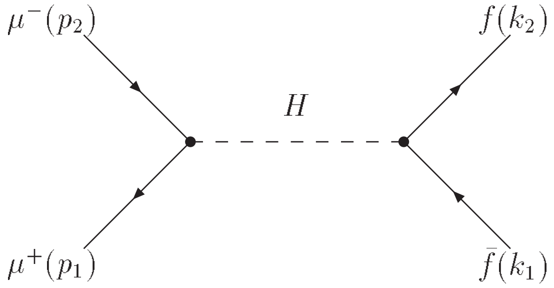

Figure 2.11: Feynman graph of the Higgs boson exchange

Since neither the Z^0 boson nor the Higgs boson is a stable particle, the propagators are substituted by *Breit-Wigner propagators*:

$$\frac{1}{q^2 - m_x^2} \longrightarrow \frac{1}{q^2 - m_x^2 + im_x\Gamma_x}\ , \qquad (2.66)$$

where Γ_x is the decay width with $x = \{Z, H\}$.

To summarize, the complete lowest order Feynman amplitude for $\mu^+\mu^- \longrightarrow f\bar{f}$ in the *Feynman-t'Hooft gauge* ($\xi = 1$) is given. The Feynman gauge has the advantage of simple expressions for the amplitudes at the cost of the presence of the Goldstone boson contributions. With the factors

$$\mathcal{T}_\gamma = i\,\frac{e^2 Q_\mu Q_f}{q^2}\ , \qquad (2.67)$$

$$\mathcal{T}_{Z^0} = i\,\frac{e^2}{4\sin^2\theta_W\cos^2\theta_W}\,\frac{1}{(q^2 - m_Z^2 + im_z\Gamma_Z)}\ , \qquad (2.68)$$

$$\mathcal{T}_{G^0} = i \, \frac{e^2 \, g_A^\mu g_A^f}{\sin^2\theta_W \cos^2\theta_W} \, \frac{m_\mu m_f}{m_Z^2} \, \frac{1}{(q^2 - m_Z^2 + i m_z \Gamma_Z)} \, , \tag{2.69}$$

$$\mathcal{T}_H = -i \, \frac{e^2}{4\sin^2\theta_W \cos^2\theta_W} \, \frac{m_\mu m_f}{m_Z^2} \, \frac{1}{(q^2 - m_H^2 + i m_H \Gamma_H)} \, , \tag{2.70}$$

where the relations (2.21) and (2.61) have been used, the complete Feynman amplitude can be written in a compact form:

$$\mathcal{M} = \mathcal{M}_\gamma + \mathcal{M}_{Z^0} + \mathcal{M}_{G^0} + \mathcal{M}_H \tag{2.71}$$

with

$$\mathcal{M}_\gamma = \mathcal{T}_\gamma \; \bar{v}(p_1)\,\gamma_\alpha\,u(p_2)\;\bar{u}(k_2)\,\gamma^\alpha\,v(k_1) \, , \tag{2.72}$$

$$\begin{aligned}\mathcal{M}_{Z^0} = {} & \mathcal{T}_{Z^0} \; \bar{v}(p_1)\,\gamma_\alpha\,(g_V^\mu - g_A^\mu\gamma_5)\;u(p_2) \\ & \bar{u}(k_2)\,\gamma^\alpha(g_V^f - g_A^f\gamma_5)\,v(k_1) \, ,\end{aligned} \tag{2.73}$$

$$\mathcal{M}_{G^0} = \mathcal{T}_{G^0} \; \bar{v}(p_1)\,\gamma_5\,u(p_2)\;\bar{u}(k_2)\,\gamma^5\,v(k_1) \, , \tag{2.74}$$

$$\mathcal{M}_H = \mathcal{T}_H \; \bar{v}(p_1)\,u(p_2)\;\bar{u}(k_2)\,v(k_1) \, . \tag{2.75}$$

2.3.2 Squared Matrix Elements

Here, the squared Feynman amplitudes for unpolarized muons and averaged quark spin will be calculated by making use of the Feynman amplitudes presented above in (2.72) - (2.75).

Photon

$$\begin{aligned}|\mathcal{M}|_\gamma^2 = \frac{1}{4}\cdot|\mathcal{T}_\gamma|^2 \quad \cdot \quad & \mathrm{Tr}\;[\gamma_\alpha\,(\not{p}_1 - m_\mu)\,\gamma_\beta\,(\not{p}_2 + m_\mu)] \\ \cdot \quad & \mathrm{Tr}\;\left[\gamma^\alpha\,(\not{k}_1 + m_f)\,\gamma^\beta\,(\not{k}_2 - m_f)\right] \\ = 8\cdot|\mathcal{T}_\gamma|^2 \quad \cdot \quad & \left[2m_\mu^2 m_f^2 + m_\mu^2(k_1k_2) + m_f^2(p_1p_2)\right. \\ & \left. +(p_1k_1)(p_2k_2) + (p_1k_2)(p_2k_1)\right]\end{aligned} \tag{2.76}$$

Photon Z-Boson Interference

$$\begin{aligned}
\mathcal{M}_\gamma \mathcal{M}_{Z^0}^\dagger + \mathcal{M}_\gamma^\dagger \mathcal{M}_{Z^0} &= 2 \cdot \Re e \left(\mathcal{M}_\gamma \mathcal{M}_{Z^0}^\dagger \right) \\
&= \frac{1}{4} \cdot \left(\mathcal{T}_\gamma \mathcal{T}_{Z^0}^* + \mathcal{T}_\gamma^* \mathcal{T}_{Z^0} \right) \\
&\quad \cdot \mathrm{Tr} \left[\gamma_\alpha \left(\not{p}_1 - m_\mu \right) \gamma_\beta \left(g_V^\mu - g_A^\mu \gamma_5 \right) \left(\not{p}_2 + m_\mu \right) \right] \\
&\quad \cdot \mathrm{Tr} \left[\gamma^\alpha \left(\not{k}_1 + m_f \right) \gamma^\beta (g_V^f - g_A^f \gamma^5) \left(\not{k}_2 - m_f \right) \right] \\
&= 8 \cdot \left(\mathcal{T}_\gamma \mathcal{T}_{Z^0}^* + \mathcal{T}_\gamma^* \mathcal{T}_{Z^0} \right) \\
&\quad \cdot \{ g_V^\mu g_V^f \cdot [2 m_\mu^2 m_f^2 + m_\mu^2 (k_1 k_2) + m_f^2 (p_1 p_2) \\
&\qquad\qquad + (p_1 k_1)(p_2 k_2) + (p_1 k_2)(p_2 k_1)] \\
&\quad + g_A^\mu g_A^f \cdot [(p_1 k_1)(p_2 k_2) - (p_1 k_2)(p_2 k_1)] \} \qquad (2.77)
\end{aligned}$$

Photon Goldstone-Boson Interference

$$\mathcal{M}_\gamma \mathcal{M}_{G^0}^\dagger + \mathcal{M}_\gamma^\dagger \mathcal{M}_{G^0} = 0 \qquad (2.78)$$

(A vector-pseudoscalar-interference vanishes.)

Photon Higgs-Boson Interference

$$\begin{aligned}
\mathcal{M}_\gamma \mathcal{M}_H^\dagger + \mathcal{M}_\gamma^\dagger \mathcal{M}_H &= 2 \cdot \Re e \left(\mathcal{M}_\gamma \mathcal{M}_H^\dagger \right) \\
&= \frac{1}{4} \cdot \left(\mathcal{T}_\gamma \mathcal{T}_H^* + \mathcal{T}_\gamma^* \mathcal{T}_H \right) \\
&\quad \cdot \mathrm{Tr} \left[\gamma_\alpha \left(\not{p}_1 - m_\mu \right) \left(\not{p}_2 + m_\mu \right) \right] \\
&\quad \cdot \mathrm{Tr} \left[\gamma^\alpha \left(\not{k}_1 + m_f \right) \left(\not{k}_2 - m_f \right) \right] \\
&= 4 \cdot \left(\mathcal{T}_\gamma \mathcal{T}_H^* + \mathcal{T}_\gamma^* \mathcal{T}_H \right) \cdot m_\mu m_f \\
&\quad \cdot [-(p_1 k_1) + (p_1 k_2) + (p_2 k_1) - (p_2 k_2)] \qquad (2.79)
\end{aligned}$$

Z-Boson

$$
\begin{aligned}
|\mathcal{M}|^2_{Z^0} = \frac{1}{4}\cdot|\mathcal{T}_{Z^0}|^2 \quad \cdot \quad & \mathrm{Tr}\Big[\gamma_\alpha\,(g_V^\mu - g_A^\mu\gamma_5)\,(\not{p}_1 - m_\mu) \\
& \quad \cdot\gamma_\beta\,(g_V^\mu - g_A^\mu\gamma_5)\,(\not{p}_2 + m_\mu)\Big] \\
& \cdot\ \mathrm{Tr}\Big[\gamma^\alpha(g_V^f - g_A^f\gamma^5)\,(\not{k}_1 + m_f) \\
& \quad \cdot\gamma^\beta(g_V^f - g_A^f\gamma^5)\,(\not{k}_2 - m_f)\Big] \\
= 8\cdot|\mathcal{T}_{Z^0}|^2 \quad \cdot \quad & \Big\{2m_\mu^2 m_f^2\Big[\Big({g_V^\mu}^2 - {g_A^\mu}^2\Big)\cdot\Big({g_V^f}^2 - {g_A^f}^2\Big)\Big] \\
& +m_\mu^2(k_1k_2)\Big[\Big({g_V^\mu}^2 - {g_A^\mu}^2\Big)\Big({g_V^f}^2 + {g_A^f}^2\Big)\Big] \\
& +m_f^2(p_1p_2)\Big[\Big({g_V^\mu}^2 + {g_A^\mu}^2\Big)\Big({g_V^f}^2 - {g_A^f}^2\Big)\Big] \\
& +(p_1k_1)(p_2k_2)\Big[\Big({g_V^\mu}^2 + {g_A^\mu}^2\Big)\Big({g_V^f}^2 + {g_A^f}^2\Big)\Big] \\
& +(p_1k_2)(p_2k_1)\Big[\Big({g_V^\mu}^2 + {g_A^\mu}^2\Big)\Big({g_V^f}^2 + {g_A^f}^2\Big)\Big] \\
& +4g_V^\mu g_A^\mu g_V^f g_A^f \\
& \quad \cdot\Big[(p_1k_1)(p_2k_2) - (p_1k_2)(p_2k_1)\Big]\Big\}
\end{aligned}
\tag{2.80}
$$

Z-Boson Goldstone-Boson Interference

$$
\begin{aligned}
\mathcal{M}_{Z^0}\mathcal{M}^\dagger_{G^0} + \mathcal{M}^\dagger_{Z^0}\mathcal{M}_{G^0} &= 2\cdot\Re e\Big(\mathcal{M}_{Z^0}\mathcal{M}^\dagger_{G^0}\Big) \\
&= \frac{1}{4}\cdot(\mathcal{T}_{Z^0}\mathcal{T}^*_{G^0} + \mathcal{T}^*_{Z^0}\mathcal{T}_{G^0}) \\
&\quad \cdot\ \mathrm{Tr}\Big[\gamma_\alpha\,(g_V^\mu - g_A^\mu\gamma_5)\,(\not{p}_1 - m_\mu)\,\gamma_5\,(\not{p}_2 + m_\mu)\Big] \\
&\quad \cdot\ \mathrm{Tr}\Big[\gamma^\alpha(g_V^f - g_A^f\gamma^5)\,(\not{k}_1 + m_f)\,\gamma^5\,(\not{k}_2 - m_f)\Big] \\
&= -4\cdot(\mathcal{T}_{Z^0}\mathcal{T}^*_{G^0} + \mathcal{T}^*_{Z^0}\mathcal{T}_{G^0})\cdot m_\mu m_f\cdot g_A^\mu g_A^f \\
&\quad \cdot[(p_1k_1) + (p_1k_2) + (p_2k_1) + (p_2k_2)]
\end{aligned}
\tag{2.81}
$$

Z-Boson Higgs-Boson Interference

$$\begin{aligned}
\mathcal{M}_{Z^0}\mathcal{M}_H^\dagger + \mathcal{M}_{Z^0}^\dagger\mathcal{M}_H &= 2\cdot\Re e\left(\mathcal{M}_{Z^0}\mathcal{M}_H^\dagger\right) \\
&= \frac{1}{4}\cdot\left(\mathcal{T}_{Z^0}\mathcal{T}_H^* + \mathcal{T}_{Z^0}^*\mathcal{T}_H\right) \\
&\quad \cdot\ \mathrm{Tr}\left[\gamma_\alpha\left(g_V^\mu - g_A^\mu\gamma_5\right)\left(\not{p}_1 - m_\mu\right)\left(\not{p}_2 + m_\mu\right)\right] \\
&\quad \cdot\ \mathrm{Tr}\left[\gamma^\alpha\left(g_V^f - g_A^f\gamma^5\right)\left(\not{k}_1 + m_f\right)\left(\not{k}_2 - m_f\right)\right] \\
&= 4\cdot\left(\mathcal{T}_{Z^0}\mathcal{T}_H^* + \mathcal{T}_{Z^0}^*\mathcal{T}_H\right)\cdot m_\mu m_f\cdot g_V^\mu g_V^f \\
&\quad \cdot\left[-(p_1k_1) + (p_1k_2) + (p_2k_1) - (p_2k_2)\right] \qquad (2.82)
\end{aligned}$$

Goldstone-Boson

$$\begin{aligned}
|\mathcal{M}|_{G^0}^2 = \frac{1}{4}\cdot|\mathcal{T}_{G^0}|^2 \quad &\cdot \quad \mathrm{Tr}\left[\gamma_5\left(\not{p}_1 - m_\mu\right)\gamma_5\left(\not{p}_2 + m_\mu\right)\right] \\
&\cdot \quad \mathrm{Tr}\left[\gamma^5\left(\not{k}_1 + m_f\right)\gamma^5\left(\not{k}_2 - m_f\right)\right] \\
= 4\cdot|\mathcal{T}_{G^0}|^2 \quad &\cdot \quad \Big[m_\mu^2 m_f^2 + m_\mu^2(k_1k_2) \\
&\qquad + m_f^2(p_1p_2) + (p_1p_2)(k_1k_2)\Big] \qquad (2.83)
\end{aligned}$$

Goldstone-Boson Higgs-Boson Interference

$$\mathcal{M}_{G^0}\mathcal{M}_H^\dagger + \mathcal{M}_{G^0}^\dagger\mathcal{M}_H = 0 \qquad (2.84)$$

(A scalar-pseudoscalar-interference vanishes.)

Higgs-Boson

$$\begin{aligned}
|\mathcal{M}|_H^2 = \frac{1}{4}\cdot|\mathcal{T}_H|^2 \quad &\cdot \quad \mathrm{Tr}\left[\left(\not{p}_1 - m_\mu\right)\left(\not{p}_2 + m_\mu\right)\right] \\
&\cdot \quad \mathrm{Tr}\left[\left(\not{k}_1 + m_f\right)\left(\not{k}_2 - m_f\right)\right] \\
= 4\cdot|\mathcal{T}_H|^2 \quad &\cdot \quad \Big[m_\mu^2 m_f^2 - m_\mu^2(k_1k_2) \\
&\qquad - m_f^2(p_1p_2) + (p_1p_2)(k_1k_2)\Big] \qquad (2.85)
\end{aligned}$$

2.3.3 Differential Cross Section

From the squared Feynman amplitudes given in (2.76) - (2.85) and from (2.52) one obtains the differential cross section

$$\frac{d\sigma}{d\Omega} = 3\alpha^2 \sqrt{\frac{\lambda_f}{\lambda_\mu}} \sum_k f_k \left(R_k \cos^2\theta + I_k \cos\theta + S_k\right) \tag{2.86}$$

with the prefactors

$$f_\gamma = Q_\mu^2 Q_f^2 \frac{1}{s^2} , \tag{2.87}$$

$$f_{\gamma Z^0} = \frac{Q_\mu Q_f}{\cos^2\theta_W \sin^2\theta_W} \frac{s - m_Z^2}{(s-m_Z^2)^2 + m_Z^2\Gamma_Z^2} \frac{1}{s} , \tag{2.88}$$

$$f_{\gamma G^0} = 0 , \tag{2.89}$$

$$f_{\gamma H} = \frac{Q_\mu Q_f}{\sin^2\theta_W} \frac{m_\mu m_f}{m_W^2} \frac{s - m_H^2}{(s-m_H^2)^2 + m_H^2\Gamma_H^2} \frac{1}{s} , \tag{2.90}$$

$$f_{Z^0} = \frac{1}{\cos^4\theta_W \sin^4\theta_W} \frac{1}{(s-m_Z^2)^2 + m_Z^2\Gamma_Z^2} , \tag{2.91}$$

$$f_{Z^0 G^0} = \frac{1}{\cos^4\theta_W \sin^4\theta_W} \frac{m_\mu m_f}{m_Z^2} \frac{1}{(s-m_Z^2)^2 + m_Z^2\Gamma_Z^2} , \tag{2.92}$$

$$\begin{aligned} f_{Z^0 H} = {} & \frac{1}{\cos^2\theta_W \sin^4\theta_W} \frac{m_\mu m_f}{m_W^2} \\ & \cdot \frac{(s-m_Z^2)(s-m_H^2) + m_Z\Gamma_Z m_H\Gamma_H}{\left[(s-m_Z^2)^2 + m_Z^2\Gamma_Z^2\right]\left[(s-m_H^2)^2 + m_H^2\Gamma_H^2\right]} , \end{aligned} \tag{2.93}$$

$$f_{G^0} = \frac{1}{\cos^4\theta_W \sin^4\theta_W} \frac{m_\mu^2 m_f^2}{m_Z^4} \frac{1}{(s-m_Z^2)^2 + m_Z^2\Gamma_Z^2} , \tag{2.94}$$

$$f_{G^0 H} = 0 , \tag{2.95}$$

$$f_H = \frac{1}{\sin^4\theta_W} \frac{m_\mu^2 m_f^2}{m_W^4} \frac{1}{(s-m_H^2)^2 + m_H^2\Gamma_H^2} , \tag{2.96}$$

and the factors R_k, I_k and S_k listed in Tab. 2.1. It is worth mentioning, that the mass dependence of the Feynman amplitudes is completely contained in the prefactors f_k.

k	R_k	I_k	S_k
γ	$\frac{s}{4} - \left(m_\mu^2 + m_f^2\right) + \frac{4}{s} m_\mu^2 m_f^2$	–	$\frac{s}{4} + \left(m_\mu^2 + m_f^2\right)$
γZ^0	$\frac{1}{2} g_V^\mu g_V^f \left[\frac{s}{4} - \left(m_\mu^2 + m_f^2\right) + \frac{4}{s} m_\mu^2 m_f^2\right]$	$\frac{1}{4s} g_A^\mu g_A^f \sqrt{\lambda_\mu \lambda_f}$	$\frac{1}{2} g_V^\mu g_V^f \left[\frac{s}{4} + \left(m_\mu^2 + m_f^2\right)\right]$
γG^0	–	–	–
γH	–	$\frac{1}{2s^2} m_\mu m_f \sqrt{\lambda_\mu \lambda_f}$	–
Z^0	$\frac{1}{16} \left({g_V^\mu}^2 + {g_A^\mu}^2\right) \left({g_V^f}^2 + {g_A^f}^2\right) \left[\frac{s}{4} - \left(m_\mu^2 + m_f^2\right) + \frac{4}{s} m_\mu^2 m_f^2\right]$	$\frac{1}{8s} g_V^\mu g_A^\mu g_V^f g_A^f \sqrt{\lambda_\mu \lambda_f}$	$\frac{1}{16} \left({g_V^\mu}^2 + {g_A^\mu}^2\right) \left({g_V^f}^2 + {g_A^f}^2\right) \cdot \left[\frac{s}{4} + \left(m_\mu^2 + m_f^2\right)\right]$ $-\frac{1}{8} \left[m_\mu^2 {g_A^\mu}^2 \left({g_V^f}^2 + {g_A^f}^2\right) + m_\mu^2 {g_A^f}^2 \left({g_V^\mu}^2 + {g_A^\mu}^2\right)\right]$ $+\frac{1}{4s} m_\mu^2 m_f^2 \left(2 {g_A^\mu}^2 {g_A^f}^2 - {g_V^\mu}^2 {g_A^f}^2 - {g_A^\mu}^2 {g_V^f}^2\right)$
$Z^0 G^0$	–	–	$-\frac{1}{2} {g_A^\mu}^2 {g_A^f}^2 m_\mu m_f$
$Z^0 H$	–	$\frac{1}{8s^2} g_V^\mu g_V^f m_\mu m_f \sqrt{\lambda_\mu \lambda_f}$	–
G^0	–	–	$\frac{s}{4} {g_A^\mu}^2 {g_A^f}^2$
$G^0 H$	–	–	–
H	–	–	$\frac{1}{16} \left[\frac{s}{4} - \left(m_\mu^2 + m_f^2\right) + \frac{4}{s} m_\mu^2 m_f^2\right]$

Table 2.1: Coefficients in the differential cross section (2.86) predicted by the Standard Model

2.3.4 Total Cross Section

The total cross section is derived from the integration of the differential cross section over the whole phase space, this means by integrating over all directions:

$$\sigma = \int_0^{2\pi} \int_0^{\pi} \frac{d\sigma}{d\Omega} \sin\theta \, d\theta \, d\phi \, . \tag{2.97}$$

2.4 Higgs Boson Effects in $t\bar{t}$-Production

Since the coupling of a Higgs boson to a fermion is proportional to the fermion mass, the process

$$\mu^+\mu^- \longrightarrow t\bar{t}. \tag{2.98}$$

promises the largest sensitivity to the Higgs boson.

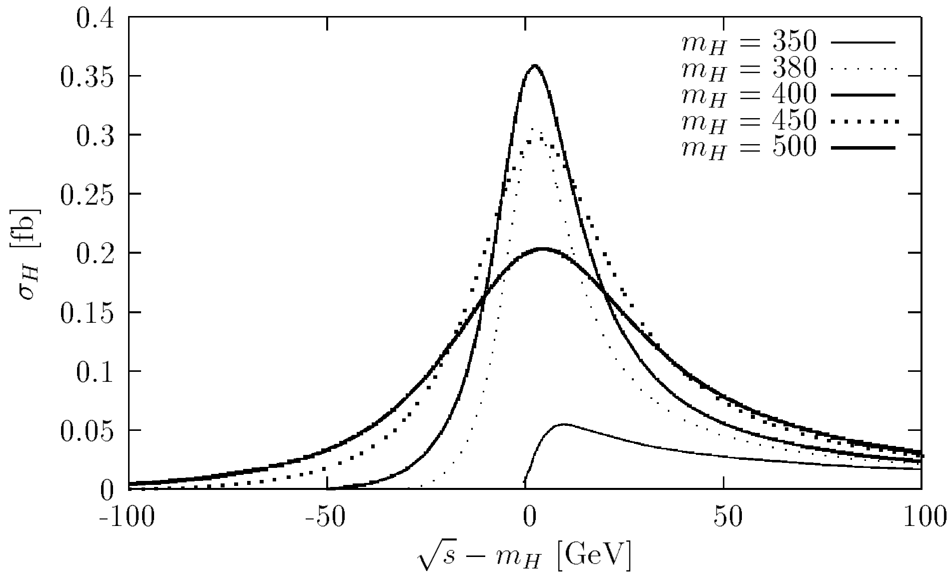

Figure 2.12: The Higgs resonance cross section σ_H for different Higgs boson masses m_H

In Fig. 2.12 the contribution of the Higgs boson resonance cross section σ_H to the total cross section is plotted for different Higgs boson masses m_H at an energy range around the Higgs resonance. The remaining part of the total cross section, that will be named background $\sigma_{\text{back}} = \sigma_{\text{tot}} - \sigma_H$, is presented in Fig. 2.13. The contributions to the differential cross section (2.86) from interferences of the Higgs boson with γ and Z^0 vanish in σ_{back}

upon integration over $\cos\theta$. A comparison of Fig. 2.12 and Fig. 2.13 reveals that in general the Higgs signal is more than three orders of magnitude smaller than the background, and can therefore not be observed (see the next section). The reason for this behaviour is the large mass of the Higgs boson. Since $m_H \geq 2\,m_t$ in order to allow for a resonant s-channel $t\bar{t}$-production, the corresponding large decay width (Fig. 2.5) leads to a decrease of the resonance height.

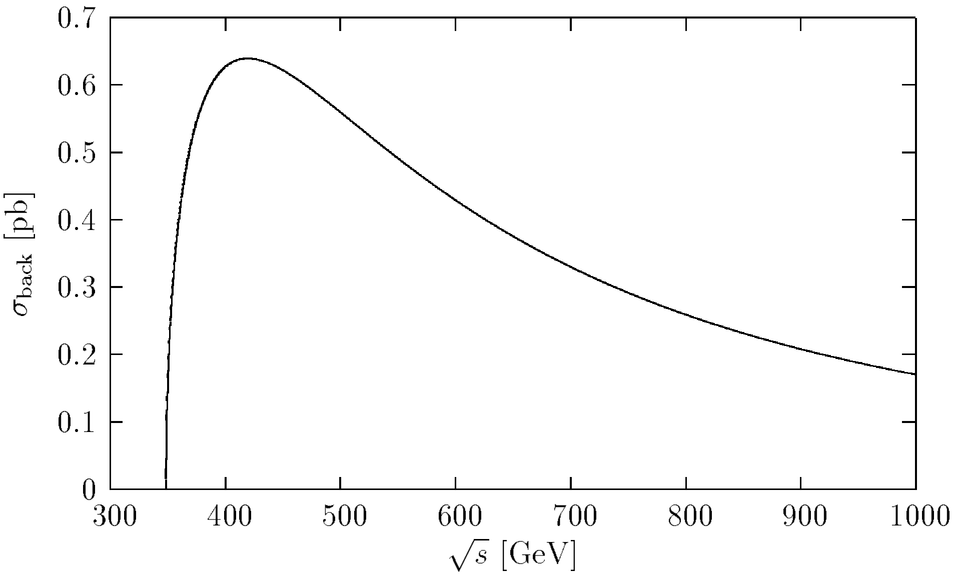

Figure 2.13: The total cross section without the part caused by the Higgs boson ($\sigma_{\rm back}$)

Finally the asymmetry of the resonances in Fig. 2.12 will be discussed. It has two reasons:

1. the production of top-quarks is impossible for $\sqrt{s} < 2\,m_t$ (threshold effect);
2. σ_H increases from lower to higher center of mass energies $\sqrt{s}$ around the resonances.

The first effect contributes significantly only to the asymmetry of those plots corresponding to small Higgs boson masses ($m_H < 450$ GeV), where the resonances are close to the threshold. Due to the vanishing influence of the threshold effect, the energy dependence of σ_H becomes gradually important for large Higgs boson masses.

2.5 Higgs Boson Effects in $b\bar{b}$-Production

Lighter Higgs bosons with smaller decay widths can be produced resonantly in the $b\bar{b}$-channel:

$$\mu^+\mu^- \longrightarrow b\bar{b}\ . \tag{2.99}$$

This case will be studied below. As will be seen, the chances for observing the Higgs boson are much better than in top-quark production.

2.5.1 Total Cross Section

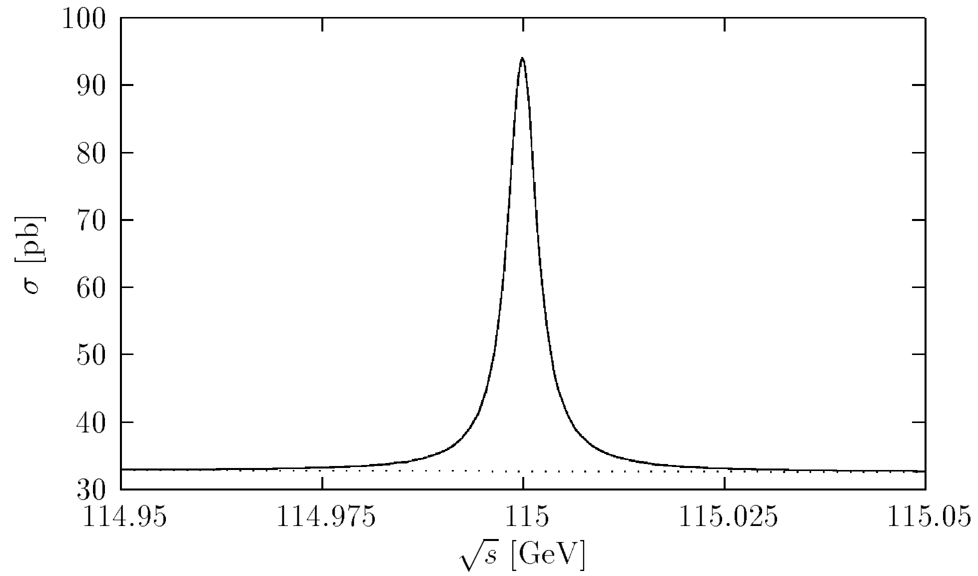

Figure 2.14: Total cross section for $\mu^+\mu^- \longrightarrow b\bar{b}$ in the presence of a Higgs boson with $m_H = 115$ GeV and $\Gamma_H = 4.5$ MeV. The dotted curve indicates the background cross section σ_{back} defined in section 2.4.

In Fig. 2.14 a Higgs boson mass of 115 GeV is assumed. In the framework of the Standard Model this mass is about the lightest one allowed by the measurements at LEP2 [16, 17, 18, 22]. The resonance cross section due to the Higgs boson exchange reaches a value of $\sigma_H \approx 60$ pb at $\sqrt{s} = m_H$, while the continuum cross section is $\sigma_{\text{back}} \approx 30$ pb resulting from the background. The width of the resonance is 4.5 MeV.

If the decay channel into W-bosons is open, a significant increase of the decay width (Fig. 2.5) at the cost of the peak cross section occurs. As an example, a Higgs boson with a mass of 165 GeV is assumed. Its decay width is 240 MeV. In this case as shown in Fig. 2.15 the Higgs resonance cross section amounts

$$\begin{aligned}\sigma_H\,(165\text{ GeV}) &= \sigma_{\text{tot}}\,(165\text{ GeV}) - \sigma_{\text{back}}\,(165\text{ GeV}) \\ &= 5.524\text{ pb} - 5.504\text{ pb} \\ &= 0.020\text{ pb}\end{aligned} \tag{2.100}$$

or about half a percent of the total cross section:

$$\frac{\sigma_H}{\sigma_{\text{tot}}} \approx 0.4\%\ . \tag{2.101}$$

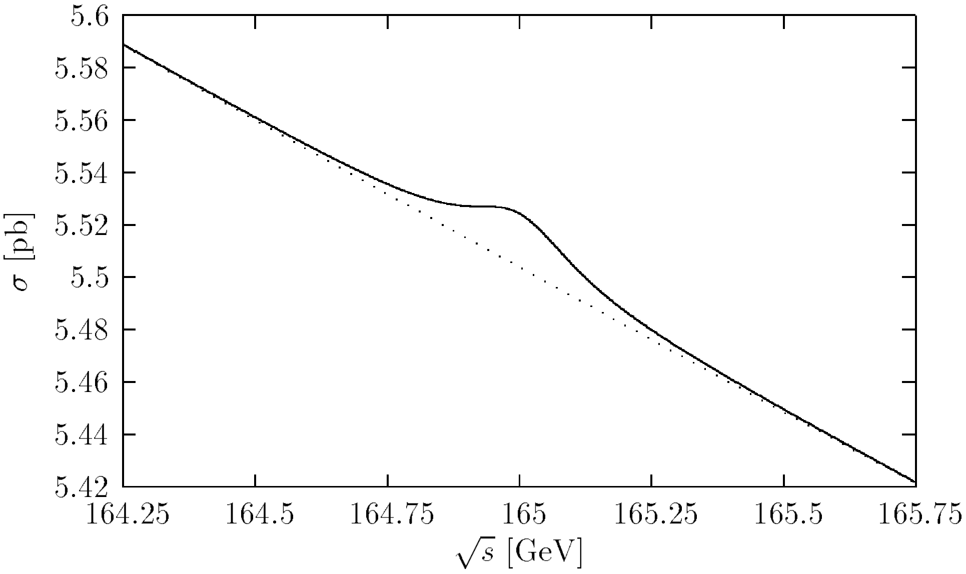

Figure 2.15: Same as Fig. 2.14 for a Higgs boson with $m_H = 165$ GeV and $\Gamma_H = 240$ MeV

If one assumes an optimistic integrated luminosity $L = 20\,(\text{fb})^{-1}$ [27], this leads to a background contribution of

$$N_{\text{back}} = L\,\sigma_{\text{back}} \approx 10^5\text{ events.} \tag{2.102}$$

On the supposition that these events are normally distributed, the 1-σ-error is

$$\sqrt{N_{\text{back}}} \approx 300\text{ events} \tag{2.103}$$

corresponding to an uncertainty of

$$\frac{1}{\sqrt{N_{\mathrm{back}}}} \approx 0.3\% \; . \tag{2.104}$$

Therefore a detection of the Higgs boson signal will be difficult.

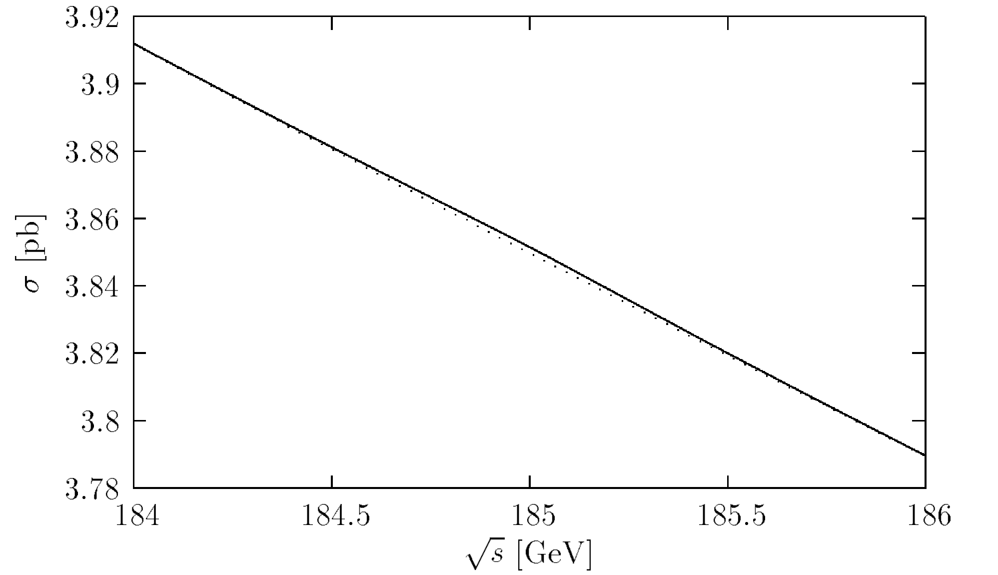

Figure 2.16: Same as Fig. 2.14 for a Higgs boson with $m_H = 185$ GeV and $\Gamma_H = 820$ MeV

The situation becomes even more difficult when the Higgs boson mass reaches the region where the additional decay into Z^0 bosons is possible. This is illustrated in Fig. 2.16 for a Higgs boson mass of 185 GeV and a decay width of 820 MeV. In this case the peak cross section of the signal falls to

$$\begin{aligned} \sigma_H\,(185\text{ GeV}) &= \sigma_{\mathrm{tot}}\,(185\text{ GeV}) - \sigma_{\mathrm{back}}\,(185\text{ GeV}) \\ &= 3.852\text{ pb} - 3.850\text{ pb} \\ &= 0.002\text{ pb} \end{aligned} \tag{2.105}$$

and the resonance disappears in the continuum.

This clearly demonstrates that the Higgs search in the $b\bar{b}$-channel is most promising for 115 GeV $\lesssim m_H < 2\,m_W$ [36].

2.5.2 Angular Distribution

To show the angular distribution the resonance peak shown in Fig. 2.14 is discussed. All other scenarios with larger Higgs masses will show the same behaviour, but the differential cross section of the Higgs exchange is less apparent.

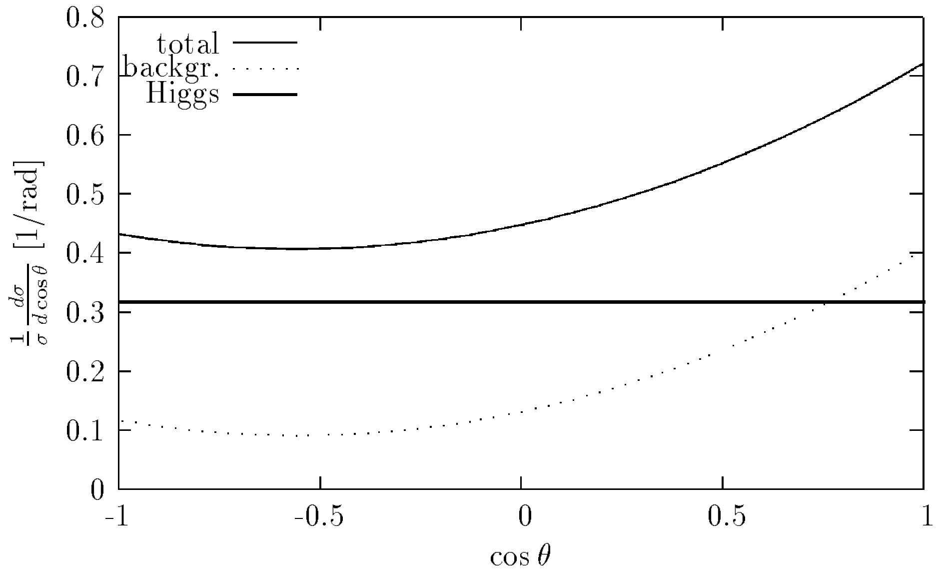

Figure 2.17: Angular distribution at $\sqrt{s} = 115$ GeV due to Higgs exchange (solid), continuum (dotted) and total (thin).

The Higgs interferences give negligible contributions, that are six orders of magnitude smaller than those plotted in Fig. 2.17. Therefore, since the differential cross section of the Higgs boson exchange is independent of the scattering angle θ, the variation with θ results practically solely from the background processes.

2.5.3 Forward-Backward-Asymmetry

In Fig. 2.18 the forward-backward-asymmetry

$$A_{fb} = \frac{\sigma(\cos\theta > 0) - \sigma(\cos\theta < 0)}{\sigma(\cos\theta > 0) + \sigma(\cos\theta < 0)} \tag{2.106}$$

of the scenario for $m_H = 115$ GeV with respect to the center-of-mass energy is investigated. The Higgs resonance leads to a significant decrease of the asymmetry, because of the isotropic Higgs cross section. Hence, the forward-backward-asymmetry is a very useful tool in the search for the missing Higgs boson.

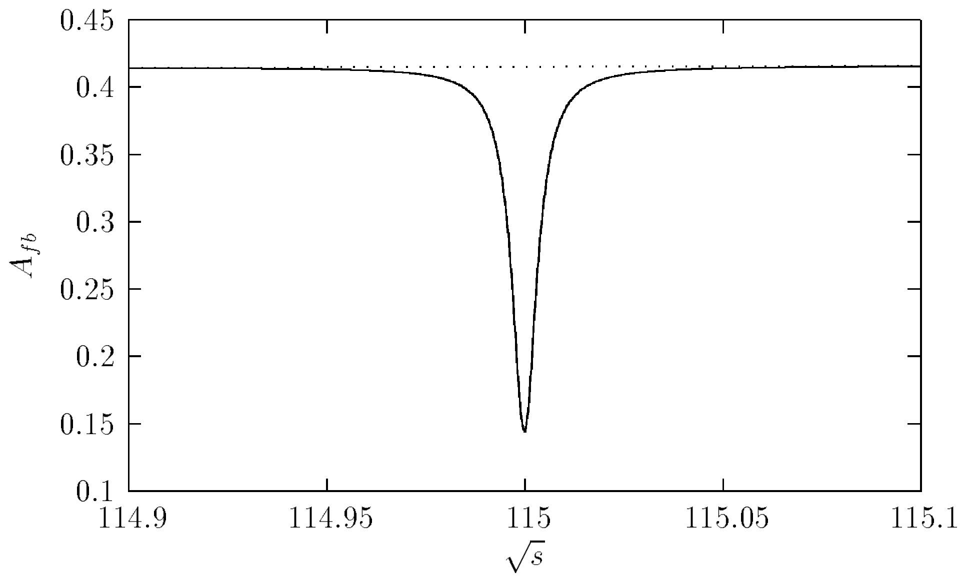

Figure 2.18: The forward-backward-asymmetry of the process $\mu^+\mu^- \longrightarrow b\bar{b}$ in the presence of a Higgs boson at $m_H = 115$ GeV. The continuum is indicated by the dotted line.

2.6 Influence of the Energy Resolution of the Collider

The extremely narrow decay width for a Higgs boson with $m_H < 2\,m_W$ requires a very high energy resolution. An e^+e^--collider will have an energy resolution $R \sim 0.1\%$ [37], whereas with a $\mu^+\mu^-$-collider $R = 0.01\%$ [31] can be realized.

The energy resolution is an alternative description to the root mean square spread in center-of-mass energy $\sigma_{\sqrt{s}}$. These two parameters are related through [29]:

$$\sigma_{\sqrt{s}} = (7 \text{ MeV}) \left(\frac{R}{0.01\%}\right) \left(\frac{\sqrt{\tilde{s}}}{100 \text{ GeV}}\right). \tag{2.107}$$

The estimation of the energy resolution of future colliders given above together with equation (2.107) leads to $\sigma_{\sqrt{s}} = 80$ MeV for an e^+e^--collider and

$\sigma_{\sqrt{s}} = 8$ MeV for a $\mu^+\mu^-$-collider $\left(\sqrt{\tilde{s}} = m_H = 115 \text{ GeV}\right)$.

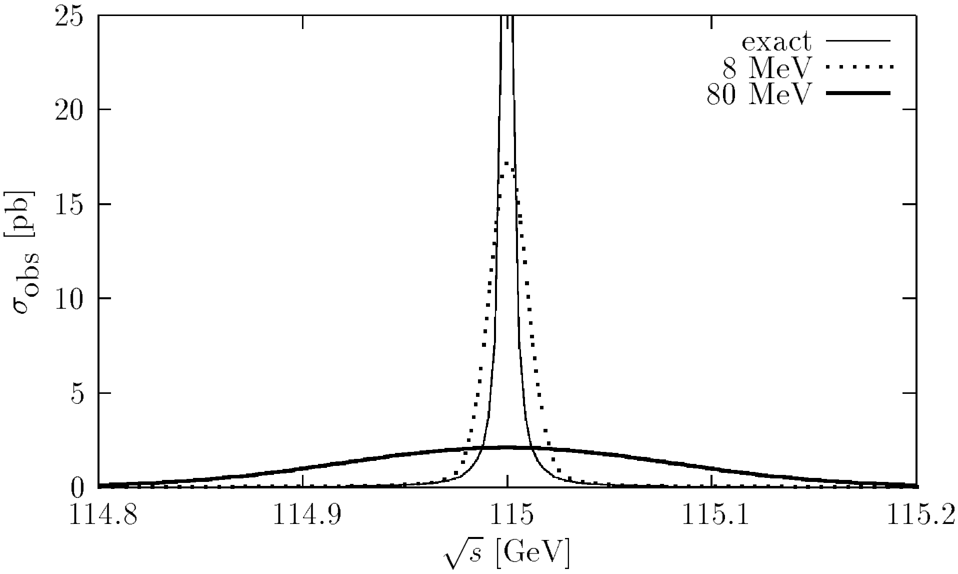

Figure 2.19: The Higgs resonance vs. $\sqrt{s}$ for different $\sigma_{\sqrt{s}}$

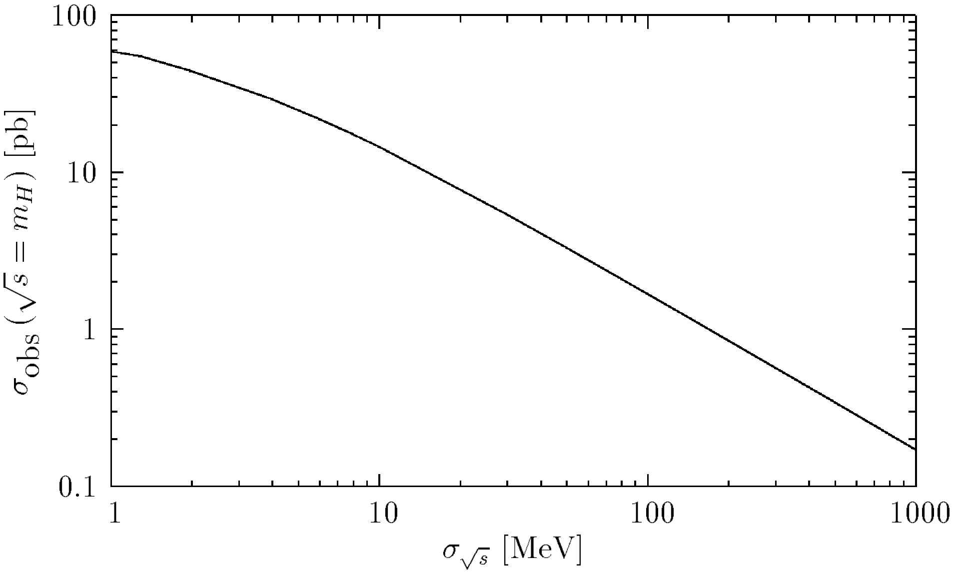

Figure 2.20: Cross section peak vs. $\sigma_{\sqrt{s}}$ at $\sqrt{s} = 115$ GeV

To get the observable resonance cross section σ_{obs} is is necessary to convolute the theoretical cross section σ_H with a normalized Gaussian distribution in $\sqrt{\hat{s}}$ centered at $\sqrt{\hat{s}} = \sqrt{s}$ and of the width $\sigma_{\sqrt{s}}$:

$$\sigma_{\mathrm{obs}}\left(\sqrt{s}\right) = \frac{1}{\sqrt{s\pi}\sigma_{\sqrt{s}}} \int \sigma_H\left(\sqrt{\hat{s}}\right) \exp\left[-\frac{\left(\sqrt{\hat{s}}-\sqrt{s}\right)^2}{2\sigma^2_{\sqrt{s}}}\right] d\sqrt{\hat{s}}. \qquad (2.108)$$

In Fig. 2.19 the resonance cross section for $m_H = 115$ GeV is plotted for different $\sigma_{\sqrt{s}}$. With the resolution of an e^+e^--collider the resonance is reduced significantly. In Fig. 2.20 the decreasing peak heigt σ_{obs} is illustrated.

The insufficient energy resolution of an e^+e^--collider compared to a $\mu^+\mu^-$-collider is a result of beamstrahlung, which is absent in muon-colliders due to the higher mass of the muons. This phenomenon induces not only a loss of energy resolution, but is difficult to monitor precisely [36].

The search for the Standard Model Higgs boson is one of the most important goals of a muon-collider. For Higgs bosons below the WW threshold then it cannot be directly measured anywhere else, but the fine energy spread and large s-channel Higgs coupling to the muon allow this unique possibility [38].

Chapter 3

The MSSM with Additional CP Violation

An attractive way to extend the Higgs sector of the Standard Model is to introduce a so-called Two Higgs Doublet Model (2HDM) [39]:

- it satisfies the relation $\frac{m_W^2}{m_Z^2 \cos^2 \theta_W} = 1$ at tree-level;
- it avoids tree-level Flavour Changing Neutral Currents (FCNCs) if the Higgs fermion couplings are appropriately chosen;
- such a Higgs sector is required in the Minimal Supersymmetric Standard Model (MSSM).

After a brief motivation of supersymmetry and an introduction of supersymmetry transformations the Higgs sector of the MSSM and the influence of additional CP violation will be discussed in more detail.

3.1 Motivation

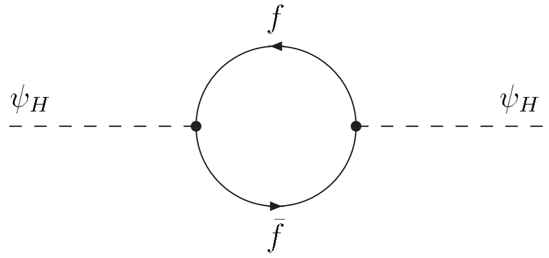

Figure 3.1: Fermion loop correction to the Higgs field

If the Higgs field ψ_H couples to the fermions f with a term in the lagrangian

$$-\lambda_f \psi_H f \bar{f}, \tag{3.1}$$

then the Feynman diagram in Fig. 3.1 yields a correction to the squared Higgs boson mass. A calculation of the radiative corrections results in [23]

$$\Delta m_H^2 = \frac{|\lambda_f|^2}{16\pi^2} \cdot \left[-2\Lambda_{\mathrm{UV}}^2 + 6m_f^2 \ln\left(\frac{\Lambda_{\mathrm{UV}}}{m_f}\right) + \ldots \right], \tag{3.2}$$

where Λ_{UV} is the so-called cut-off parameter. Such a cut-off parameter is needed to regularize the loop-diagrams. From a more physical point of view Λ_{UV} is the energy that marks the boundary to new physics at larger energies.

In the case that there is no new physics up to the Planck scale, the cut-off parameter is of order

$$M_{Planck} = \frac{1}{\sqrt{8\pi G_{Newton}}} = 2.4 \cdot 10^{18} \text{ GeV} . \tag{3.3}$$

This implies that the correction Δm_H^2 is 32 orders larger than the parameter m_H^2 to be corrected. This paradox is called the "hierarchy problem".

Now consider there are scalar particles that are too heavy to have been detected and couple to the Higgs field through the lagrangian term

$$-\lambda_S |\psi_H|^2 |S|^2 . \tag{3.4}$$

They contribute to Δm_H^2 by the Feynman graph shown in Fig. 3.2.

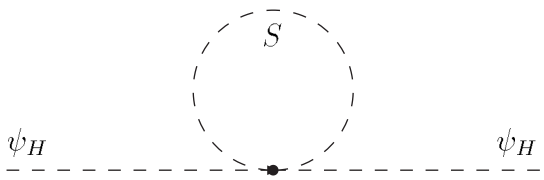

Figure 3.2: Scalar particle loop correction to the Higgs field

This yields

$$\Delta m_H^2 = \frac{\lambda_S}{16\pi^2} \cdot \left[\Lambda_{\mathrm{UV}}^2 - 2m_S^2 \ln\left(\frac{\Lambda_{\mathrm{UV}}}{m_S}\right) + \ldots \right] . \tag{3.5}$$

Comparing (3.2) with (3.5) reveals that the terms proportional to Λ_{UV} have a relative minus sign. So if there are two heavy scalar particles for every fermion that fulfill the relation

$$\lambda_S = |\lambda_f|^2 \tag{3.6}$$

there seems to be a good chance of cancelling the fermionic and the bosonic corrections to Δm_H^2. Such a cancellation is guaranteed if there is a symmetry relating fermions and bosons, called *supersymmetry* [23].

3.2 Supersymmetry Transformations

A supersymmetry transformation turns a bosonic state into a fermionic state, and vice versa. Therefore a fermionic operator Q, that carries spin angular momentum $\frac{1}{2}$, is needed:

$$Q\ |\text{Boson}\rangle = |\text{Fermion}\rangle\ , \tag{3.7}$$
$$Q\ |\text{Fermion}\rangle = |\text{Boson}\rangle\ . \tag{3.8}$$

Because spinors are intrinsically complex objects, the hermitian conjugate of Q is also a symmetry generator:

$$Q^\dagger\ |\text{Boson}\rangle = |\text{Fermion}\rangle\ , \tag{3.9}$$
$$Q^\dagger\ |\text{Fermion}\rangle = |\text{Boson}\rangle\ . \tag{3.10}$$

The fermionic nature of the symmetry generators implies that supersymmetry is a spacetime symmetry [23]. The realization of such symmetries in an interacting quantum field theory is highly restricted. For realistic theories, like the Standard Model, that have chiral fermions and thus the possibility of parity-violating interactions, the *Coleman-Mandula* theorem implies that the generators Q and $Q^\dagger$ must satisfy an algebra with the schematic form

$$\{Q, Q^\dagger\} = P^\mu, \tag{3.11}$$
$$\{Q, Q\} = \{Q^\dagger, Q^\dagger\} = 0\ , \tag{3.12}$$
$$[P^\mu, Q] = [P^\mu, Q^\dagger] = 0\ , \tag{3.13}$$

where P^μ is the momentum generator of spacetime translations.

3.3 Supermultiplets

The single-particle states of a supersymmetric theory fall naturally into irreducible representations of the supersymmetry algebra that are called *supermultiplets*. Each supermultiplet contains both fermion and boson states that are commonly known as *superpartners* of each other [23]:

- each supermultiplet contains the same number of bosonic and fermionic degrees of freedom $n_B = n_F$;
- each particle and its superpartner must have equal masses.

3.3.1 Matter Supermultiplets of the MSSM

The most obviously way of creating a supermultiplet is to combine a single Weyl fermion ($n_F = 2$) with two scalar bosons ($n_B = 2$), or alternatively with a complex scalar boson. This combination is called *chiral* or *matter* supermultiplet. The matter supermultiplets of the MSSM are listed in Tab. 3.1, classified according to their transformation properties under the Standard Model gauge group $SU(3)_C \times SU(2)_L \times U(1)_Y$ [23].

Names		spin 0	spin 1/2	$SU(3)_C$,$SU(2)_L$, $U(1)_Y$
squarks, quarks (×3 families)	Q	$\left(\tilde{u}_L\ \tilde{d}_L\right)$	$(u_L d_L)$	$(\mathbf{3}, \mathbf{2}, +\frac{1}{6})$
	$\bar{u}$	$\tilde{u}^*_R$	$u^\dagger_R$	$(\bar{\mathbf{3}}, \mathbf{1}, -\frac{2}{3})$
	$\bar{d}$	$\tilde{d}^*_R$	$d^\dagger_R$	$(\bar{\mathbf{3}}, \mathbf{1}, \frac{1}{3})$
sleptons, leptons (×3 families)	L	$(\tilde{\nu}_L\ \tilde{e}_L)$	(ν_L, e_L)	$(\mathbf{1}, \mathbf{2}, -\frac{1}{2})$
	$\bar{e}$	$\tilde{e}^*_R$	$e^\dagger_R$	$(\mathbf{1}, \mathbf{1}, +1)$
Higgs bosons, higgsinos	$\widehat{H}_u$	$(H^+_u\ H^0_u)$	$\left(\tilde{H}^+_u\ \tilde{H}^0_u\right)$	$(\mathbf{1}, \mathbf{2}, +\frac{1}{2})$
	$\widehat{H}_d$	$(H^0_d\ H^-_d)$	$\left(\tilde{H}^0_d\ \tilde{H}^-_d\right)$	$(\mathbf{1}, \mathbf{2}, -\frac{1}{2})$

Table 3.1: Matter supermultiplets of the MSSM

The electric charge Q of the particles is computed with

$$Q = T_Z + Y \ , \tag{3.14}$$

where $T_Z = \pm\frac{1}{2}$ is the *third component of the weak isospin* and Y is the *hypercharge*.

3.3.2 Gauge Supermultiplets of the MSSM

A *vector* or a *gauge* supermultiplet consists of a massless spin-1 vector boson ($n_B = 2$) and a massless spin-$\frac{1}{2}$ Weyl fermion ($n_F = 2$). The gauge supermultiplets of the MSSM are presented in Tab. 3.2 [23].

Names	spin 1/2	spin 1	$SU(3)_C$,$SU(2)_L$, $U(1)_Y$
gluino, gluon	$\tilde{g}$	g	$(\mathbf{8},\mathbf{1},0)$
winos, W bosons	$\tilde{W}^{\pm}$ $\tilde{W}^{0}$	$W^{\pm}$ W^{0}	$(\mathbf{1},\mathbf{3},0)$
bino, B boson	$\tilde{B}^{0}$	B^{0}	$(\mathbf{1},\mathbf{1},0)$

Table 3.2: Gauge supermultiplets of the MSSM

3.3.3 Remarks and Nomenclature

In theories with one pair of symmetry generators like the MSSM each supermultiplet can be reduced to a combination of the supermultiplets described above.

The two Higgs supermultiplets have opposite hypercharges $\left(Y = \pm\frac{1}{2}\right)$ to avoid triangle gauge anomalies and for another completely different reason: because of the structure of supersymmetric theories, only a $Y = +\frac{1}{2}$ Higgs chiral supermultiplet can have the Yukawa couplings necessary to give masses to up-type-quarks with a charge of $Q = \frac{2}{3}$, and only a $Y = -\frac{1}{2}$ Higgs field can have the Yukawa couplings necessary to give masses to down-type quarks with $Q = -\frac{1}{3}$ and to charged leptons [23]. This is indicated by the indices u and d in Tab 3.1. The upper indices are the electric charges of the Higgs supermultiplets.

The neutral Higgs boson of the Standard Model is a linear combination of H_u^0 and H_d^0. In a similar way the W^0 and B^0 gauge eigenstates mix to give the Standard Model mass eigenstates Z^0 and γ (Photon). Their supersymmetric partners are called $\tilde{Z}^0$ (Zino) and $\tilde{\gamma}$ (Photino) which are a mixture of $\tilde{W}^0$ and $\tilde{B}^0$.

The superpartners of the quarks and leptons with spin 0 are named by prepending a "s-" to the Standard Model name, which stands for "scalar". The nomenclature for a spin 1/2 superpartner is to append a "-ino". The symbols of the superpartners are the normal symbols used for the Standard Model particles, but with a tilde on it. The indices L and R of the squarks and sleptons denote the helicity of the superpartners.

3.4 The Superpotential

The Higgs potential of the Minimal Supersymmetric Standard Model is fixed by a superpotential of the form [23]

$$W = \bar{u}\mathbf{y_u}Q\widehat{H}_u - \bar{d}\mathbf{y_d}Q\widehat{H}_d - \bar{e}\mathbf{y_e}L\widehat{H}_d + \mu\widehat{H}_u\widehat{H}_d \ , \tag{3.15}$$

where all of the gauge and family indices are suppressed and the chiral supermultiplets given in Tab. 3.1 have been used. The dimensionless Yukawa coupling parameters $\mathbf{y_u}$, $\mathbf{y_d}$ and $\mathbf{y_e}$ are 3×3-matrices in family space.

The term proportional to μ is unique, because terms like $\widehat{H}_u^*\widehat{H}_u$ or $\widehat{H}_d^*\widehat{H}_d$ are not allowed, since the superpotential has to be analytic in the chiral superfields.

As mentioned above the two Higgs supermultiplets $\widehat{H}_u$ and $\widehat{H}_d$ are necessary to give mass to the up-type quarks, the down-type quarks and the leptons. A substitution like $\bar{u}\mathbf{y_u}Q\widehat{H}_d^*$ for the first term or $-\bar{d}\mathbf{y_d}Q\widehat{H}_u^*$ and $-\bar{e}\mathbf{y_e}L\widehat{H}_u^*$ for the others is not possible, due to the just noted fact, that the superpotential (3.15) must be analytic.

3.5 Supersymmetry Breaking

The fact that superpartners are not yet discovered implies that supersymmetry is broken. Otherwise the equality between the mass of the Standard model particles and the mass of their counterparts would have lead to a detection of the supersymmetric particles. The “hierarchy problem” gives hints what type of symmetry breaking is realized in nature. If broken supersymmetry is still to provide a solution to this paradox the relationship (3.6) must be satisfied. Otherwise a correction to the squared Higgs boson mass of the structure

$$\Delta m_H^2 = \frac{1}{8\pi^2}\left(\lambda_S - |\lambda_f|^2\right)\Lambda_{\mathrm{UV}} + \cdots \tag{3.16}$$

could not be avoided. Therefore only soft symmetry breaking is acceptable:

$$\mathcal{L} = \mathcal{L}_{\mathrm{SUSY}} + \mathcal{L}_{\mathrm{soft}} \ , \tag{3.17}$$

where $\mathcal{L}_{\mathrm{SUSY}}$ preserves supersymmetry invariance and $\mathcal{L}_{\mathrm{soft}}$ violates it, but contains only mass terms and couplings with positive mass dimension [23]. The largest mass term shall be denoted m_{soft}. The remaining correction to m_H^2 is then given by

$$\Delta m_H^2 = m_{\mathrm{soft}}^2\left[\frac{\lambda}{16\pi^2}\ln\left(\frac{\Lambda_{\mathrm{UV}}}{m_{\mathrm{soft}}}\right) + \cdots\right], \tag{3.18}$$

which vanishes for $m_{\rm soft} \to 0$. The parameter λ stands for various dimensionless couplings. To solve the "hierarchy problem", $m_{\rm soft}$ must not be too large. Since it is responsible for the mass splittings between the known particles and their superpartners, the masses of the supersymmetric particles are not too heavy. Assuming in (3.18)

$$\Lambda_{\rm UV} \sim M_{\rm Planck} , \tag{3.19}$$
$$\lambda \sim 1 \tag{3.20}$$

the masses of the lightest superpartners should be of order 1 TeV, giving experimentalists a good chance to find them at the next generation colliders.

The most general term that can be added to the lagrangian to break supersymmetry softly is given by [23]

$$\begin{aligned} \mathcal{L}_{\rm soft} = & -\frac{1}{2}\left(M_{\tilde g}\tilde g\tilde g + M_{\tilde W}\tilde W\tilde W + M_{\tilde B}\tilde B\tilde B\right) + \text{c.c.} \\ & -\left(\tilde{\bar u}\mathbf{a_u}\tilde Q H_u - \tilde{\bar d}\mathbf{a_d}\tilde Q H_d - \tilde{\bar e}\mathbf{a_e}\tilde Q H_d\right) + \text{c.c.} \\ & -\tilde Q^\dagger \mathbf{m^2_Q}\tilde Q - \tilde L^\dagger \mathbf{m^2_L}\tilde L - \tilde{\bar u}^\dagger \mathbf{m^2_{\bar u}}\tilde{\bar u} - \tilde{\bar d}^\dagger \mathbf{m^2_{\bar d}}\tilde{\bar d} - \tilde{\bar e}^\dagger \mathbf{m^2_{\bar e}}\tilde{\bar e} \\ & -m^2_{H_u}H_u^* H_u - m^2_{H_d}H_d^* H_d - (bH_u H_d + \text{c.c.}) \end{aligned} \tag{3.21}$$

where $M_{\tilde g}$, $M_{\tilde W}$ and $M_{\tilde B}$ are the gluino, wino and bino mass terms. The 3×3-matrices $\mathbf{a_u}$, $\mathbf{a_d}$ and $\mathbf{a_e}$ correspond to the Yukawa couplings in the superpotential (3.15) and are of the dimension (mass), while the 3×3-matrices $\mathbf{m^2_Q}$, $\mathbf{m^2_{\bar u}}$, $\mathbf{m^2_{\bar d}}$, $\mathbf{m^2_L}$ and $\mathbf{m^2_{\bar e}}$ are of the dimension (mass)^2 and can have complex entries as long as the lagrangian is hermitian. The last line in (3.21) represents the supersymmetry breaking contributions to the Higgs potential.

The soft supersymmetry breaking lagrangian (3.21) introduces many new parameters in the MSSM lagrangian. There are more than 100 masses, phases and mixing angles, which cannot be rotated away by redefining the phases and flavor basis for the quark and lepton supermultiplets, and that have no counterpart in the ordinary Standard Model [23].

3.6 CP Violation

In this section the more detailed discussion in [40, 41] is outlined.

While in the Standard Model CP violation occurs only explicitly by complex Yukawa couplings of the Higgs boson to the quarks, CP-symmetry may be additionally broken spontaneously by the ground state of the Higgs potential in theories with an extended Higgs sector. However, in the MSSM the Higgs potential is invariant under CP at tree-level. Hence, any explicit or spontaneous breakdown of CP symmetry can arise only via radiative corrections [40]. For example, loop-effects may violate the MSSM Higgs potential and cause important phenomenological consequences [42].

3.6.1 Complex Parameters

The MSSM includes many possible CP-odd phases that are absent in the Standard Model. In (3.15) and (3.21) the following parameters may be complex:

- the mass parameter μ of the two Higgs chiral superfields in the superpotential;
- the soft supersymmetry-breaking gaugino masses $M_{\tilde{g}}$, $M_{\tilde{W}}$ and $M_{\tilde{B}}$ of the gauge groups $SU(3)_C$, $SU(2)_L$ and $U(1)_Y$;
- the soft bilinear Higgs-mixing parameter $b \equiv B\mu$;
- the soft supersymmetry-breaking trilinear couplings $\mathbf{a_u}$, $\mathbf{a_d}$ and $\mathbf{a_e}$ of the Higgs bosons to the sfermions;
- flavor off-diagonal soft supersymmetry-breaking masses of squarks and sleptons: $\mathbf{m^2_Q}$, $\mathbf{m^2_{\bar{u}}}$, $\mathbf{m^2_{\bar{d}}}$, $\mathbf{m^2_L}$ and $\mathbf{m^2_{\bar{e}}}$.

Large CP-odd phases in the squark and slepton mass matrices can be avoided by assuming that the off-diagonal masses are small, or more concretely that the matrices are nearly flavor-blind:

$$\begin{array}{c} \mathbf{m^2_Q} = m^2_Q \mathbf{1} \ , \ \ \mathbf{m^2_{\bar{u}}} = m^2_{\bar{u}} \mathbf{1} \ , \ \ \mathbf{m^2_{\bar{d}}} = m^2_{\bar{d}} \mathbf{1} \ , \\ \mathbf{m^2_L} = m^2_L \mathbf{1} \ , \ \ \mathbf{m^2_{\bar{e}}} = m^2_{\bar{e}} \mathbf{1} \ . \end{array} \tag{3.22}$$

More CP-odd phases can be eliminated if one postulates that at a unification scale M_X the following simplifications occur:

$$\mathbf{a}\,(M_X) \ \equiv \ \mathbf{a_u} = \mathbf{a_d} = \mathbf{a_e} \ , \tag{3.23}$$

$$M_\lambda\,(M_X) \ \equiv \ M_{\tilde{g}} = M_{\tilde{W}} = M_{\tilde{B}} \ . \tag{3.24}$$

The remaining complex parameters

$$\{\mu, b, M_\lambda, \mathbf{a}\} \tag{3.25}$$

can be further reduced by global symmetries. Following [40] the focus is on the two CP-violating phases

$$\arg\,(\mu) \quad \wedge \quad \arg\,(\mathbf{a_{t,b}}) \ , \tag{3.26}$$

where t and b indicate that the third generation quarks and their supersymmetric partners play the key-role.

3.6.2 One-Loop Effective Potential

The one-loop CP-violating effective potential (Fig. 3.3) is determined by

$$-\mathcal{L}_V = -\mathcal{L}_V^0 + \frac{3}{32\pi^2} \sum_{q=t,b} \left[\tilde{m}_q^4 \left(\ln \frac{\tilde{m}_q^2}{Q^2} - \frac{3}{2} \right) - \bar{m}_q^4 \left(\frac{\ln \bar{m}_q^2}{Q^2} - \frac{3}{2} \right) \right] . \quad (3.27)$$

Herein the squared masses $\bar{m}_q^2$ and $\tilde{m}_q^2$ are the eigenvalues of the quark and squark mass matrices, which depend on the Higgs background fields and among other parameters on (3.26). They are calculated explicitly in [40]. The parameter Q is the scale of the heaviest third generation squark, which is assumed to be higher than the electroweak scale.

The tree-level Higgs potential $\mathcal{L}_V^0$ in the MSSM is given by

$$\begin{aligned} \mathcal{L}_V^0 \;=\; & -\left(m_{H_d}^2 + |\mu|^2\right)\left(H_d^* H_d\right) - \left(m_{H_u}^2 + |\mu|^2\right)\left(H_u^* H_u\right) \\ & + b\left(H_d^* H_u\right) + b^*\left(H_u^* H_d\right) \\ & + \lambda_1 \left(H_d^* H_d\right)^2 + \lambda_2 \left(H_u^* H_u\right)^2 + \lambda_3 \left(H_d^* H_d\right)\left(H_u^* H_u\right) \\ & + \lambda_4 \left(H_d^* H_u\right)\left(H_u^* H_d\right) \end{aligned} \quad (3.28)$$

with the couplings

$$\lambda_1 = \lambda_2 = -\frac{1}{8}\left(g^2 + g'^2\right) , \quad (3.29)$$

$$\lambda_3 = -\frac{1}{4}\left(g^2 - g'^2\right) , \quad (3.30)$$

$$\lambda_4 = \frac{1}{2} g^2 , \quad (3.31)$$

where g is the gauge coupling of the $SU(2)_L$ symmetry and g' that of the $U(1)_Y$ symmetry.

In a next step the Higgs doublets will be expanded around their ground states as follows [41]:

$$\widehat{H}_u = \begin{pmatrix} \phi_1^+ \\ \frac{1}{\sqrt{2}}\left(v_1 + \eta_1 + i a_1\right) \end{pmatrix} , \quad (3.32)$$

$$\widehat{H}_d = e^{i\xi} \begin{pmatrix} \phi_2^+ \\ \frac{1}{\sqrt{2}}\left(v_2 + \phi_2 + i a_2\right) \end{pmatrix} . \quad (3.33)$$

Herein v_1 and v_2 are the moduli of the *vacuum expectation values* (VEVs) of the Higgs doublets. Their relative phase ξ can be set zero [40].

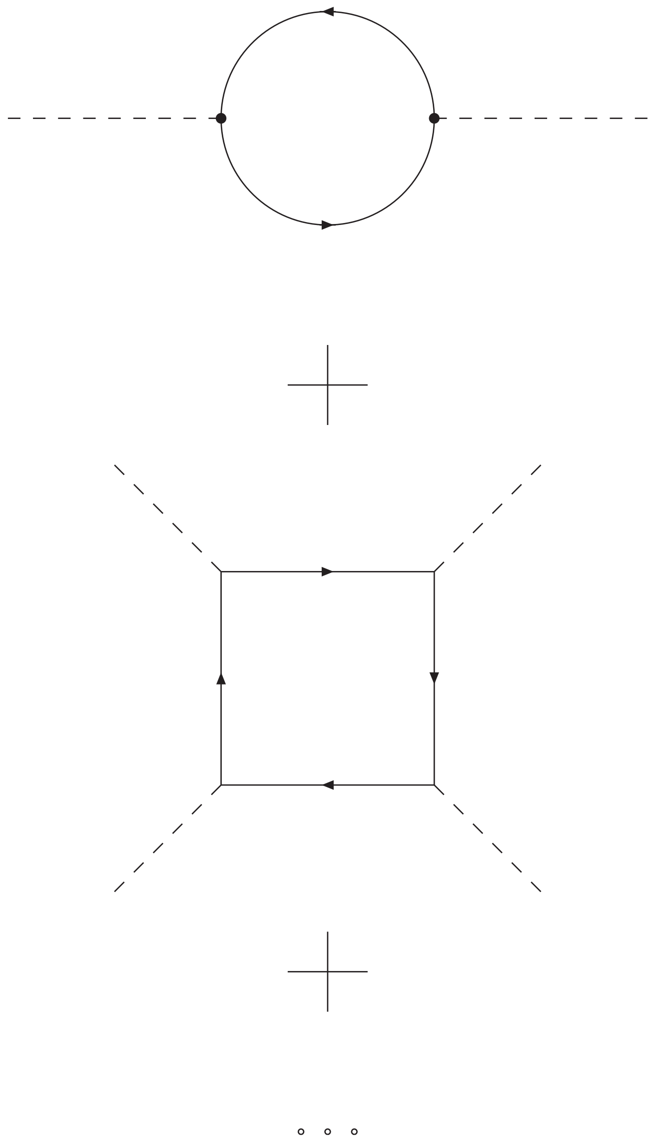

Figure 3.3: The fermion contribution to the effective potential. The directed lines represent fermions. Note that in the fermion sum only graphs with an even number of external lines occur [43].

3.6.3 The Neutral Higgs Boson Mass Matrix

In the basis $\{\phi_1, \phi_2, a_1, a_2\}$ the mass-matrix of the neutral Higgs bosons possesses the following form [40, 41]

$$\mathcal{M}_0^2 = \left(\begin{array}{cc} (\mathcal{M}_S^2)_{ij} & (\mathcal{M}_{SP}^2)_{ij} \\ (\mathcal{M}_{SP}^2)_{ij}^T & (\mathcal{M}_P^2)_{ij} \end{array} \right), \tag{3.34}$$

where the entries are 2×2-matrices. The index S refers to the scalar and P to the pseudoscalar states. The presence of CP-violating self-energy terms leads to mass eigenstates with no well-defined CP quantum numbers [40]. Using

$$\tan\beta = \frac{v_1}{v_2} \tag{3.35}$$

and

$$\left(\begin{array}{c} G^0 \\ a \end{array} \right) = \left(\begin{array}{cc} \cos\beta & -sin\beta \\ \sin\beta & \cos\beta \end{array} \right) \left(\begin{array}{c} a_1 \\ a_2 \end{array} \right) \tag{3.36}$$

the mass-matrix reduces to a 3×3-matrix, since G^0 does not mix with the other neutral fields. The orthogonal rotation (3.36) gives rise to a flat direction of the Higgs potential with respect to the G^0 field, i.e.

$$\left\langle \frac{\partial \mathcal{L}_V}{\partial G^0} \right\rangle = 0\ . \tag{3.37}$$

In the newly defined basis the G^0 field becomes the would-be Goldstone boson, that is absorbed by the longitudinal component of the Z^0 boson [42]. So (3.34) can be rewritten as

$$\mathcal{M}_N^2 = \left(\begin{array}{ccc} (\mathcal{M}_S^2)_{11} & (\mathcal{M}_S^2)_{12} & \frac{1}{\cos\beta}\ (\mathcal{M}_{SP}^2)_{12} \\ (\mathcal{M}_S^2)_{21} & (\mathcal{M}_S^2)_{22} & -\frac{1}{\sin\beta}\ (\mathcal{M}_{SP}^2)_{21} \\ \frac{1}{\cos\beta}\ (\mathcal{M}_{SP}^2)_{12} & -\frac{1}{\sin\beta}\ (\mathcal{M}_{SP}^2)_{21} & -\frac{1}{\sin\beta\cos\beta}\ (\mathcal{M}_P^2)_{12} \end{array} \right) \tag{3.38}$$

In (3.38) the relations

$$\left(\mathcal{M}_{SP}^2\right)_{11} \quad = \quad -\tan\beta \left(\mathcal{M}_{SP}^2\right)_{12}, \tag{3.39}$$

$$\left(\mathcal{M}_{SP}^2\right)_{22} = -\cot\beta\left(\mathcal{M}_{SP}^2\right)_{21}, \tag{3.40}$$
$$\left(\mathcal{M}_{P}^2\right)_{12} = \left(\mathcal{M}_{P}^2\right)_{21}, \tag{3.41}$$
$$\left(\mathcal{M}_{P}^2\right)_{11} = -\tan\beta\left(\mathcal{M}_{P}^2\right)_{12}, \tag{3.42}$$
$$\left(\mathcal{M}_{P}^2\right)_{22} = -\cot\beta\left(\mathcal{M}_{P}^2\right)_{21} \tag{3.43}$$

have been taken into account. To get the mass eigenstates of the neutral Higgs bosons the above mass matrix has to be diagonalised by an orthogonal transformation O:

$$O^T M_N^2(m_t)\,O = \mathrm{diag}\left[m_{H_1}^2(m_t), m_{H_2}^2(m_t), m_{H_3}^2(m_t)\right], \tag{3.44}$$

where the definitions m_{H_i} are chosen in such a way that the masses satisfy the relation

$$m_{H_1}^2(m_t) \le m_{H_2}^2(m_t) \le m_{H_3}^2(m_t). \tag{3.45}$$

3.6.4 The Charged Higgs Boson Mass Matrix

Similar to the (3×3)-mass matrix of the neutral Higgs bosons a (2×2)-mass matrix of the charged Higgs bosons exist. The masses of the charged and neutral Higgs bosons are interrelated. If m_A is the mass of the neutral CP-odd Higgs scalar in the CP-conserving case, the following relation can be found [41]:

$$m_A^2 = m_{H^\pm}^2 - \frac{1}{2}\lambda_4\left(v_1^2 + v_2^2\right). \tag{3.46}$$

Herein $m_{H^\pm}$ is the mass of the charged Higgs bosons in the CP-conserving scenario.

3.6.5 Fermion Couplings

The couplings of the neutral Higgs bosons to the down-type (to the leptons respectively) and to the up-type fermions are given by [40]

$$\begin{aligned}\mathcal{L}_{Hff} = -\sum_{i=1}^{3} H_i \Big[& \frac{gm_d}{2m_W}\cdot\bar{d}\left(g_{S_i}^d + ig_{P_i}^d\gamma_5\right)d + \\ & \frac{gm_l}{2m_W}\cdot\bar{l}\left(g_{S_i}^d + ig_{P_i}^d\gamma_5\right)l + \\ & \frac{gm_u}{2m_W}\cdot\bar{u}\left(g_{S_i}^u + ig_{P_i}^u\gamma_5\right)u\Big],\end{aligned} \tag{3.47}$$

where the coupling constants are functions of the elements of the transformation Matrix O defined in (3.44):

$$g^d_{S_i} = O_{1i}\,\frac{1}{\cos\beta}\;, \qquad g^d_{P_i} = -\,O_{3i}\,\tan\beta\;, \tag{3.48}$$

$$g^u_{S_i} = O_{2i}\,\frac{1}{\sin\beta}\;, \qquad g^u_{P_i} = -\,O_{3i}\,\frac{1}{\tan\beta}\;. \tag{3.49}$$

In the decoupling limit of a heavy charged Higgs boson ($m_{H^+} \gg m_Z$) in the MSSM one has [40]

$$O_{31} \longrightarrow 0\;,\;\; O_{11} \longrightarrow \cos\beta\;,\;\; O_{21} \longrightarrow \sin\beta\;. \tag{3.50}$$

In this limit, the scalar components of the H_1dd and H_1uu couplings aquire the known SM form, given by

$$\frac{g\,m_d}{2\,m_W} \quad \wedge \quad \frac{g\,m_u}{2\,m_W}\;. \tag{3.51}$$

3.6.6 Gauge Boson Couplings

To complete the discussion the interaction lagrangian for the coupling of the neutral Higgs bosons to the gauge bosons is presented [40]:

$$\mathcal{L}_{HVV} = g\,m_W \sum_{i=1}^{3} g_{H_iVV}\left(H_i W^+_\mu W^{-,\mu} + \frac{1}{2\cos^2\theta_W} H_i Z_\mu Z^\mu\right) \tag{3.52}$$

with $V = \{W, Z\}$. The coupling constants that appear in (3.52) are given in elements of the transformation matrix O (3.44) as

$$g_{H_iVV} = O_{1i}\,\cos\beta + O_{2i}\,\sin\beta\;. \tag{3.53}$$

This leads to

$$g_{H_1VV} \longrightarrow 1 \tag{3.54}$$

in the decoupling limit (3.50). Further unitary requires

$$\sum_{i=1}^{3} g^2_{H_iVV} = 1. \tag{3.55}$$

Together with the relation

$$g_{H_kVV} = \varepsilon_{ijk}\,g_{H_iH_jZ}, \tag{3.56}$$

where ε_{ijk} is the three-dimensional totally antisymmetric ε-tensor defined in (A.41), all couplings of neutral Higgs bosons to gauge bosons can be calculated if two of these couplings are known.

3.7 Higgs Boson Masses and Couplings

To reveal the effects which are caused by the above described CP-violating scenario it seems to be natural to distinguish between two cases. They are presented in 3.7.1 and 3.7.2 and defined by the value of the charged Higgs boson mass m_{H^+}, that determines mainly the mass of the two heavier neutral Higgs bosons and, with strong restrictions, that of the lightest neutral Higgs particle. Unless otherwise mentioned the following parameters are used:

$$\begin{aligned} M_{SUSY} = |\mathbf{m_Q}| = |\mathbf{m_t}| = |\mathbf{m_b}| = 0.5 \text{ TeV}, \\ |\mathbf{a_t}| = |\mathbf{a_b}| = 1 \text{ TeV}, \quad \mu = 2 \text{ TeV}, \\ |M_{\tilde{B}}| = |M_{\tilde{W}}| = 0.3 \text{ TeV}, \\ |M_{\tilde{g}}| = 1 \text{ TeV}, \quad \arg(M_{\tilde{g}}) = \tfrac{\pi}{2}. \end{aligned} \tag{3.57}$$

The μ parameter shall be real, so that the only CP-violating phase is due to (3.26)

$$\arg(\mathbf{a_t}) = \arg(\mathbf{a_b}). \tag{3.58}$$

The plots in this chapter are made with the help of [44].

3.7.1 Heavy Charged Higgs Scenario

The goal of this scenario is to describe the circumstances that are required to detect one of the neutral Higgs particles in top-quark production at a muon-collider. Therefore it is necessary that one Higgs boson has a mass that is at least two times larger than m_t.

This can only be achieved in the presence of a heavy charged Higgs boson H^+. As shown in Fig. 3.4 the masses of the two heavier Higgs bosons m_{H_2} and m_{H_3} increase nearly linear with the charged Higgs boson mass m_{H^+}. This is a result of the relation given in (3.46). In contrast the mass of the lightest Higgs boson m_{H_1} is practically constant at values above $m_{H^+} = 170$ GeV. Below that value a level-crossing of the two lightest Higgs bosons occurs, which vanishes in the CP-conserving case, i.e. if the CP-violating phase is set to $\arg(\mathbf{a_t}) = 0°$ (dotted lines). The mass of the heaviest Higgs boson H_3 is not visibly affected by CP-violation.

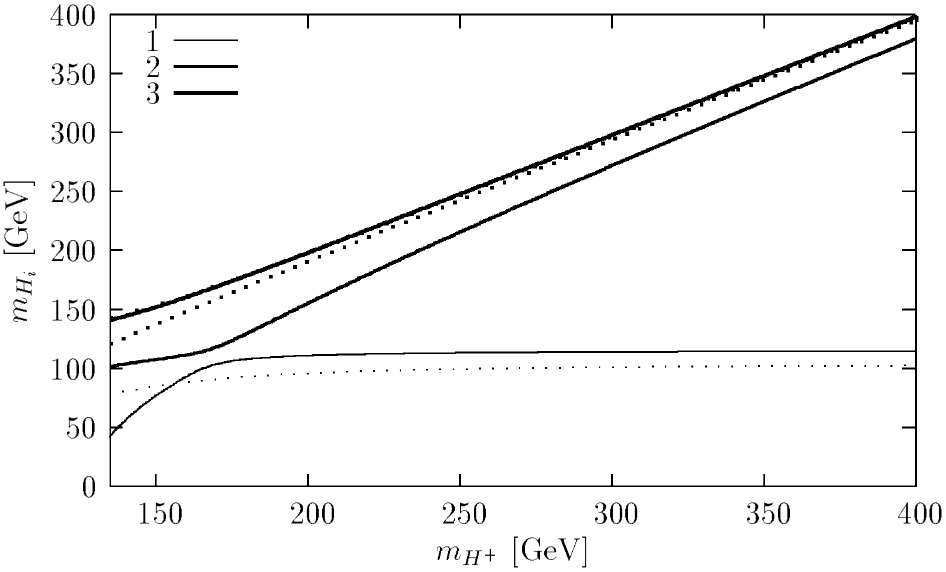

Figure 3.4: m_{H_i} versus m_{H^+} with $\tan\beta = 4$ and $\arg(\mathbf{a_t}) = 0°$ (dotted lines), $\arg(\mathbf{a_t}) = 90°$ (solid lines).

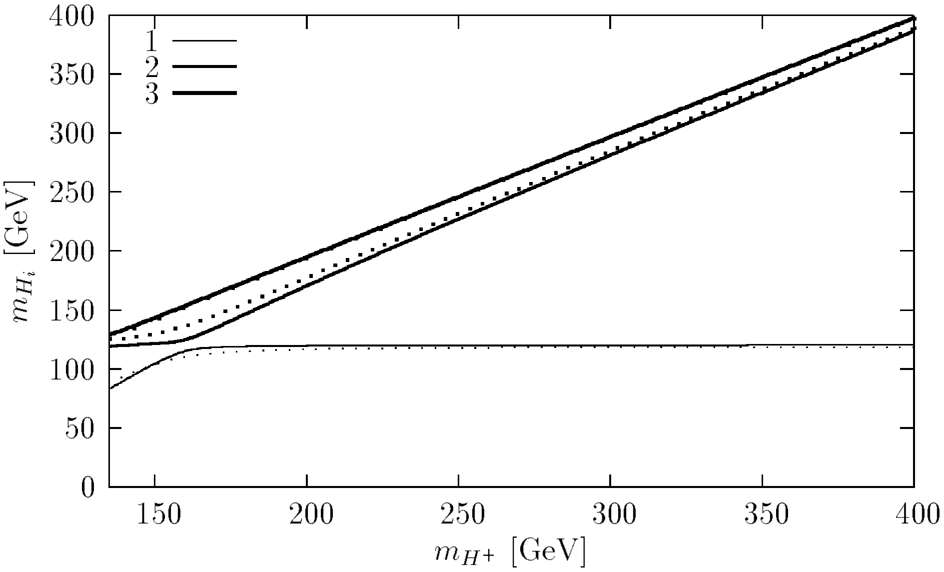

Figure 3.5: m_{H_i} versus m_{H^+} with $\tan\beta = 20$ and $\arg(\mathbf{a_t}) = 0°$ (dotted lines), $\arg(\mathbf{a_t}) = 90°$ (solid lines)

In order for the heaviest neutral Higgs boson to be resonantly exchanged in top-quark production the following relation must be satisfied:

$$m_{H^+} \geq 350 \text{ GeV}. \tag{3.59}$$

In Fig. 3.5 the same plot as in Fig. 3.4 is presented taking $\tan\beta = 20$. Comparing Fig. 3.4 with Fig. 3.5 reveals that the two scenarios differ in some aspects: the mass of the lightest Higgs boson is increased, the splitting between the two heavy particles is reduced and the effect of CP-violation is less significant in the scenario with $\tan\beta = 20$. To understand the last point it is important to notice that the radiative corrections to the lightest Higgs boson depend crucially on the stop mixing parameter [40]:

$$|X_t| = |\mathbf{a_t} - \mu\cot\beta| = \left|\mathbf{a_t} - \frac{\mu}{\tan\beta}\right|. \tag{3.60}$$

The mass m_{H_1} reaches a maximum at $|X_t|/M_{SUSY} \approx 2.45$. In low $\tan\beta$ scenarios a variation of $\arg(\mathbf{a_t})$ causes large differences of the stop mixing parameter $|X_t|$ since the second term of (3.60) is comparable to the first one. The situation changes significantly for large $\tan\beta$, where the first term is dominating. This leads to $|X_t| \approx |\mathbf{a_t}|$ and therefore $\arg(\mathbf{a_t})$ has little influence.

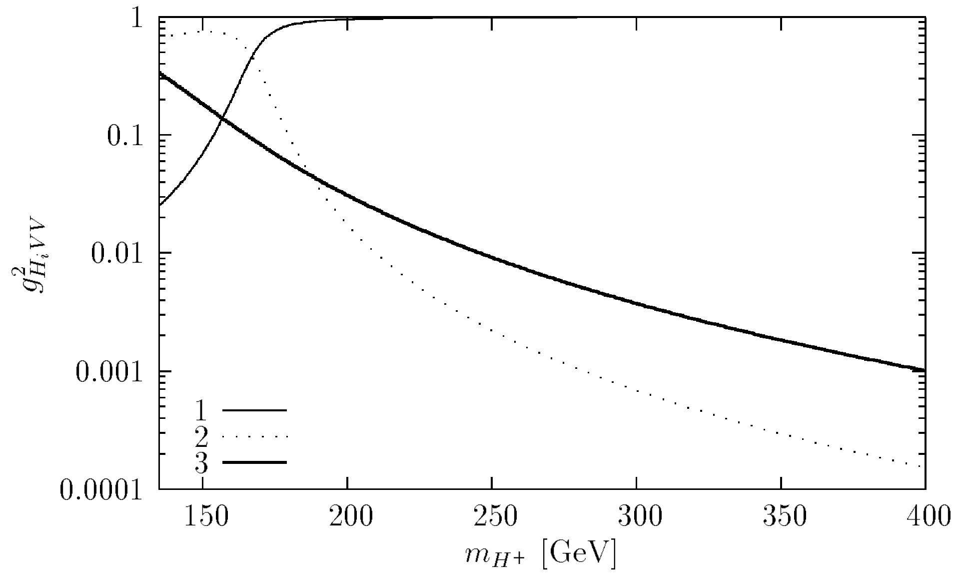

Figure 3.6: $g^2_{H_iVV}$ versus m_{H^+} with $\tan\beta = 4$ and $\arg(\mathbf{a_t}) = 90°$

In Fig. 3.6 the squared coupling constants $g^2_{H_iVV}$ of the Higgs bosons H_i to the gauge bosons (3.53) are plotted. After a significant depression $g^2_{H_1VV}$ is nearly identical to unity. On the other hand, $g^2_{H_2VV}$ reaches a maximum of about 0.75 around $m_{H^+} = 150$ GeV and decreases to $1.5 \cdot 10^{-4}$ at $m_{H^+} = 400$ GeV. The third squared coupling constant $g^2_{H_3VV}$ decreases monotonously from a value of about 0.3 at $m_{H^+} = 135$ GeV to 0.001 at $m_{H^+} = 400$ GeV. The sum of the three squared coupling constants is unity according to (3.55).

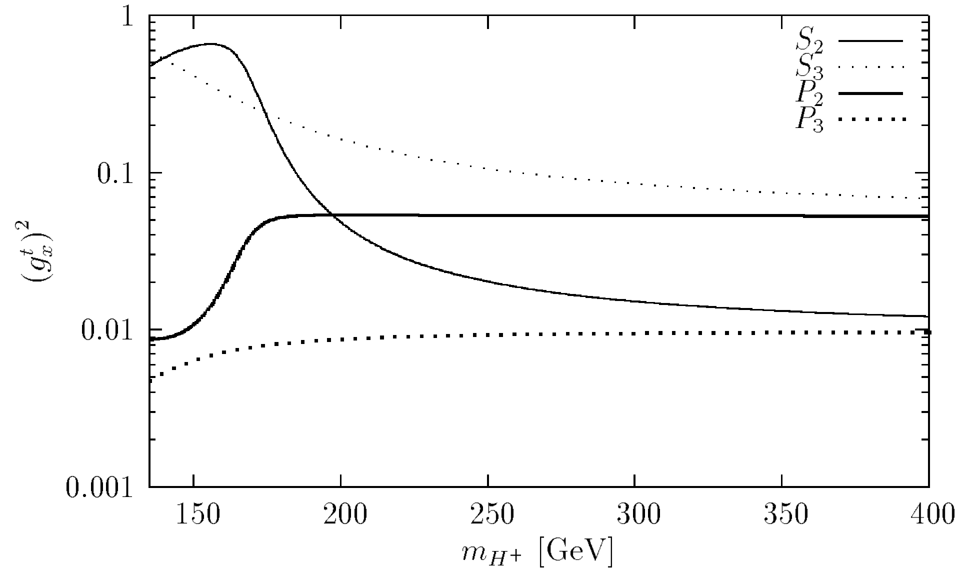

Figure 3.7: $(g^t_x)^2$ versus m_{H^+} for $i = S_2, S_3, P_2, P_3$ with $\tan\beta = 4$ and $\arg(\mathbf{a_t}) = 90°$

To complete the discussion the scalar and pseudoscalar squared coupling constants of the two heavy neutral Higgs bosons to the top quark and the muon are shown in Fig. 3.7 and Fig. 3.8 respectively. At small values of m_{H^+} the scalar as well as the pseudoscalar couplings have the same order of magnitude in each figure. Oppositely, at high values of m_{H^+}, $g^2_{S_2}$ becomes similar to $g^2_{P_3}$ and $g^2_{S_3}$ to $g^2_{P_2}$.

Furthermore, in the interesting range $m_{H^+} > 350$ GeV all couplings can be treated as practically constant. Since the coupling constants to the top quark are small in this range, searches for the Higgs boson in the top-channel will be difficult, similarily as have been found in the Standard Model. The coupling constants of the two heavy neutral Higgs bosons to the muon are according to (3.48) and (3.49) two orders of magnitude larger than those to the top quark.

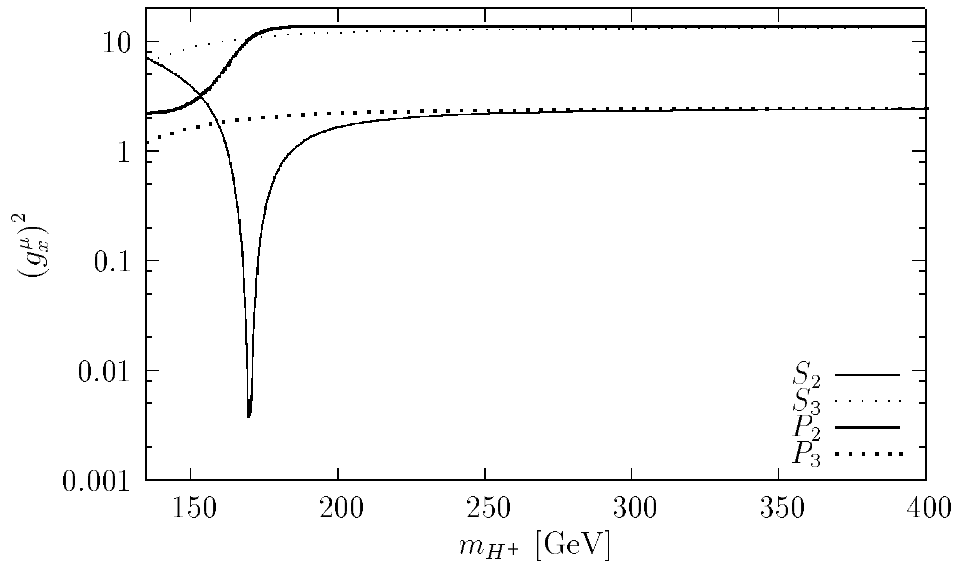

Figure 3.8: $(g_x^\mu)^2$ versus m_{H^+} for $i = S_2, S_3, P_2, P_3$ with $\tan\beta = 4$ and $\arg(\mathbf{a_t}) = 90°$

However, another scenario presented in 3.7.2 is the focus of attention.

3.7.2 Light Charged Higgs Scenario

As mentioned in the introduction a mass bound on the lightest neutral Higgs boson of 115 GeV [18] has been derived from LEP2. This result is based on the process

$$e^+e^- \longrightarrow Z^* \longrightarrow ZH_1 \tag{3.61}$$

with $g_{H_1ZZ} = 1$. However, as shown in Fig. 3.6 in CP-violating scenarios the coupling constant can be well below that value if the charged Higgs mass m_{H^+} is smaller than 180 GeV. In this case a much lower bound than 115 GeV would result from the LEP2 search. Since this possibility is particularly interesting, in the following

$$m_{H^+} = 150 \text{ GeV} \tag{3.62}$$

is assumed.

As explained above with respect to (3.60) it is important to distinguish between low and high values of $\tan\beta$. In the *Low*-$\tan\beta$-*Scenario* (LTS) $\tan\beta = 4$, and in the *High*-$\tan\beta$-*Scenario* (HTS) $\tan\beta = 20$ is assumed.

Low-$\tan\beta$-Scenario (LTS)

As shown in Fig. 3.9 $g^2_{H_1VV}$ is almost equal to the value in the Standard Model in the low range of $\arg(\mathbf{a_t})$, while at $\arg(\mathbf{a_t}) \geq 60°$ this coupling is highly suppressed and $g^2_{H_2VV}$ becomes the strongest coupling constant. The squared coupling of the heaviest Higgs boson H_3 to the gauge bosons is nearly constant $\left(g^2_{H_3VV} \approx 0.2\right)$.

Values $\arg(\mathbf{a_t}) \geq 109°$ are unphysical, since in this case a complex or negative eigenvalue of the neutral Higgs boson mass matrix (3.38) develops.

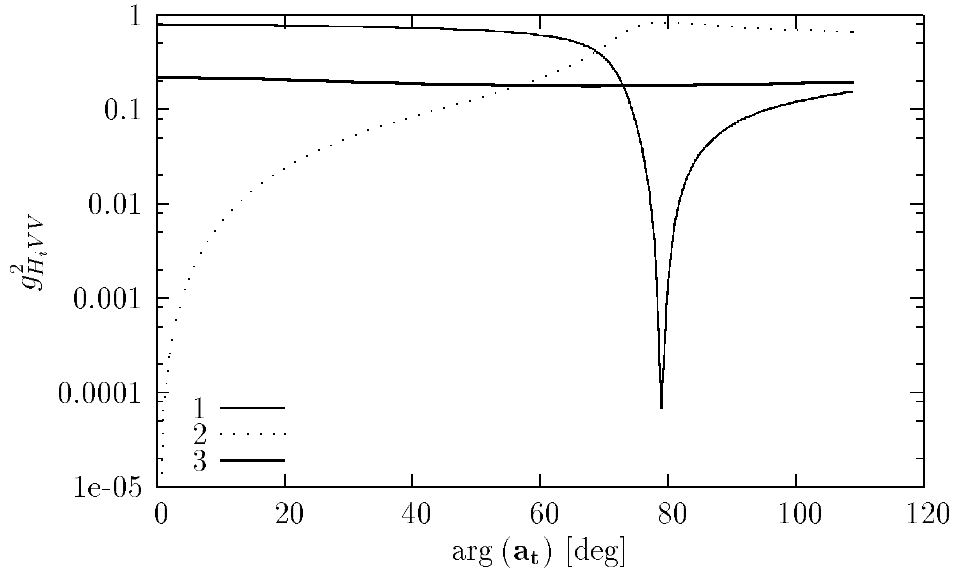

Figure 3.9: $g^2_{H_iVV}$ versus $\arg(\mathbf{a_t})$ with $\tan\beta = 4$ and $m_{H^+} = 150$ GeV

Fig. 3.10 shows the corresponding values of the masses of the three neutral Higgs bosons. Note that for $75° \lesssim \arg(A_t) \lesssim 95°$ the squared coupling constant $g^2_{H_1VV}$ is smaller than 0.1 (Fig. 3.9). Hence one may have missed H_1 at LEP 2, despite the fact that H_1 is much lighter than 115 GeV.

On the other hand $g^2_{H_2VV} \approx 0.8$ is large enough in this range to allow for a detection of the next to lightest Higgs boson, that possesses a mass around 110 GeV.

Therefore the excess found at LEP2 in the last year [16, 17, 18, 19, 20] may have been a signal of the *intermediate* Higgs boson [45].

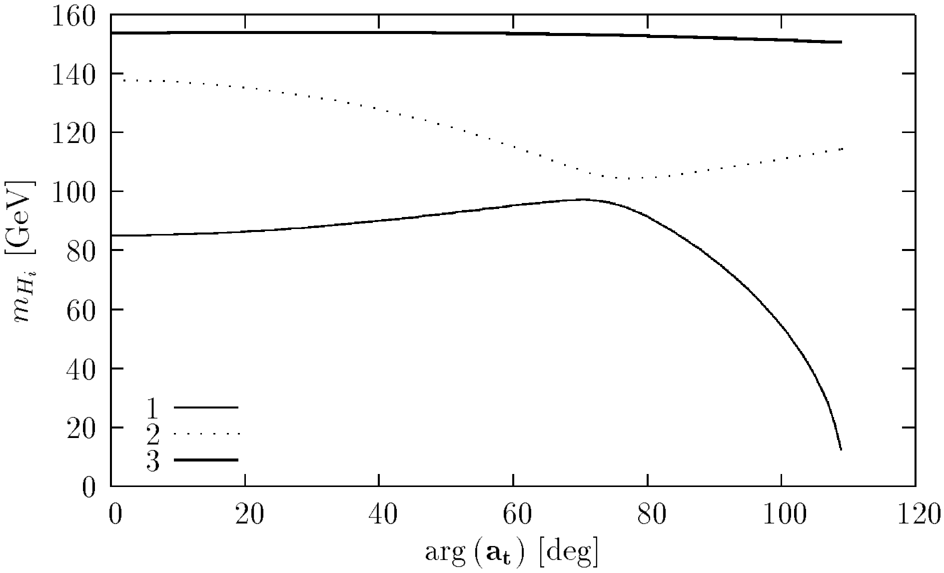

Figure 3.10: m_{H_i} versus arg $(\mathbf{a_t})$ with $\tan\beta = 4$ and $m_{H^+} = 150$ GeV

High-$\tan\beta$**-Scenario (HTS)**

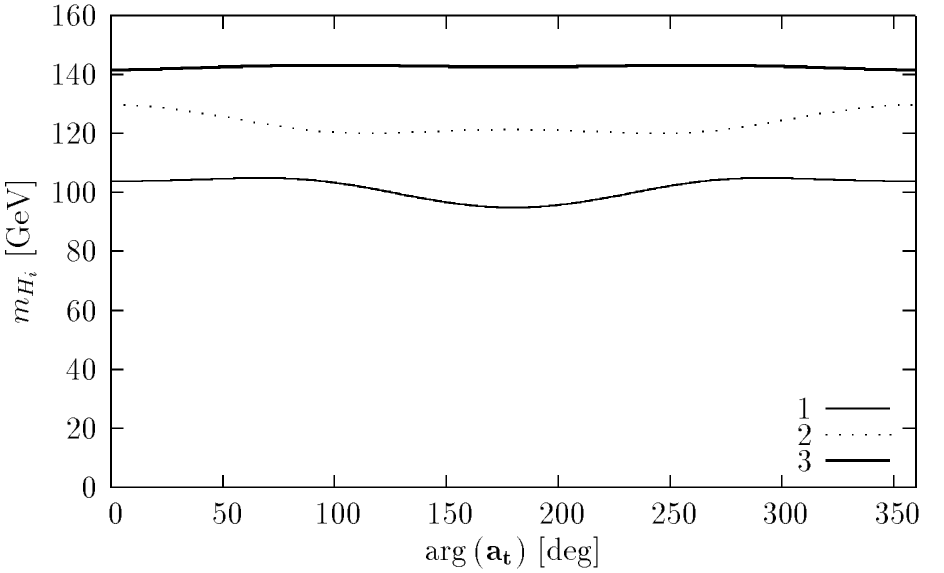

Figure 3.11: m_{H_i} versus arg $(\mathbf{a_t})$ with $\tan\beta = 20$ and $m_{H^+} = 150$ GeV

The situation for $\tan\beta = 20$ is illustrated in Fig. 3.11 and Fig. 3.12. Firstly, in the HTS the mass splitting between the three neutral Higgs bosons is smaller than in the LTS. Secondly, $|X_t|$ becomes according to (3.60) less dependent of $\arg(\mathbf{a_t})$. Therefore the masses vary less with $\arg(\mathbf{a_t})$ than in the LTS considered in Fig. 3.10.

In contrast, as depicted in Fig. 3.12, the squared coupling constants $g^2_{H_1VV}$ and $g^2_{H_3VV}$ vary dramatically with $\arg(\mathbf{a_t})$ over five orders of magnitude, whereas $0.55 \lesssim g^2_{H_2VV} \lesssim 0.98$.

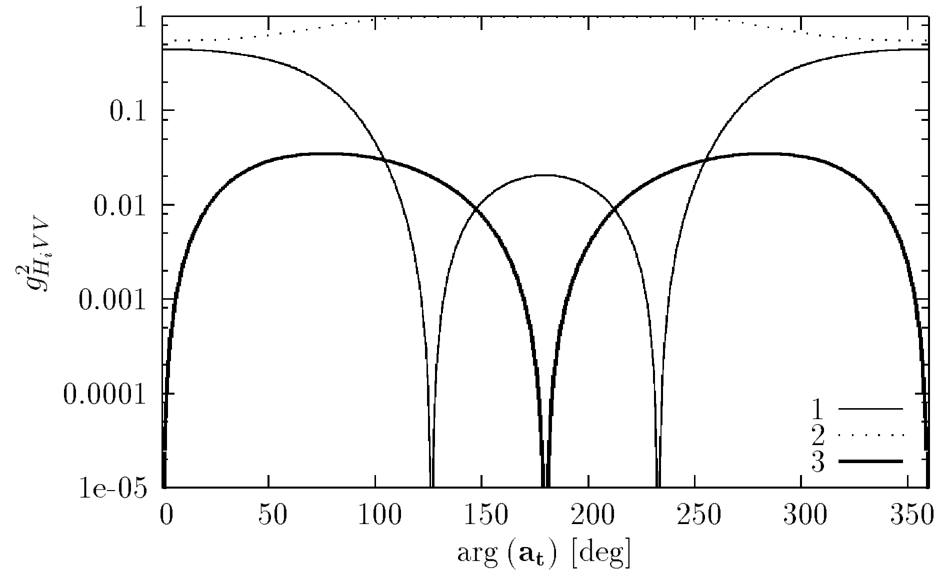

Figure 3.12: $g^2_{H_iVV}$ versus $\arg(\mathbf{a_t})$ with $\tan\beta = 20$ and $m_{H^+} = 150$ GeV

An explanation of the "spikes" in Fig. 3.12 is not obvious. Taking $\tan\beta = 20$, i.e. $\sin\beta = 20\cos\beta$, into account leads to an approximation of (3.53):

$$g_{H_iVV} \approx O_{2i}\,\sin\beta\ . \tag{3.63}$$

Therefore the coupling constants g_{H_1VV} and g_{H_3VV} depend on the off-diagonal elements of the transformation matrix O (3.44). These off-diagonal elements scale with the size of the CP-violating off-diagonal terms in the Higgs-boson mass matrix (3.34), estimated by [40]

$$\mathcal{M}^2_{SP} \propto \sin(\mathbf{a_t})\,. \tag{3.64}$$

The coupling of the heaviest Higgs boson H_3 to the gauge bosons shows exactly this depedency, while in the case of g_{H_1VV} the "spikes" drift to $\arg(\mathbf{a_t}) = 180°$.

Chapter 4

Signatures of a CP-Violating Higgs Sector in $\mu^+\mu^- \longrightarrow b\bar{b}$

4.1 Higgs Boson Decay

4.1.1 Decay into Fermions

According to the model introduced in chapter 3 the CP-even Standard Model Higgs boson with its scalar coupling is substituted by three Higgs bosons with mixed CP and couplings described by the interaction lagrangian presented in (3.47). More formally, the Higgs coupling of the Standard Model is modified by

$$1 \quad \longrightarrow \quad g^f_{S_i} + i g^f_{P_i}\gamma_5 \ , \qquad i = \{1,2,3\} \ , \tag{4.1}$$

where $g^f_{S_i}$ and $g^f_{P_i}$ are shown numerically in appendix C.

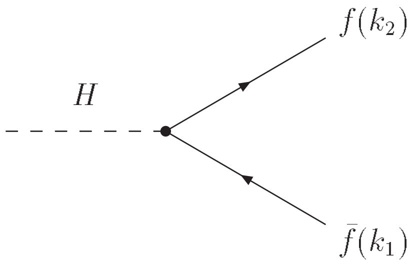

Figure 4.1: Higgs boson decay into fermions

Therefore the Feynman amplitude describing Fig. 4.1 is given by

$$\mathcal{M} = \bar{u}(k_2)\left[-\frac{1}{2} i g \,\frac{m_f}{m_W}\left(g^f_{S_i} + i g^f_{P_i}\gamma_5\right)\right] v(k_1). \tag{4.2}$$

This yields

$$|\mathcal{M}|^2 = g^2 \left(\frac{m_f}{m_W}\right)^2 \left[{g^f_{S_i}}^2 \left(k_1 k_2 - m_f^2\right) + {g^f_{P_i}}^2 \left(k_1 k_2 + m_f^2\right)\right] . \tag{4.3}$$

Now one can compute with (2.18) the decay width

$$\begin{aligned}\Gamma\left(H_i \to f\bar{f}\right) &= N_c^f \frac{1}{8\pi m_{H_i}^2} \left|\vec{k}_f\right| g^2 \left(\frac{m_f}{m_W}\right)^2 \\ &\quad \cdot \left[{g^f_{S_i}}^2 \left(k_1 k_2 - m_f^2\right) + {g^f_{P_i}}^2 \left(k_1 k_2 + m_f^2\right)\right] \\ &\overset{\text{(restfr.)}}{=} N_c^f \frac{g^2}{32\pi} m_{H_i} \left(\frac{m_f}{m_W}\right)^2 \\ &\quad \cdot \left[{g^f_{S_i}}^2 \left(1 - \frac{4m_f^2}{m_{H_i}^2}\right) + {g^f_{P_i}}^2\right] \sqrt{1 - \frac{4m_f^2}{m_{H_i}^2}} \end{aligned} \tag{4.4}$$

with the colour factor N_c^f defined in (2.22).

4.1.2 Decay into Gauge Bosons

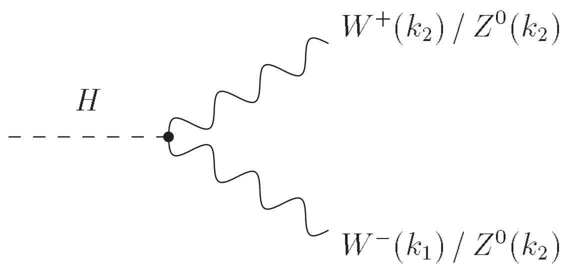

Figure 4.2: Higgs boson decay into gauge bosons

The results are with exception of the squared coupling constant $g^2_{H_iVV}$ derived from (3.52) identical to the SM calculations (2.30) and (2.34):

$$\begin{aligned}\Gamma\left(H_i \to W^+W^-\right) = g^2_{H_iVV} &\cdot \frac{g^2}{64\pi} m_{H_i} \left(\frac{m_{H_i}}{m_W}\right)^2 \sqrt{1 - \frac{4m_W^2}{m_{H_i}^2}} \\ &\cdot \left(1 - 4\frac{m_W^2}{m_{H_i}^2} + 12\frac{m_W^4}{m_{H_i}^4}\right)\end{aligned} \tag{4.5}$$

and

$$\Gamma\left(H_i \to Z^0 Z^0\right) = g^2_{H_i VV} \cdot \frac{g^2}{128\pi}\, m_{H_i} \left(\frac{m_{H_i}}{m_W}\right)^2 \sqrt{1 - \frac{4m_Z^2}{m_{H_i}^2}} \cdot \left(1 - 4\frac{m_Z^2}{m_{H_i}^2} + 12\frac{m_Z^4}{m_{H_i}^4}\right). \tag{4.6}$$

4.1.3 Numerical Results

Low-$\tan\beta$-Scenario

The *LTS* is defined in chapter 4 as a CP-violating scenario with the parameters given in (3.57) and

$$\tan\beta = 4\ , \tag{4.7}$$
$$m_{H^+} = 150\ \text{GeV}. \tag{4.8}$$

In Fig. 3.9 the squared coupling constants of the three neutral Higgs bosons to the gauge bosons are presented. Their masses are plotted in Fig. 3.10, and their squared scalar and pseudoscalar coupling constants to down-type (to leptons respectively) and to up-type fermions are illustrated in appendix C. The dependence of the Higgs boson decay widths on the CP-violating phase $\arg(\mathbf{a_t})$ within this scenario is shown in Fig. 4.3.

While being nearly constant between 0.023 GeV and 0.027 GeV at low CP-violating phases $\arg(\mathbf{a_t}) \leq 50°$, the decay width of the lightest Higgs particle Γ_{H_1} reaches a maximum at $\arg(\mathbf{a_t}) \approx 80°$ before rapidly decreasing for $\arg(\mathbf{a_t}) > 80°$. In contrast, the decay width of the intermediate Higgs boson Γ_{H_2} reaches a minimum around 80°. The third Higgs boson possesses a decay width Γ_{H_3} that is nearly independent of CP violation and varies only between 0.053 GeV and 0.057 GeV. For the special case $\arg(\mathbf{a_t}) = 80°$, where the coupling of H_1 to the gauge bosons is heavily suppressed (see Fig. 3.9), the relevant parameters are listed in Tab. 4.1, and the branching ratios in Tab. 4.2.

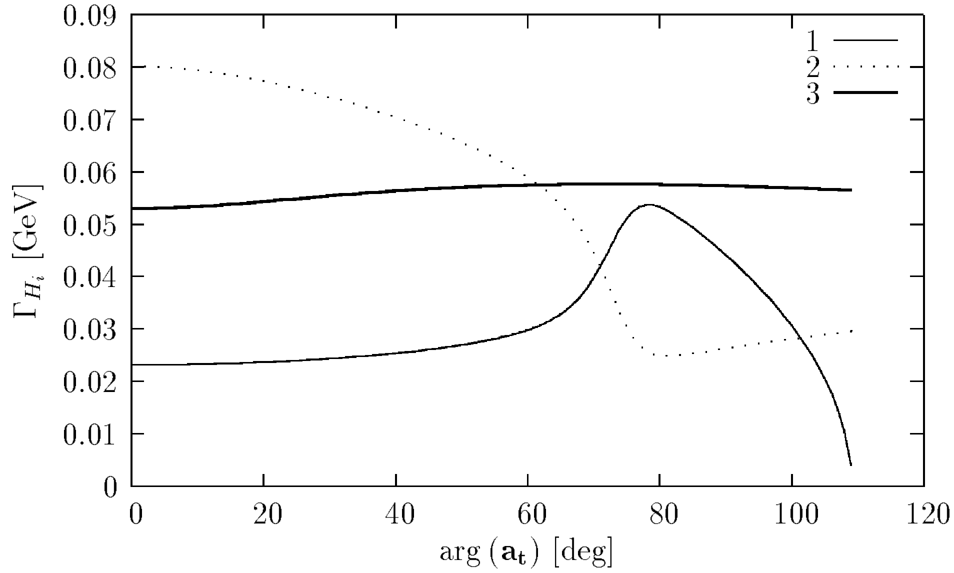

Figure 4.3: Decay width Γ_{H_i} for $i = 1, 2, 3$ versus arg $(\mathbf{a_t})$ for $\tan\beta = 4$ and $m_{H^+} = 150$ GeV (LTS)

Higgs boson	H_1	H_2	H_3
mass [GeV]	**91.534**	**104.741**	**152.747**
g_{H_iVV}	0.0373	0.905	0.424
$g^d_{S_i}$	1.23	2.48	-3.05
$g^d_{P_i}$	-3.81	0.636	-1.02
$g^u_{S_i}$	-0.0374	0.806	0.641
$g^u_{P_i}$	-0.238	0.0397	-0.0639

Table 4.1: Masses and coupling constants of the neutral Higgs bosons for arg $(\mathbf{a_t}) = 80°$, $\tan\beta = 4$ and $m_{H^+} = 150$ GeV (LTS)

channel	Γ_{H_1} [MeV]	BR [%]	Γ_{H_2}[MeV]	BR [%]	Γ_{H_3} [MeV]	BR [%]
$b\bar{b}$	50.23	94.22	23.40	93.45	54.10	93.94
$c\bar{c}$	0.02	0.03	0.21	0.83	0.19	0.33
$s\bar{s}$	0.04	0.08	0.02	0.08	0.05	0.08
$\tau^+\tau^+$	3.01	5.65	1.41	5.62	3.24	5.62
$\mu^-\mu^+$	0.01	0.02	< 0.01	0.02	0.01	0.02
total	**53.31**	100%	**25.04**	100%	**57.59**	100%

Table 4.2: Branching Ratios of the neutral Higgs bosons for $\arg(\mathbf{a_t}) = 80°$, $\tan\beta = 4$ and $m_{H^+} = 150$ GeV (LTS)

High-$\tan\beta$-Scenario

The *HTS* is also defined in chapter 4 as a CP-violating scenario with the parameters given in (3.57) and

$$\tan\beta = 20\ , \quad (4.9)$$

$$m_{H^+} = 150 \text{ GeV}. \quad (4.10)$$

The corresponding masses of the three neutral Higgs bosons as a function of $\arg(\mathbf{a_t})$ are shown in Fig. 3.11, their squared coupling constants to the gauge bosons in Fig. 3.12, and the squared scalar and pseudoscalar coupling constants to down-type (to leptons respectively) and to up-type fermions are plotted in appendix C. The dependence of the decay widths from the CP-violating phase $\arg(\mathbf{a_t})$ is illustrated in Fig. 4.4.

The decay widths are generally one order of magnitude larger than in the LTS. In the scenario discussed here the graphs do not intersect, but the value of the decay width of the medium Higgs boson Γ_{H_2} lies below the values of Γ_{H_1} and Γ_{H_3} and is < 20 MeV for $162° \leq \arg(\mathbf{a_t}) \leq 198°$. The reason is the suppressed coupling of the intermediate Higgs boson to the up-type fermions in this range (see appenix C).

If the CP-violating phase $\arg(\mathbf{a_t})$ is fixed again at 80°, where the coupling of the lightest Higgs boson to the gauge bosons g_{H_1VV} reaches a minimum, the coupling constants listed in Tab. 4.3 and the branching ratios shown in Tab. 4.4 are found.

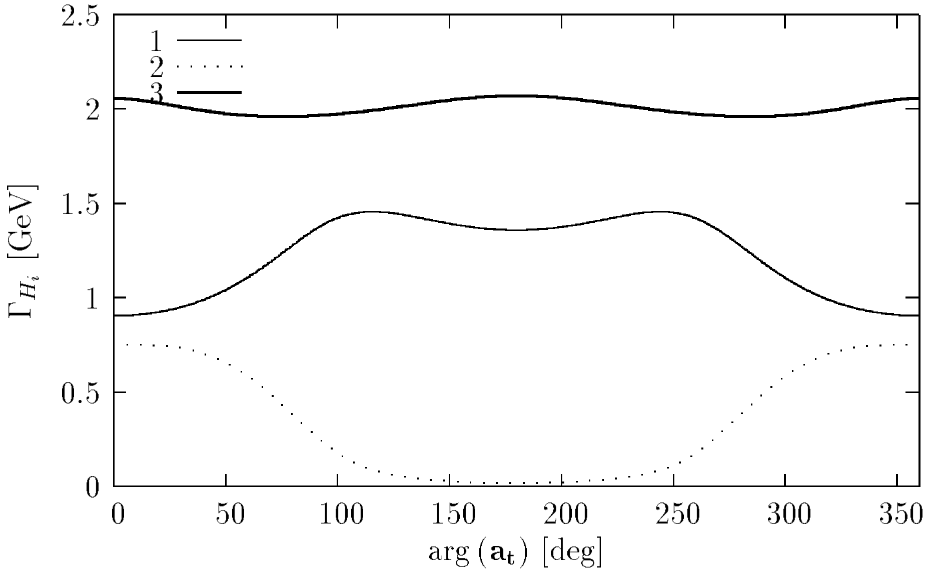

Figure 4.4: Decay width Γ_{H_i} for $i = 1, 2, 3$ versus $\arg(\mathbf{a_t})$ with $\tan\beta = 20$ and $m_{H^+} = 150$ GeV (HTS)

Higgs boson	H_1	H_2	H_3
mass [GeV]	**104.664**	**121.859**	**142.838**
g_{H_iVV}	0.405	0.895	-0.187
$g^d_{S_i}$	2.61	3.99	19.45
$g^d_{P_i}$	18.15	-8.36	-0.720
$g^u_{S_i}$	0.399	0.887	-0.236
$g^u_{P_i}$	0.0454	-0.0209	-0.00180

Table 4.3: Masses and coupling constants of the neutral Higgs bosons for $\arg(\mathbf{a_t}) = 80°$, $\tan\beta = 20$ and $m_{H^+} = 150$ GeV (HTS)

channel	Γ_{H_1} [MeV]	BR [%]	Γ_{H_2}[MeV]	BR [%]	Γ_{H_3} [MeV]	BR [%]
$b\bar{b}$	1204.51	94.25	357.94	94.18	1847.37	94.25
$c\bar{c}$	0.05	< 0.01	0.29	0.08	0.02	< 0.01
$s\bar{s}$	1.07	0.08	0.32	0.08	1.64	0.08
$\tau^+\tau^+$	72.07	5.64	21.42	5.64	110.70	5.65
$\mu^-\mu^+$	0.26	0.02	0.08	0.02	0.39	0.02
total	**1277.96**	100%	**380.04**	100%	**1960.13**	100%

Table 4.4: Branching Ratios of the neutral Higgs bosons for $\arg(\mathbf{a_t}) = 80°$, $\tan\beta = 20$ and $m_{H^+} = 150$ GeV (HTS)

4.2 Cross Section

4.2.1 Squared amplitudes

Similarly to the SM results given in (2.76) - (2.85) the squared matrix elements for $\mu^+\mu^- \longrightarrow b\bar{b}$ within the CP-violating scenarios discussed above are calculated. Obviously, only the squared matrix elements involving a Higgs boson (2.79), (2.82), (2.84) and (2.85) have to be recalculated. The analytic results are summarized below.

Photon Higgs-Bosons Interference

$$\begin{aligned}
\mathcal{M}_\gamma \mathcal{M}_H^\dagger + \mathcal{M}_\gamma^\dagger \mathcal{M}_H &= 2 \cdot \Re e \left(\mathcal{M}_\gamma \mathcal{M}_H^\dagger \right) \\
&= 4 \cdot \sum_{i=1}^{3} \left(\mathcal{T}_\gamma \mathcal{T}_{H_i}^* + \mathcal{T}_\gamma^* \mathcal{T}_{H_i} \right) \cdot m_\mu m_b \cdot g_{S_i}^\mu g_{S_i}^b \\
&\quad \cdot \left[-(p_1 k_1) + (p_1 k_2) + (p_2 k_1) - (p_2 k_2) \right] \qquad (4.11)
\end{aligned}$$

Z-Boson Higgs-Bosons Interference

$$\begin{aligned}
\mathcal{M}_{Z^0}\mathcal{M}_H^\dagger + \mathcal{M}_{Z^0}^\dagger\mathcal{M}_H &= 2\cdot\Re e\left(\mathcal{M}_{Z^0}\mathcal{M}_H^\dagger\right) \\
&= 4\cdot\sum_{i=1}^{3}\left(\mathcal{T}_{Z^0}\mathcal{T}_{H_i}^* + \mathcal{T}_{Z^0}^*\mathcal{T}_{H_i}\right)\cdot m_\mu m_b \\
&\cdot \Big\{g_{S_i}^\mu g_{S_i}^b g_V^\mu g_V^b \\
&\quad \cdot[-(p_1k_1)+(p_1k_2)+(p_2k_1)-(p_2k_2)] \\
&\quad + g_{P_i}^\mu g_{P_i}^b g_A^\mu g_A^b \\
&\quad \cdot[(p_1k_1)+(p_1k_2)+(p_2k_1)+(p_2k_2)]\Big\} \qquad (4.12)
\end{aligned}$$

Goldstone-Boson Higgs-Bosons Interference

$$\begin{aligned}
\mathcal{M}_{G^0}\mathcal{M}_H^\dagger + \mathcal{M}_{G^0}^\dagger\mathcal{M}_H &= 2\cdot\Re e\left(\mathcal{M}_{G^0}\mathcal{M}_H^\dagger\right) \\
&= -4\cdot\sum_{i=1}^{3}\left(\mathcal{T}_{G^0}\mathcal{T}_{H_i}^* + \mathcal{T}_{G^0}^*\mathcal{T}_{H_i}\right)\cdot g_{P_i}^\mu g_{P_i}^b \\
&\quad \cdot\Big[m_\mu^2 m_b^2 + m_\mu^2(k_1k_2) \\
&\quad\quad + m_b^2(p_1p_2) + (p_1p_2)(k_1k_2)\Big] \qquad (4.13)
\end{aligned}$$

Higgs-Bosons

$$\begin{aligned}
|\mathcal{M}|_H^2 = 4 &\cdot \sum_{i,j=1}^{3}\left(\mathcal{T}_{H_i}\mathcal{T}_{H_j}^* + \mathcal{T}_{H_i}^*\mathcal{T}_{H_j}\right) \\
&\cdot \Big\{m_\mu^2 m_b^2\Big[\left(-g_{S_i}^\mu g_{S_j}^\mu + g_{P_i}^\mu g_{P_j}^\mu\right)\left(-g_{S_i}^b g_{S_j}^b + g_{P_i}^b g_{P_j}^b\right)\Big] \\
&\quad + m_\mu^2(k_1k_2)\Big[\left(-g_{S_i}^\mu g_{S_j}^\mu + g_{P_i}^\mu g_{P_j}^\mu\right)\left(g_{S_i}^b g_{S_j}^b + g_{P_i}^b g_{P_j}^b\right)\Big] \\
&\quad + m_b^2(p_1p_2)\Big[\left(g_{S_i}^\mu g_{S_j}^\mu + g_{P_i}^\mu g_{P_j}^\mu\right)\left(-g_{S_i}^b g_{S_j}^b + g_{P_i}^b g_{P_j}^b\right)\Big] \\
&\quad + (p_1p_2)(k_1k_2)\Big[\left(g_{S_i}^\mu g_{S_j}^\mu + g_{P_i}^\mu g_{P_j}^\mu\right) \\
&\quad\quad \cdot\left(g_{S_i}^b g_{S_j}^b + g_{P_i}^b g_{P_j}^b\right)\Big]\Big\} \qquad (4.14)
\end{aligned}$$

4.2.2 Differential Cross Section

Putting the squared amplitudes (4.11) - (4.14) and the kinematics given in section 2.1 into (2.52), and using the unchanged part of the SM differential cross section, one gets

$$\begin{aligned}\frac{d\sigma}{d\Omega} &= 3\alpha^2 \sqrt{\frac{\lambda_f}{\lambda_\mu}} \\ &\cdot \sum_k \sum_{i,j=1}^{3} f_k \left(R_k \cos^2\theta + I_k \cos\theta + S_k\right)\end{aligned} \tag{4.15}$$

with the prefactors

$$f_\gamma = Q_\mu^2 Q_b^2 \frac{1}{s^2} , \tag{4.16}$$

$$f_{\gamma Z^0} = \frac{Q_\mu Q_b}{\cos^2\theta_W \sin^2\theta_W} \frac{s - m_Z^2}{(s - m_Z^2)^2 + m_Z^2\Gamma_Z^2} \frac{1}{s} , \tag{4.17}$$

$$f_{\gamma G^0} = 0 , \tag{4.18}$$

$$f_{\gamma H} = \frac{Q_\mu Q_b}{\sin^2\theta_W} \frac{m_\mu m_b}{m_W^2} \frac{s - m_{H_i}^2}{\left(s - m_{H_i}^2\right)^2 + m_{H_i}^2\Gamma_{H_i}^2} \frac{1}{s} , \tag{4.19}$$

$$f_{Z^0} = \frac{1}{\cos^4\theta_W \sin^4\theta_W} \frac{1}{(s - m_Z^2)^2 + m_Z^2\Gamma_Z^2} , \tag{4.20}$$

$$f_{Z^0 G^0} = \frac{1}{\cos^4\theta_W \sin^4\theta_W} \frac{m_\mu m_b}{m_Z^2} \frac{1}{(s - m_Z^2)^2 + m_Z^2\Gamma_Z^2} , \tag{4.21}$$

$$\begin{aligned}f_{Z^0 H} &= \frac{1}{\cos^2\theta_W \sin^4\theta_W} \frac{m_\mu m_b}{m_W^2} \\ &\cdot \frac{(s - m_Z^2)\left(s - m_{H_i}^2\right) + m_Z\Gamma_Z m_{H_i}\Gamma_{H_i}}{\left[(s - m_Z^2)^2 + m_Z^2\Gamma_Z^2\right]\left[\left(s - m_{H_i}^2\right)^2 + m_{H_i}^2\Gamma_{H_i}^2\right]} ,\end{aligned} \tag{4.22}$$

$$f_{G^0} = \frac{1}{\cos^4\theta_W \sin^4\theta_W} \frac{m_\mu^2 m_b^2}{m_Z^4} \frac{1}{(s - m_Z^2)^2 + m_Z^2\Gamma_Z^2} , \tag{4.23}$$

k	R_k	I_k	S_k
γ	$\frac{s}{4} - (m_\mu^2 + m_b^2) + \frac{4}{s} m_\mu^2 m_b^2$	–	$\frac{s}{4} + (m_\mu^2 + m_b^2)$
γZ^0	$\frac{1}{2} g_V^\mu g_V^b \left[\frac{s}{4} - (m_\mu^2 + m_b^2) + \frac{4}{s} m_\mu^2 m_b^2\right]$	$\frac{1}{4s} g_A^\mu g_A^b \sqrt{\lambda_\mu \lambda_b}$	$\frac{1}{2} g_V^\mu g_V^b \left[\frac{s}{4} + (m_\mu^2 + m_b^2)\right]$
γG^0	–	–	–
γH	–	$\frac{1}{2s^2} g_{S_i}^\mu g_{S_i}^b m_\mu m_b \sqrt{\lambda_\mu \lambda_b}$	–
Z^0	$\frac{1}{16} \left({g_V^\mu}^2 + {g_A^\mu}^2\right) \left({g_V^b}^2 + {g_A^b}^2\right) \cdot \left[\frac{s}{4} - (m_\mu^2 + m_b^2) + \frac{4}{s} m_\mu^2 m_b^2\right]$	$\frac{1}{8s} g_V^\mu g_A^\mu g_V^b g_A^b \sqrt{\lambda_\mu \lambda_b}$	$\frac{1}{16} \left({g_V^\mu}^2 + {g_A^\mu}^2\right) \left({g_V^b}^2 + {g_A^b}^2\right) \left[\frac{s}{4} + (m_\mu^2 + m_b^2)\right] - \frac{1}{8} \left[m_\mu^2 {g_A^\mu}^2 \left({g_V^b}^2 + {g_A^b}^2\right) + m_b^2 {g_A^b}^2 \left({g_V^\mu}^2 + {g_A^\mu}^2\right)\right] + \frac{1}{4s} m_\mu^2 m_b^2 \left(2 {g_A^\mu}^2 {g_A^b}^2 - {g_V^\mu}^2 {g_A^b}^2 - {g_A^\mu}^2 {g_V^b}^2\right)$
$Z^0 G^0$	–	–	$-\frac{1}{2} {g_A^\mu}^2 {g_A^b}^2 m_\mu m_b$
$Z^0 H$	–	$\frac{1}{8s^2} g_{S_i}^\mu g_V^\mu g_{S_i}^b g_V^b m_\mu m_b \sqrt{\lambda_\mu \lambda_b}$	$-\frac{1}{8} g_{P_i}^\mu g_A^\mu g_{P_i}^b g_A^b m_\mu m_b$
G^0	–	–	$\frac{s}{4} {g_A^\mu}^2 {g_A^b}^2$
$G^0 H$	–	–	$\frac{s}{8} g_{P_i}^\mu g_A^\mu g_{P_i}^b g_A^b$
H	–	–	$\frac{1}{16} \left\{ \left(g_{S_i}^\mu g_{S_j}^\mu + g_{P_i}^\mu g_{P_j}^\mu\right) \left(g_{S_i}^b g_{S_j}^b + g_{P_i}^b g_{P_j}^b\right) \frac{s}{4} + \frac{4}{s} m_\mu^2 m_b^2 g_{S_i}^\mu g_{S_j}^\mu g_{S_i}^b g_{S_j}^b - \left[m_b^2 \left(g_{S_i}^\mu g_{S_j}^\mu + g_{P_i}^\mu g_{P_j}^\mu\right) g_{S_i}^b g_{S_j}^b + m_\mu^2 \left(g_{S_i}^b g_{S_j}^b + g_{P_i}^b g_{P_j}^b\right) g_{S_i}^\mu g_{S_j}^\mu\right] \right\}$

Table 4.5: Coefficients in the differential cross section (4.15) with scalar and pseudoscalar Higgs couplings

$$
\begin{aligned}
f_{G^0 H} &= \frac{1}{\cos^2\theta_W \sin^4\theta_W} \frac{m_\mu^2 m_b^2}{m_W^2 m_Z^2} \\
&\cdot \frac{\left(s-m_Z^2\right)\left(s-m_{H_i}^2\right)+m_Z\Gamma_Z m_{H_i}\Gamma_{H_i}}{\left[\left(s-m_Z^2\right)^2+m_Z^2\Gamma_Z^2\right]\left[\left(s-m_{H_i}^2\right)^2+m_{H_i}^2\Gamma_{H_i}^2\right]}\,, \qquad (4.24)\\
f_H &= \frac{1}{\sin^4\theta_W}\frac{m_\mu^2 m_b^2}{m_W^4} \\
&\cdot \frac{\left(s-m_{H_i}^2\right)\left(s-m_{H_j}^2\right)+m_{H_i}\Gamma_{H_i} m_{H_j}\Gamma_{H_j}}{\left[\left(s-m_{H_i}^2\right)^2+m_{H_i}^2\Gamma_{H_i}^2\right]\left[\left(s-m_{H_j}^2\right)^2+m_{H_j}^2\Gamma_{H_j}^2\right]}\,, \qquad (4.25)
\end{aligned}
$$

and R_k, I_k and S_k listed in Tab. 4.5.

4.2.3 Numerical Results

Before having a look at the numerical results within the LTS / HTS it is important to discuss the γ-Z^0-background that gives the dominant contribution to the cross section in these scenarios except close to a Higgs resonance.

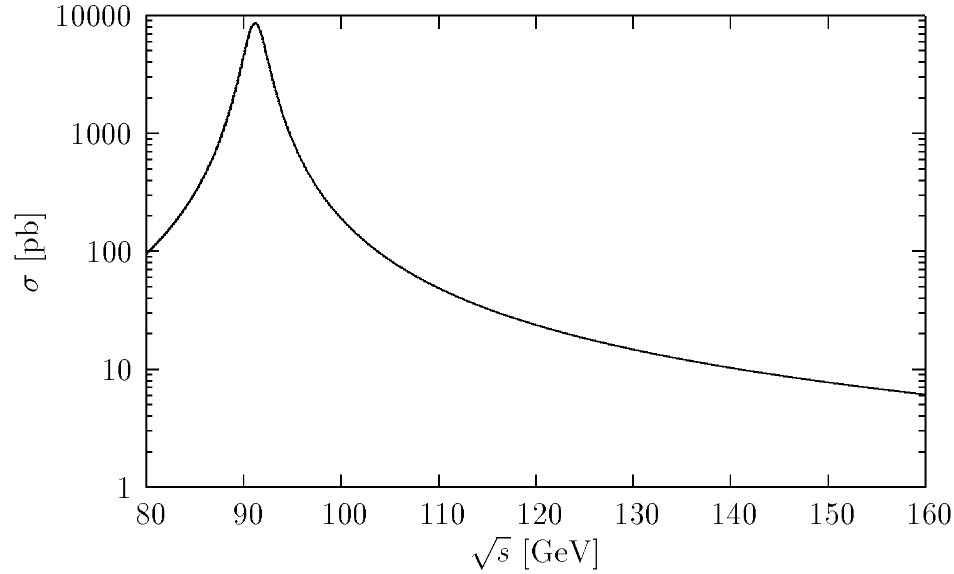

Figure 4.5: Total cross section due to γ and Z^0 exchange in the process $\mu^+\mu^- \longrightarrow b\bar{b}$

The plots presented below are calculated with the parameters given above in Tab. 4.1 and Tab. 4.3 and the constants listed in appendix B. Again the background is depicted by a dotted line.

Low-$\tan\beta$ **Scenario (LTS)**

In Fig. 4.6 - Fig. 4.8 the total cross section of $\mu^+\mu^- \longrightarrow b\bar{b}$ in the presence of the three Higgs bosons in the LTS considered here is shown. According to Fig. 4.5 the background cross section is about 8100 pb at $\sqrt{s} = m_{H_1}$ (Fig. 4.6) and 7 pb at $\sqrt{s} = m_{H_3}$ (Fig. 4.8). Since the resonance Higgs cross section is about $\approx$ 90 pb for H_1 and H_2 and 39 pb for H_3, the detection of all three resonances should be possible, if a muon-collider with its high energy resolution is used.

The energy resolution discussed in section 2.6 will be also very important due to the fact, that the resonace of the lightest neutral Higgs boson H_1 is very close to the Z^0-resonance:

$$m_{H_1} - m_{Z^0} \approx 0.34 \text{ GeV} . \tag{4.26}$$

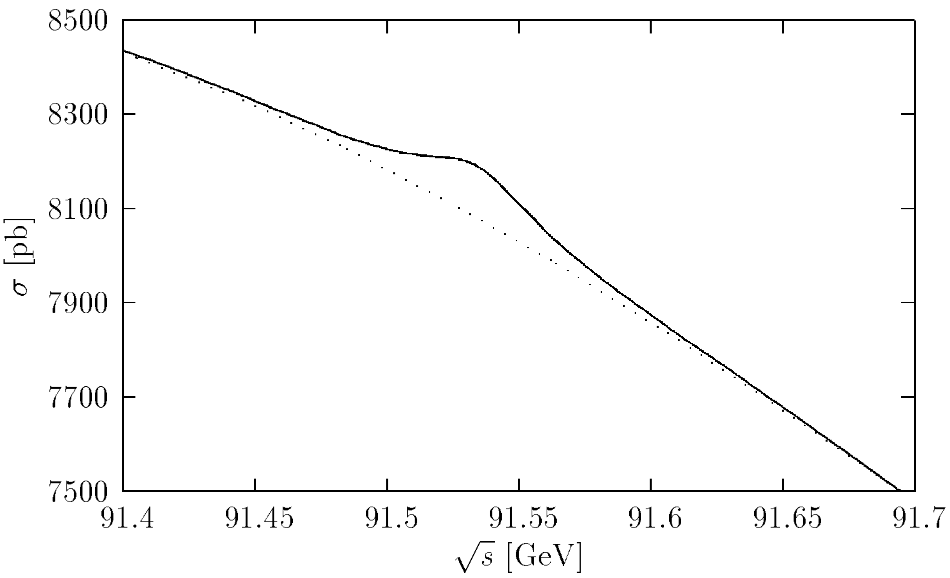

Figure 4.6: The total cross section of $\mu^+\mu^- \longrightarrow b\bar{b}$ around the resonance of the lightest Higgs boson at $m_{H_1} = 91.534$ GeV (LTS). The γ-Z^0-background is dotted.

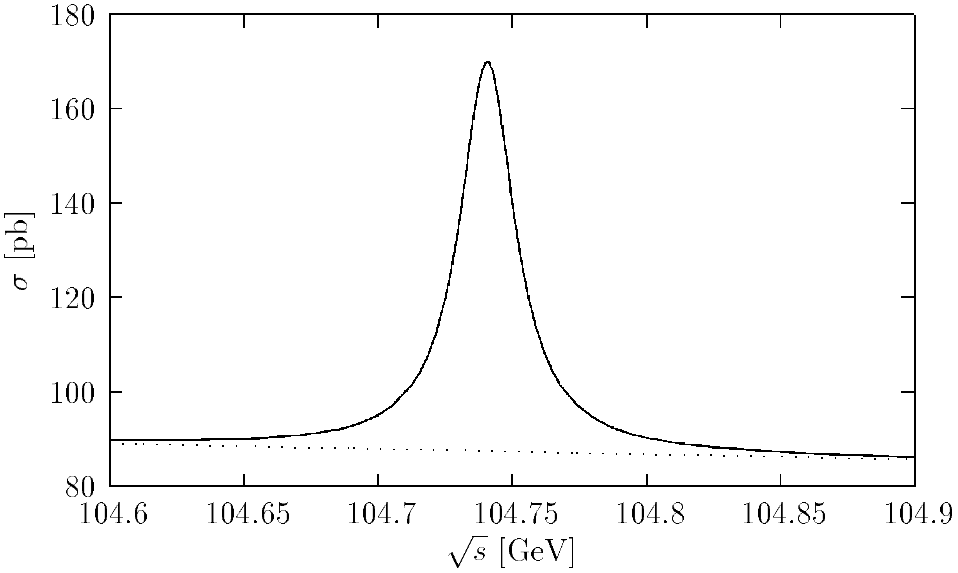

Figure 4.7: The total cross section of $\mu^+\mu^- \longrightarrow b\bar{b}$ around the resonance of the intermediate Higgs boson at $m_{H_2} = 104.741$ GeV (LTS). The γ-Z^0-background is dotted.

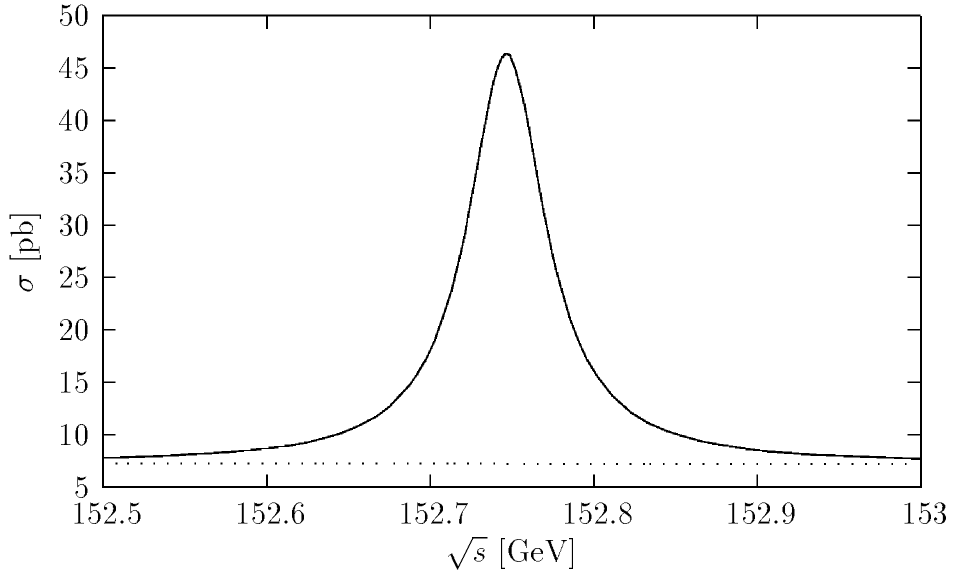

Figure 4.8: The total cross section of $\mu^+\mu^- \longrightarrow b\bar{b}$ around the resonance of the heaviest Higgs boson at $m_{H_3} = 152.747$ GeV (LTS). The γ-Z^0-background is dotted.

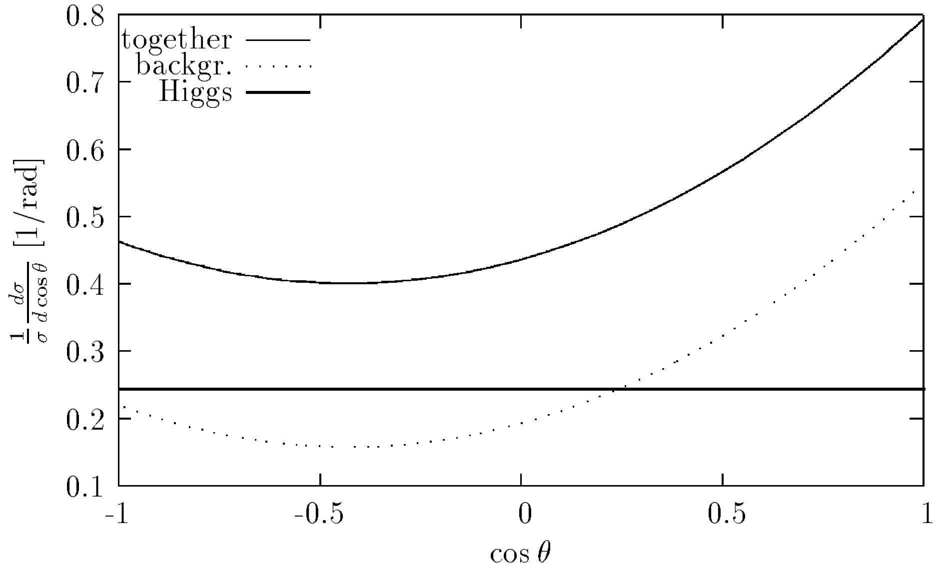

Figure 4.9: Angular distribution of the peak cross section σ_H, the background cross section σ_{back} and the total cross section $\sigma_{\text{back}} + \sigma_H$ at $\sqrt{s} = m_{H_2} =$ 104.741 GeV (LTS).

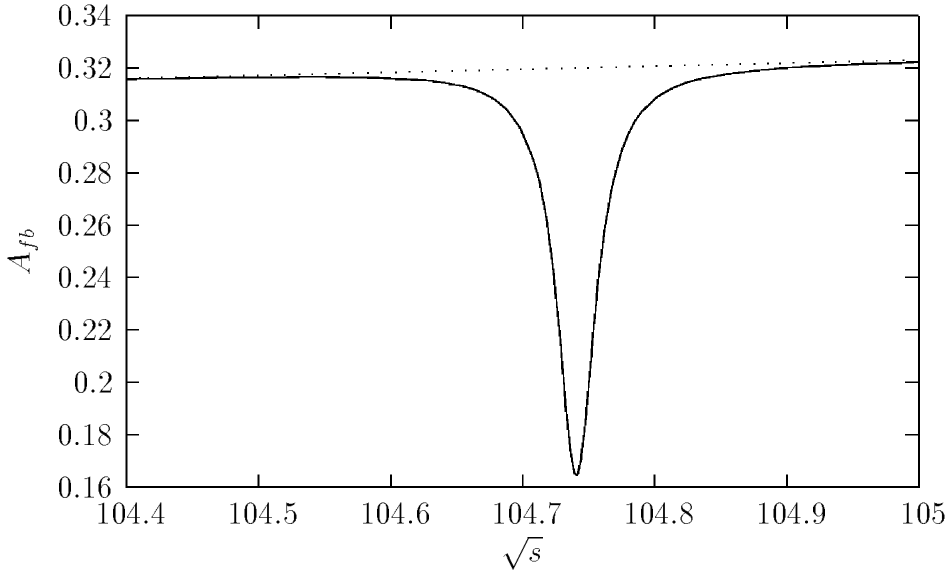

Figure 4.10: The forward-backward-asymmetry of the process $\mu^+\mu^- \longrightarrow b\bar{b}$ in the presence of the intermediate Higgs boson at $m_{H_2} = 104.741$ GeV (LTS). The asymmetry of the γ-Z^0-background is dotted.

Fig. 4.9 shows the angular distribution of the intermediate Higgs boson H_2 at a center-of-mass energy equal to $m_{H_2} = 104.741$ GeV. The choice of the next to lightest Higgs boson is made due to the fact that H_2 is with respect to the mass and the decay width more SM-like than H_1 and H_3. Since the coupling to the gauge bosons is reduced, this or a similar Higgs boson is a possible explanation for the excess found at LEP2 [16, 17, 18, 19, 20]. However, it is instructive to compare this plot with Fig. 2.17. One sees that the signal to background ratio is smaller in the LTS than in the SM.

This also can be seen in the forward-backward-asymmetry depicted in Fig. 4.10.

High-$\tan\beta$ Scenario (HTS)

Since the decay widths are much larger in the HTS than in the LTS, the three Higgs resonances in the HTS can be plotted in a single figure (Fig. 4.11). So one can easy compare the different heights and widths of the resonances.

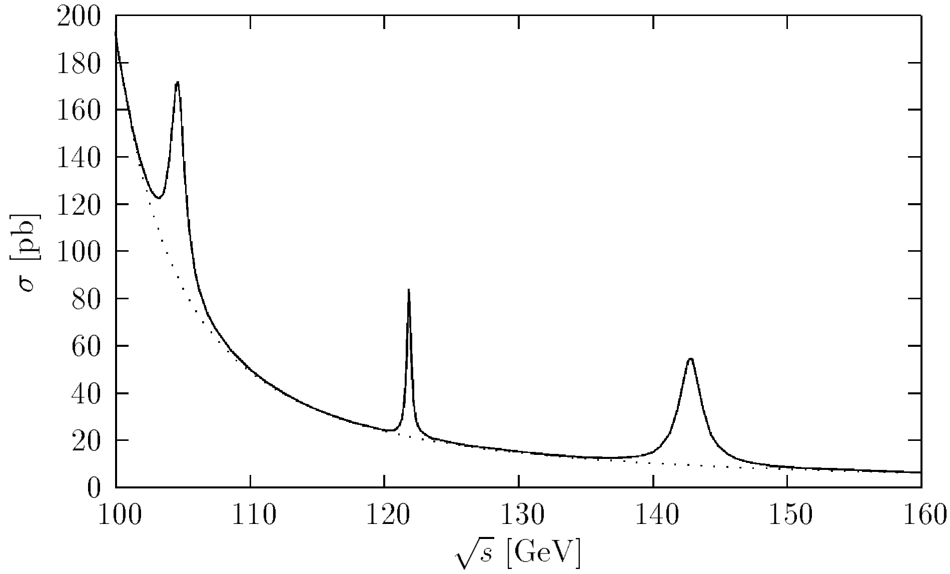

Figure 4.11: The total cross section around the resonances of the Higgs bosons (HTS). The γ-Z^0-background is dotted.

Finally, the asymmetry of the three Higgs bosons is presented in Fig. 4.12. Compared to the asymmetry of the background the asymmetry of the total cross section is decreased over the whole range of values of the center-of-mass energy $\sqrt{s}$ that has been plotted. This is a result of the large decay widths. Therefore such a scenario is detectable in experiments sensible to the forward-backward-asymmetry even at those center-of-mass energies $\sqrt{s}$ that are not close to the resonances.

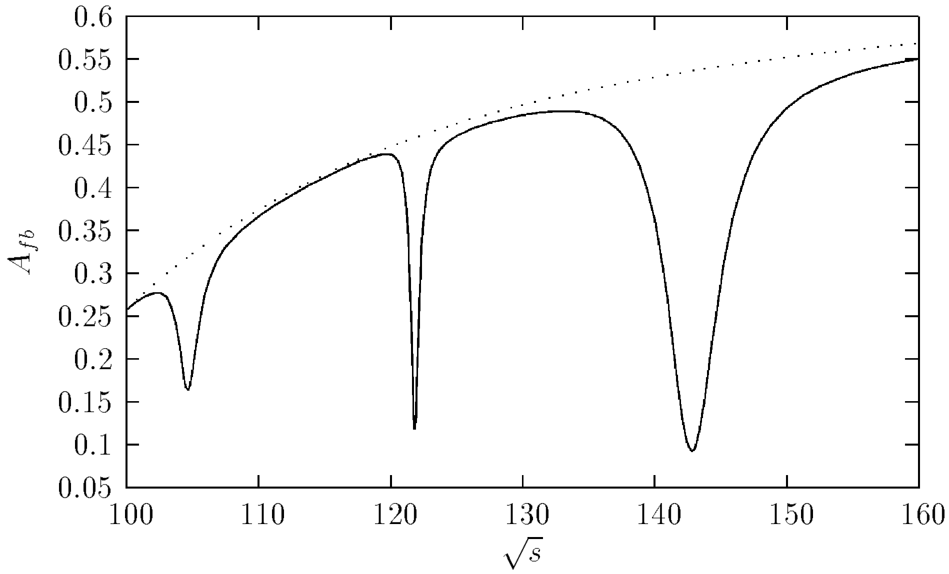

Figure 4.12: The forward-backward-asymmetry of the process $\mu^+\mu^- \longrightarrow b\bar{b}$ (HTS). The asymmetry of the γ-Z^0-background is dotted.

The analysis indicates that a muon-collider offers a unique opportunity to probe the Higgs boson mass spectrum of the MSSM sytematically. In particular, such a collider will help to unravel the CP-nature of the Higgs sector of the MSSM. As has been discussed, CP-violation in the MSSM can, in principle, be large, and may be tested at muon-colliders [46].

Chapter 5

Longitudinal Polarized $\mu^{\pm}$-beams

5.1 Bouchiat-Michel-Formulae

In this chapter the benefits of using longitudinal polarized muon-beams will be discussed. The Bouchiat-Michel-formula given in (A.53) that describes the polarization of particles can be written in the high energy limit ($m_\mu \equiv 0$)* as

$$u(p,s_1)\bar{u}(p,s_2) = \underbrace{\frac{1}{2}(1+P\gamma_5)\,\not{p}\,\delta_{s_1 s_2}}_{\text{longitudinal pol.}} + \underbrace{\frac{1}{2}\gamma_5\left(\not{s}^1\sigma^1_{s_1 s_2} + \not{s}^2\sigma^2_{s_1 s_2}\right)\,\not{p}}_{\text{transverse pol.}}\ , \tag{5.1}$$

where σ^1 and σ^2 are the Pauli matrices defined in (A.7) and (A.8). The parameter

$$-1 \le P_\pm \le 1 \tag{5.2}$$

describes the degree of the longitudinal polarization of the muon beams (P_- for the μ^--beam and P_+ for the μ^+-beam). In this chapter only longitudinal polarization will be considered, which leads to a simplification of (5.1):

$$\begin{aligned} u(p,s)\bar{u}(p,s) &= \frac{1}{2}(1+P_-\gamma_5)\,\not{p} \\ &= \left[\left(\frac{1+P_-}{2}\right)\left(\frac{1+\gamma_5}{2}\right) + \left(\frac{1-P_-}{2}\right)\left(\frac{1-\gamma_5}{2}\right)\right]\not{p} \\ &= \left[\left(\frac{1+P_-}{2}\right)P_R + \left(\frac{1-P_-}{2}\right)P_L\right]\not{p}\ , \end{aligned} \tag{5.3}$$

*The justification of that assumption will be given in section 5.4

where the projection operators (A.22) and (A.23) have been used. Similarly, one gets with (A.54)

$$\begin{aligned} v(p,s)\bar{v}(p,s) &= \frac{1}{2}\left(1 - P_{+}\gamma_5\right) \not{p} \\ &= \left[\left(\frac{1-P_{+}}{2}\right) P_R + \left(\frac{1+P_{+}}{2}\right) P_L\right] \not{p}\,. \end{aligned} \tag{5.4}$$

5.2 Squared Amplitudes

The squared Feynman amplitudes given in (2.76) - (2.85) are recalculated with (4.1), (5.3) and (5.4). Therefore with exception of the Higgs boson couplings given in (2.70) all muon masses m_μ are set to zero.

Even the muon masses within the Goldstone vertex (2.69) and hence the Goldstone contribution to the Feynman amplitude must be dropped to maintain the gauge invariance (2.64), because for massless muons the second term of the Z^0-propagator (2.57) vanishes due to (2.58).

Photon

$$\begin{aligned} |\mathcal{M}|^2_\gamma &= 8 \cdot |\mathcal{T}_\gamma|^2 \\ &\cdot \left[m_f^2(p_1p_2) + (p_1k_1)(p_2k_2) + (p_1k_2)(p_2k_1)\right] \\ &\cdot \left(1 - P_{-}P_{+}\right) \end{aligned} \tag{5.5}$$

Photon/Z^0-Boson

$$\begin{aligned} \mathcal{M}_\gamma\mathcal{M}^\dagger_{Z^0} + \mathcal{M}^\dagger_\gamma\mathcal{M}_{Z^0} &= 2 \cdot \Re e\left(\mathcal{M}_\gamma\mathcal{M}^\dagger_{Z^0}\right) \\ &= 8 \cdot \left(\mathcal{T}^*_\gamma\mathcal{T}_{Z^0} + \mathcal{T}^*_{Z^0}\mathcal{T}_\gamma\right) \\ &\cdot \Bigg(\Big\{ g_V^\mu g_V^f \left[m_f^2(p_1p_2) + (p_1k_1)(p_2k_2) + (p_1k_2)(p_2k_1)\right] \\ &\qquad + g_A^\mu g_A^f \left[(p_1k_1)(p_2k_2) - (p_1k_2)(p_2k_1)\right]\Big\} \\ &\qquad\qquad \cdot \left(1 - P_{-}P_{+}\right) \\ &\quad + \Big\{ g_A^\mu g_V^f \left[m_f^2(p_1p_2) + (p_1k_1)(p_2k_2) + (p_1k_2)(p_2k_1)\right] \\ &\qquad + g_V^\mu g_A^f \left[(p_1k_1)(p_2k_2) - (p_1k_2)(p_2k_1)\right]\Big\} \\ &\qquad\qquad \cdot \left(P_{+} - P_{-}\right)\Bigg) \end{aligned} \tag{5.6}$$

Z^0-Boson

$$
\begin{aligned}
|\mathcal{M}|^2_{Z^0} &= 8 \cdot |\mathcal{T}_{Z^0}|^2 \\
&\cdot \Bigg(\Big\{ m_f^2 (p_1 p_2) \cdot \Big[\Big(g_V^{\mu\,2} + g_A^{\mu\,2} \Big) \Big(g_V^{f\,2} - g_A^{f\,2} \Big) \Big] \\
&\quad + \Big[(p_1 k_1)(p_2 k_2) + (p_1 k_2)(p_2 k_1) \Big] \\
&\qquad \cdot \Big[\Big(g_V^{\mu\,2} + g_A^{\mu\,2} \Big) \Big(g_V^{f\,2} + g_A^{f\,2} \Big) \Big] \Big\} (1 - P_- P_+) \\
&\quad + 2 \Big\{ m_f^2 (p_1 p_2) \cdot \Big[g_V^{\mu} g_A^{\mu} \Big(g_V^{f\,2} - g_A^{f\,2} \Big) \Big] \\
&\quad + \Big[(p_1 k_1)(p_2 k_2) + (p_1 k_2)(p_2 k_1) \Big] \\
&\qquad \cdot \Big[g_V^{\mu} g_A^{\mu} \Big(g_V^{f\,2} + g_A^{f\,2} \Big) \Big] \\
&\quad + \Big[(p_1 k_1)(p_2 k_2) - (p_1 k_2)(p_2 k_1) \Big] \\
&\qquad \cdot \Big[\Big(g_V^{\mu\,2} + g_A^{\mu\,2} \Big) g_V^f g_A^f \Big] \Big\} (P_+ - P_-) \\
&\quad + 4 \Big\{ g_V^{\mu} g_A^{\mu} g_V^f g_A^f \cdot [(p_1 k_1)(p_2 k_2) - (p_1 k_2)(p_2 k_1)] \Big\} \\
&\qquad \cdot (1 - P_- P_+) \Bigg) \qquad (5.7)
\end{aligned}
$$

Higgs-Bosons ‡‡

$$
\begin{aligned}
|\mathcal{M}|^2_H &= 4 \cdot \sum_{i,j=1}^{3} \Big(\mathcal{T}^*_{H_i} \mathcal{T}_{H_j} + \mathcal{T}^*_{H_j} \mathcal{T}_{H_i} \Big) \\
&\cdot \Big\{ m_f^2 (p_1 p_2) \Big[\Big(g^{\mu}_{S_i} g^{\mu}_{S_j} + g^{\mu}_{P_i} g^{\mu}_{P_j} \Big) \Big(-g^{f}_{S_i} g^{f}_{S_j} + g^{f}_{P_i} g^{f}_{P_j} \Big) \Big] \\
&\quad + (p_1 p_2)(k_1 k_2) \Big[\Big(g^{\mu}_{S_i} g^{\mu}_{S_j} + g^{\mu}_{P_i} g^{\mu}_{P_j} \Big) \Big(g^{f}_{S_i} g^{f}_{S_j} + g^{f}_{P_i} g^{f}_{P_j} \Big) \Big] \Big\} \\
&\cdot (1 + P_- P_+) \qquad (5.8)
\end{aligned}
$$

‡‡In the matrix element an additional term $\propto i \left(g^i_{P_i} g^j_{S_i} - g^i_{S_i} g^j_{P_i} \right) (P_+ + P_-)$ appears, which vanishes due to the summation.

k	R_k	I_k	S_k
γ	$\left(\frac{s}{4}-m_f^2\right)(1-P_-P_+)$	–	$\left(\frac{s}{4}+m_f^2\right)(1-P_-P_+)$
γZ^0	$\frac{1}{2}g_V^\mu g_V^f\left(\frac{s}{4}-m_f^2\right)\cdot(1-P_-P_+)+$ $\frac{1}{2}g_A^\mu g_V^f\left(\frac{s}{4}-m_f^2\right)\cdot(P_+-P_-)$	$\frac{1}{4}g_A^\mu g_A^f\sqrt{\lambda_f}\cdot(1-P_-P_+)+$ $\frac{1}{4}g_V^\mu g_A^f\sqrt{\lambda_f}\,(P_+-P_-)$	$\frac{1}{2}g_V^\mu g_V^f\left(\frac{s}{4}+m_f^2\right)\cdot(1-P_-P_+)+$ $\frac{1}{2}g_A^\mu g_V^f\left(\frac{s}{4}+m_f^2\right)\cdot(P_+-P_-)$
γG^0 γH	–	–	–
Z^0	$\frac{1}{16}\left({g_V^\mu}^2+{g_A^\mu}^2\right)\left({g_V^f}^2+{g_A^f}^2\right)\left(\frac{s}{4}-m_f^2\right)\cdot$ $(1-P_-P_+)+$ $\frac{1}{8}g_V^\mu g_A^\mu\left({g_V^f}^2+{g_A^f}^2\right)\left(\frac{s}{4}-m_f^2\right)(P_+-P_-)$	$\frac{1}{8}g_V^\mu g_A^\mu g_V^f g_A^f\sqrt{\lambda_f}\,(1-P_-P_+)+$ $\frac{1}{16}\left({g_V^\mu}^2+{g_A^\mu}^2\right)g_V^f g_A^f\sqrt{\lambda_f}\,(P_+-P_-)$	$\left[\frac{1}{16}\left({g_V^\mu}^2+{g_A^\mu}^2\right)\left({g_V^f}^2+{g_A^f}^2\right)\left(\frac{s}{4}+m_f^2\right)-\right.$ $\left.\frac{m_f^2}{8}{g_A^f}^2\left({g_V^\mu}^2+{g_A^\mu}^2\right)\right](1-P_-P_+)+$ $g_V^\mu g_A^\mu\left[\frac{1}{8}\left(\frac{s}{4}+m_f^2\right)\left({g_V^f}^2+{g_A^f}^2\right)-m_f^2{g_A^f}^2\right](P_+-P_-)$
Z^0G^0 Z^0H G^0 G^0H	–	–	–
H	–	–	$\frac{1}{16}\left[\frac{s}{4}\left(g_{S_i}^\mu g_{S_j}^\mu+g_{P_i}^\mu g_{P_j}^\mu\right)\left(g_{S_i}^f g_{S_j}^f+g_{P_i}^f g_{P_j}^f\right)-\right.$ $\left.m_f^2\left(g_{S_i}^\mu g_{S_j}^\mu+g_{P_i}^\mu g_{P_j}^\mu\right)g_{S_i}^f g_{S_j}^f\right]\cdot(1+P_-P_+)$

Table 5.1: Coefficients in the differential cross section (5.9) with massless longitudinal polarized muons

5.3 Differential Cross Section

Here the differential cross section computed with (2.52), the kinematics in section 2.1 and the squared Feynman amplitudes given in (5.5) - (5.8) is presented in the familiar way:

$$\begin{aligned}\frac{d\sigma}{d\Omega} &= 3\alpha^2 \frac{\sqrt{\lambda_f}}{s} \\ &\quad \cdot \sum_k \sum_{i,j=1}^{3} f_k \left(R_k \cos^2\theta + I_k \cos\theta + S_k\right). \end{aligned} \tag{5.9}$$

As mentioned before all masses that derive from the vertices and the propagators are within the prefactors that have the dimension $\frac{1}{s^2}$:

$$f_\gamma = Q_\mu^2 Q_f^2 \cdot \frac{1}{s^2}\,, \tag{5.10}$$

$$f_{\gamma Z^0} = \frac{Q_\mu Q_f}{\cos^2\theta_W \sin^2\theta_W} \cdot \frac{s-m_Z^2}{(s-m_Z^2)^2 + m_Z^2\Gamma_Z^2} \cdot \frac{1}{s}\,, \tag{5.11}$$

$$f_{\gamma G^0} = f_{\gamma H} = 0\,, \tag{5.12}$$

$$f_{Z^0} = \frac{1}{\cos^4\theta_W \sin^4\theta_W} \cdot \frac{1}{(s-m_Z^2)^2 + m_Z^2\Gamma_Z^2}\,, \tag{5.13}$$

$$f_{Z^0G^0} = f_{Z^0H} = f_{G^0} = f_{G^0H} = 0\,, \tag{5.14}$$

$$\begin{aligned} f_H &= \frac{1}{\sin^4\theta_W} \cdot \frac{m_\mu^2 m_f^2}{m_W^4} \\ &\quad \cdot \frac{\left(s-m_{H_i}^2\right)\left(s-m_{H_j}^2\right) + m_{H_i}\Gamma_{H_i} m_{H_j}\Gamma_{H_j}}{\left[\left(s-m_{H_i}^2\right)^2 + m_{H_i}^2\Gamma_{H_i}^2\right]\left[\left(s-m_{H_j}^2\right)^2 + m_{H_j}^2\Gamma_{H_j}^2\right]}\,. \end{aligned} \tag{5.15}$$

The factors R_k, I_k and S_k are listed in Tab. 5.1.

5.4 Numerical Results

To demonstrate the influence of the longitudinal polarization, the resonance cross section of the next to lightest Higgs boson H_2 in the LTS, that is illustrated in Fig. 4.7, will be discussed in detail as an example.

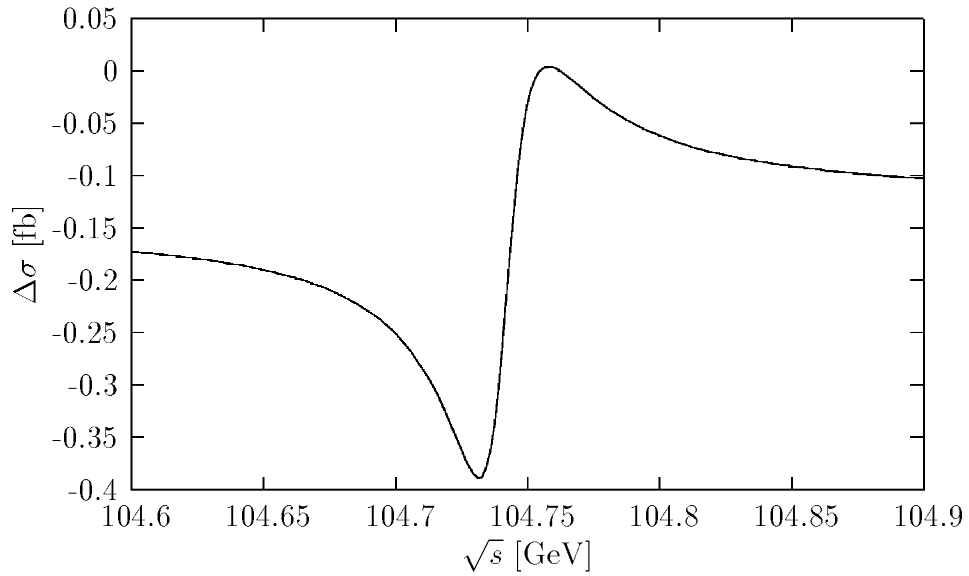

Figure 5.1: The difference $\Delta\sigma = \sigma\,(m_\mu \neq 0) - \sigma\,(m_\mu = 0)$ around the resonance of the intermediate Higgs boson

It is important to estimate the changes in the cross sections due to the neglection of the muon masses (except the Higgs boson couplings) within this chapter. Therefore the unpolarized total cross section calculated with the analytic formula (5.9) is subtracted from the total cross section given in Fig. 4.7 that include all muon masses. This leads to Fig. 5.1, which reveals that the influence of the muon masses $\Delta\sigma$ is at least six orders of magnitude smaller than the total cross section itself and can thus be ignored.

Fig. 5.2 shows what happens if the polarization of the two muon-beams is identical to P. Since

$$\begin{aligned} \sigma_H &\propto (1 + P_+ P_-) \\ &= \left(1 + P^2\right) \end{aligned} \tag{5.16}$$

the resonance cross section increases by a factor of 2 for a maximal polarization $P = \pm 1$.

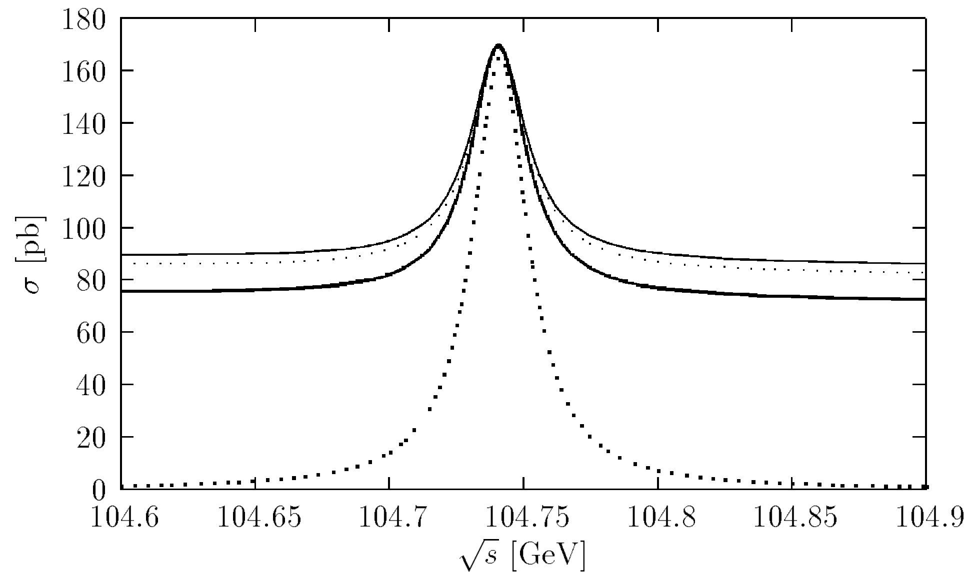

Figure 5.2: Total cross section around the resonance of the intermediate Higgs boson (LTS) assuming $P_+ = P_- = \pm 0.0$, ± 0.2, ± 0.4, ± 1.0 (from top to bottom).

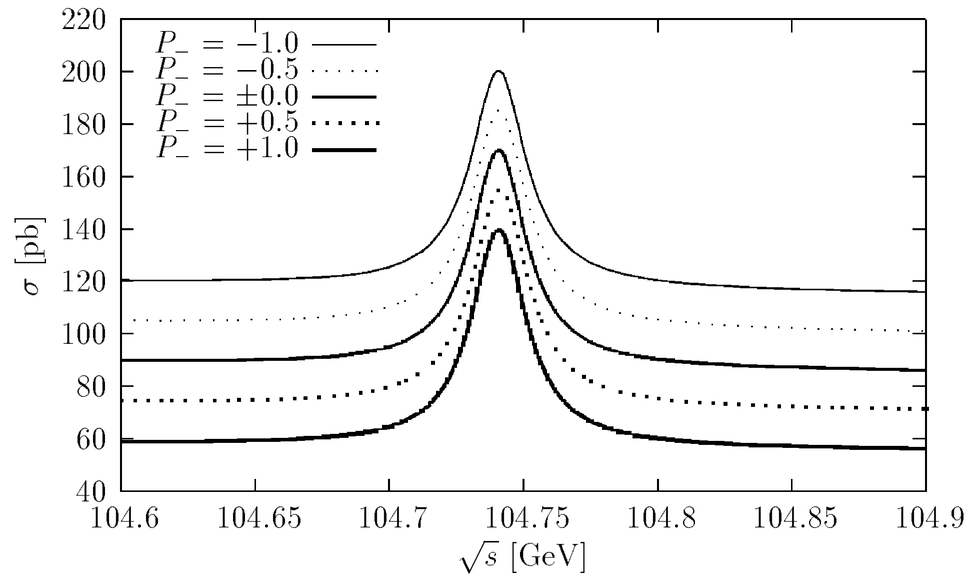

Figure 5.3: Total cross section around the resonance of the intermediate Higgs boson (LTS). The polarization of the μ^+-beam is $P_+ = 0$, while the polarization of the μ^--beam varies.

Since the terms proportional to $(P_+ - P_-)$ vanish for identical beam polarizations, the background

$$\begin{aligned}\sigma_{\text{back}} &\propto (1 - P_+ P_-) \\ &= \left(1 - P^2\right)\end{aligned} \tag{5.17}$$

is reduced to zero for $P = \pm 1$ (Fig. 5.2).

In Fig. 5.3 it is considered that the polarization of the μ^+-beam P_+ is set to zero and the polarization of the μ^--beam P_- is varied between -1 and $+1$. In this case the Higgs resonance peak does not change its height, while

$$\sigma_{\text{back}} \propto (P_+ - P_-) \tag{5.18}$$

cause a shift of the background to higher or lower values.

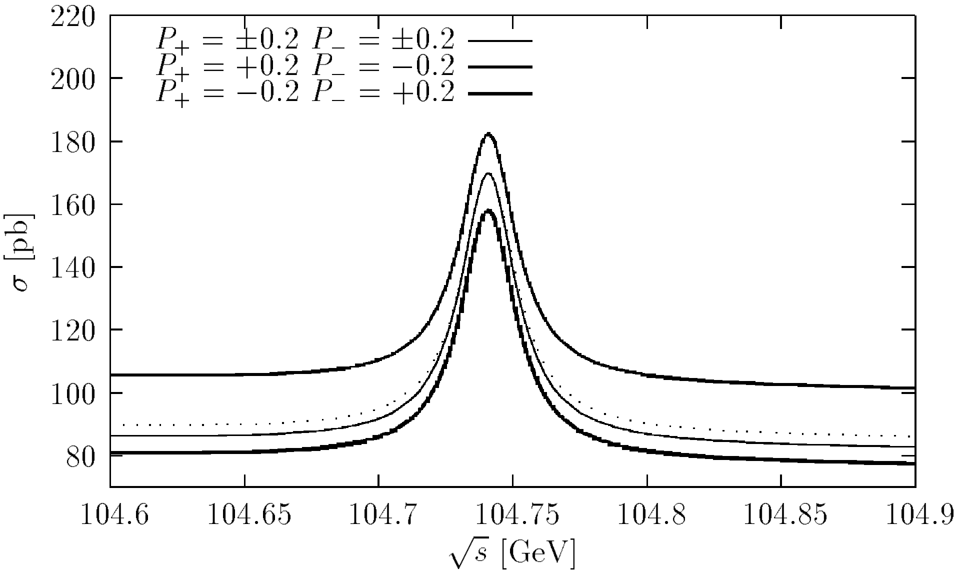

Figure 5.4: Total cross section around the resonance of the intermediate Higgs boson (LTS). A longitudinal beam polarization of 20% with different signs is assumed. The unpolarized case is dotted.

Because of the weak decay, muons produced in pion decays are 100% polarized. The average longitudinal polarization (i.e. muon helicity) is about 28% [47]. The muon spins will precess in electric and magnetic fields that are present during cooling and acceleration. It has been estimated that a longitudinal polarization of about 20% will resist all muon handling up to the injection into the collider [47]. In Fig. 5.4 the different cases for a "natural" polarization of 20% are plotted.

Since the muons are naturally polarized, highly polarized beams are possible, although the luminosity for polarized beams may be significantly reduced during the cooling and acceleration process. If a degree of polarization $\widehat{P}$ is realized for both beams, then, relative to the unpolarized case, the s-channel Higgs signal is enhanced by the factor given in (5.16) while the background is suppressed according to (5.17). Therefore a polarization $\widehat{P}$ of both beams would be useful if the luminosity reduction is less than a factor

$$\frac{\text{signal}^2}{\text{background}} = \frac{\left(1+\widehat{P}^2\right)^2}{\left(1-\widehat{P}^2\right)}\,, \tag{5.19}$$

i.e. the factor that would leave the significance of the signal unchanged. For example $\widehat{P} = 0.84$ would compensate a factor of 10 reduction in luminosity [27]. Unfortunately the reduction in luminosity is always larger than the improvement described in (5.19) if the bunches are saturated at $P = 0.2$ [28].

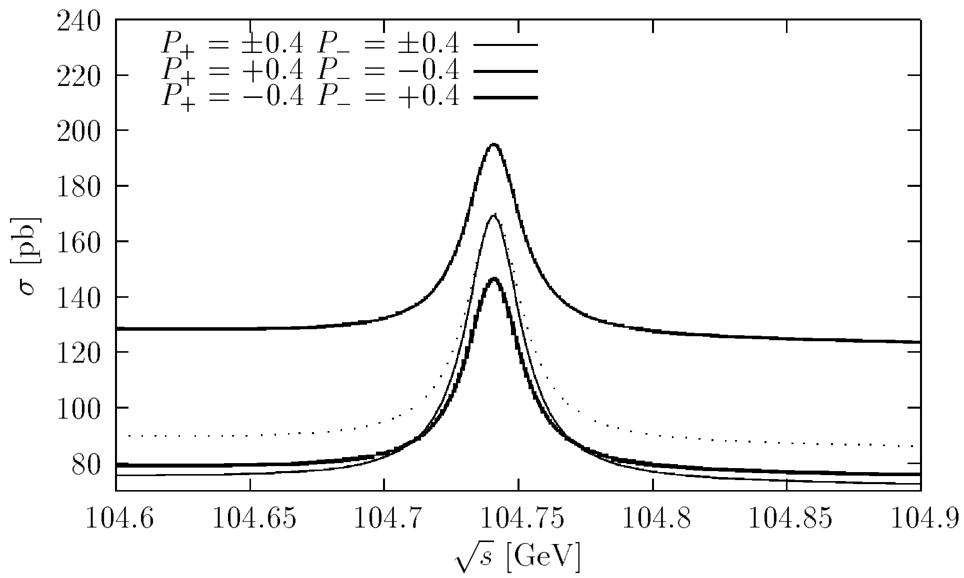

Figure 5.5: Total cross section around the resonance of the intermediate Higgs boson (LTS). A longitudinal beam polarization of 40% with different signs is assumed. The unpolarized case is dotted.

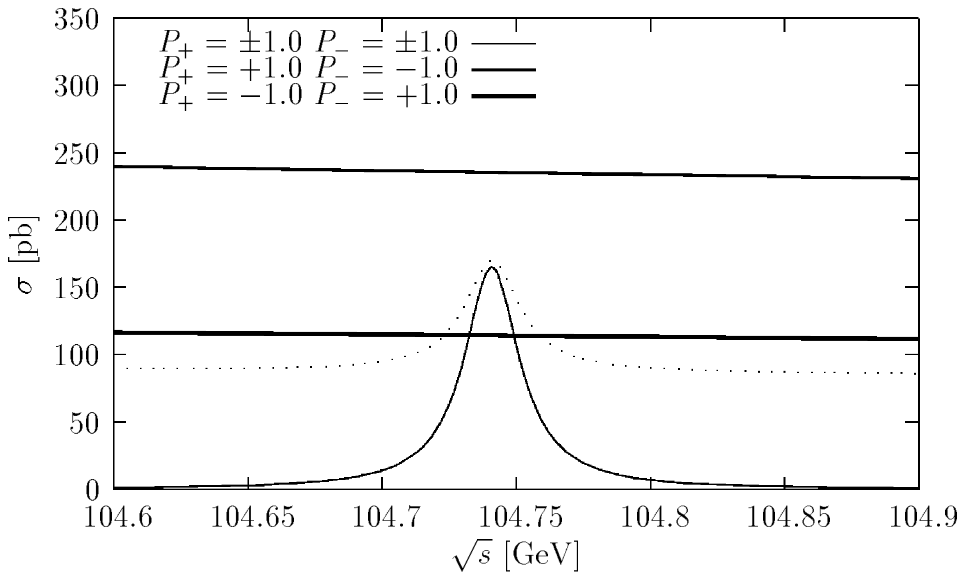

Figure 5.6: Total cross section around the resonance of the intermediate Higgs boson (LTS). A longitudinal beam polarization of 100% with different signs is assumed. The unpolarized case is dotted.

Thus, although a higher polarization P would have some advantages, if the pion intensity was such that the two muon bunches were both fully saturated at $P \gtrsim 0.4$ rather than at $P \sim 0.2$, it is usually accepted that this advantage is not sufficient to justify the expense associated with building a more intense pion source, if Standard Model processes will be studied [28].

However, if determining the CP nature of the Higgs boson couplings to muons is the goal a polarization of $P \approx 0.4$ is most efficient [28], since bunch merging techniques minimize the loss in luminosity. Therefore in Fig. 5.5 the different scenarios for a polarization of 40% are shown.

As a reference the case of full polarization is assumed in Fig. 5.6.

Chapter 6

Conclusion

The task of this diploma thesis was to discuss the heavy quark production at a $\mu^+\mu^-$-collider with respect to different models of the Higgs sector and to predict the posibilities of detecting the involved Higgs particles. All calculations should be analytical and deal with massive particles. Furthermore the influence of longitudinal polarization should be considered.

At first the cross section of the process

$$\mu^+\mu^- \longrightarrow f\bar{f}$$

in the frame of the Standard Model has been calculated. There, all masses have been taken into account. The familiar way of ignoring the masses of the relatively light incoming particles has been avoideded to get the complete analytical formula of the differential cross section, which was presented in an instructive way: all contributions are factorized according to their angular dependency. The numerical results and the plots revealed that it will be very difficult to scan or even detect a Higgs resonance with the present accelerators. The small energy spread of a muon-collider will be necessary to prevent a smearing of the Higgs resonance cross section. Additionally it has been shown that the production of top-quarks is not useful to explore the properties of the Standard Model Higgs boson.

Thereafter the MSSM has been introduced. In this model three neutral (two CP-even and one CP-odd) and two charged Higgs bosons exist. Taking the one-loop CP-violating effects in the Higgs potential into account, the three neutral as well as the two charged Higgs bosons are mixed. Further the couplings of the Higgs bosons to the fermions and the gauge bosons are modified. The couplings to the fermions now consist of a scalar and a pseodoscalar part:

$$1 \longrightarrow g_{S_i} + i\, g_{P_i}\gamma_5$$

with $i = \{1, 2, 3\}$. Using a model [41, 40] with only one extra CP-violating phase, $\arg(\mathbf{a_t})$, the dependency of the Higgs boson masses and couplings on this phase has been discussed. Focusing on relatively light Higgs bosons that are resonantly produced in the process

$$\mu^+\mu^- \longrightarrow b\bar{b}$$

a distinction between a low (LTS) and a high (HTS) value of $\tan\beta$ has been made, which causes a different sensivity to the CP-violating phase $\arg(\mathbf{a_t})$.

In the special case of $\arg(\mathbf{a_t}) = 80°$ within the LTS the coupling of the lightest Higgs boson to the gauge bosons is small. So the Higgs-strahlung process used at LEP2 may be rather inefficient as a source of Higgs bosons. Therefore the combined data of the LEP experiments may not be able to exclude an excess of events around 95 GeV at a level corresponding to a Higgs cross section about a tenth of the SM cross section [45]. It is conceivable that the apparent excess around 115 GeV gives evidence for the second-lightest Higgs boson [45]. A process like $\mu^+\mu^- \longrightarrow b\bar{b}$ would help to exclude possible misinterpretations.

Important analytical and numerical results in the framework of the Standard Model, like the decay width, the differential cross section, the total cross section, the angular distribution and the forward-backward-asymmetry have been recalculated in the frame of the MSSM with $\arg(\mathbf{a_t}) = 80°$. Therefore an easy comparison between the two models become possible.

Since natural polarization of the colliding particles is a unique feature of $\mu^+\mu^-$-colliders due to the origin of the muons in pion decays, the advantages of longitudinally polarized $\mu^\pm$-beams have been discussed. The enhancement of the signal and the reduction of the background will be very helpful in the search for one or more Higgs bosons if the luminosity of the accelerator is high enough. Furthermore it has been demonstrated that all muon masses except for those responsible for the couplings to the Higgs bosons could be ignored.

Appendix A

Useful Formulae

The formulae are adopted from [33], [34], [35], [48] and [49].

A.1 Relativistic Notation

The metric tensor is

$$g_{\mu\nu} = g^{\mu\nu} = \begin{pmatrix} 1 & 0 & 0 & 0 \\ 0 & -1 & 0 & 0 \\ 0 & 0 & -1 & 0 \\ 0 & 0 & 0 & -1 \end{pmatrix} \tag{A.1}$$

with Greek indices running over $0, 1, 2, 3$ and Roman indices over the spatial components $1, 2, 3$. Contravariant (x^μ) and covariant (x_μ) *Lorentz vectors* are formed as

$$x^\mu = \left(x^0, \vec{x}\right) = g^{\mu\nu} x_\nu \,, \tag{A.2}$$

$$x_\mu = \left(x^0, -\vec{x}\right) = g_{\mu\nu} x^\nu \,. \tag{A.3}$$

The scalar product is defined as

$$\begin{aligned} x \cdot y &= g_{\mu\nu} x^\mu y^\nu \\ &= x^0 y^0 - \vec{x} \cdot \vec{y} \,. \end{aligned} \tag{A.4}$$

The four-momentum vector of a massive particle is given by

$$p^\mu = (E, \vec{p}) \tag{A.5}$$

with

$$p^2 = p^\mu p_\mu = E^2 - |\vec{p}|^2 = m^2. \tag{A.6}$$

A.2 Pauli Matrices

Discussions of spin in quantum mechanics make use of the Pauli matrices:

$$\sigma^1 = \begin{pmatrix} 0 & 1 \\ 1 & 0 \end{pmatrix}, \tag{A.7}$$

$$\sigma^2 = \begin{pmatrix} 0 & -i \\ i & 0 \end{pmatrix}, \tag{A.8}$$

$$\sigma^3 = \begin{pmatrix} 1 & 0 \\ 0 & -1 \end{pmatrix}. \tag{A.9}$$

These matrices satisfy

$$\sigma^i \sigma^j = \delta^{ij} + i\epsilon^{ijk}\sigma^k \ , \tag{A.10}$$

which leads to

$$\left\{\sigma^i, \sigma^j\right\} = 2\delta^{ij} \ , \tag{A.11}$$

$$\left[\sigma^i, \sigma^j\right] = 2\epsilon^{ijk}\sigma^k \ . \tag{A.12}$$

A.3 Dirac Matrices

The Dirac matrices γ^μ are defined as set of matrices that satisfy the *Dirac algebra*:

$$\{\gamma^\mu, \gamma^\nu\} \equiv \gamma^\mu\gamma^\nu + \gamma^\nu\gamma^\mu = 2g^{\mu\nu}. \tag{A.13}$$

In the four-dimensional Minkowski space these matrices must be at least 4×4.

Dirac Representation

$$\gamma^0 = \begin{pmatrix} 1 & 0 \\ 0 & -1 \end{pmatrix} \tag{A.14}$$

$$\gamma^i = \begin{pmatrix} 0 & \sigma^i \\ -\sigma^i & 0 \end{pmatrix} \tag{A.15}$$

Relations

$$\gamma^5 = i\gamma^0\gamma^1\gamma^2\gamma^3 = \gamma_5 \tag{A.16}$$

$$\gamma^{0\dagger} = \gamma^0 \tag{A.17}$$

$$\gamma^{\mu\dagger} = \gamma^0\gamma^\mu\gamma^0 = g_{\mu\nu}\gamma^\nu = \gamma_\mu \tag{A.18}$$

$$\left\{\gamma^\mu, \gamma^5\right\} = 0 \tag{A.19}$$

$$
\begin{aligned}
\not{p} &= \gamma_\mu p^\mu = \gamma^\mu p_\mu && \text{(A.20)}\\
\not{p}\,\not{q} &= 2(qp) - \not{q}\,\not{p} && \text{(A.21)}
\end{aligned}
$$

$$
\begin{aligned}
P_R &= \frac{1}{2}(1+\gamma_5) && \text{(A.22)}\\
P_L &= \frac{1}{2}(1-\gamma_5) && \text{(A.23)}\\
P_R^2 &= P_R && \text{(A.24)}\\
P_L^2 &= P_L && \text{(A.25)}\\
P_{R,L}^\dagger &= P_{R,L} && \text{(A.26)}\\
P_R\gamma_5 &= \gamma_5 P_R = P_R && \text{(A.27)}\\
P_L\gamma_5 &= \gamma_5 P_L = -P_L && \text{(A.28)}
\end{aligned}
$$

Contractions

$$
\begin{aligned}
\gamma_\mu\gamma^\mu &= 4 && \text{(A.29)}\\
\gamma_\mu\gamma^\nu\gamma^\mu &= -2\gamma^\nu && \text{(A.30)}\\
\gamma_\mu\gamma^\nu\gamma^\rho\gamma^\mu &= 4g^{\nu\rho} && \text{(A.31)}\\
\gamma_\mu\gamma^\nu\gamma^\rho\gamma^\sigma\gamma^\mu &= -2\gamma^\sigma\gamma^\rho\gamma^\nu. && \text{(A.32)}
\end{aligned}
$$

Traces

$$
\begin{aligned}
Tr\,(1) &= 4 && \text{(A.33)}\\
Tr\,(\text{odd \# of } \gamma\text{'s}) &= 0 && \text{(A.34)}\\
Tr\,(\gamma^\mu\gamma^\nu) &= 4g^{\mu\nu} && \text{(A.35)}\\
Tr\,(\gamma^\mu\gamma^\nu\gamma^\rho\gamma^\sigma) &= 4\,(g^{\mu\nu}g^{\rho\sigma} - g^{\mu\rho}g^{\nu\sigma} + g^{\mu\sigma}g^{\nu\rho}) && \text{(A.36)}
\end{aligned}
$$

$$
\begin{aligned}
Tr\left(\gamma^5\right) &= 0 && \text{(A.37)}\\
Tr\,(\text{odd \# of } \gamma\text{'s and } \gamma^5) &= 0 && \text{(A.38)}\\
Tr\left(\gamma^\mu\gamma^\nu\gamma^5\right) &= 0 && \text{(A.39)}\\
Tr\left(\gamma^\mu\gamma^\nu\gamma^\rho\gamma^\sigma\gamma^5\right) &= -4i\epsilon^{\mu\nu\rho\sigma} && \text{(A.40)}
\end{aligned}
$$

A.4 Epsilon Tensor

In Three Dimensions

$$\epsilon^{ijk} = \begin{cases} +1 & : \text{ if } (ijk) \text{ is an even perm. of } (123) \\ -1 & : \text{ if } (ijk) \text{ is an odd perm. of } (123) \\ 0 & : \text{ else} \end{cases} \tag{A.41}$$

$$\epsilon^{kij}\epsilon^{klm} = \delta_{il}\delta_{jm} - \delta_{im}\delta_{jl} \tag{A.42}$$

In Four Dimensions

The definition presented here corresponds to the one given in [35], but differs from the definition in [33] and [48], where the signs are changed.

$$\epsilon^{\mu\nu\rho\sigma} = \begin{cases} +1 & : \text{ if } (\mu\nu\rho\sigma) \text{ is an even perm. of } (0123) \\ -1 & : \text{ if } (\mu\nu\rho\sigma) \text{ is an odd perm. of } (0123) \\ 0 & : \text{ else} \end{cases} \tag{A.43}$$

$$\epsilon^{\mu\nu\rho\sigma} = -\epsilon_{\mu\nu\rho\sigma} \tag{A.44}$$

Contractions

$$\epsilon^{\mu\nu\rho\sigma}\epsilon_{\mu\nu\rho\sigma} = -24 \tag{A.45}$$

$$\epsilon^{\mu\nu\rho\delta}\epsilon_{\mu\nu\rho\sigma} = -6\delta^{\delta}{}_{\sigma} \tag{A.46}$$

$$\epsilon^{\mu\nu\gamma\delta}\epsilon_{\mu\nu\rho\sigma} = -2\left(\delta^{\gamma}{}_{\rho}\delta^{\delta}{}_{\sigma} - \delta^{\gamma}{}_{\sigma}\delta^{\delta}{}_{\rho}\right) \tag{A.47}$$

$$\begin{aligned} \epsilon^{\mu\beta\gamma\delta}\epsilon_{\mu\nu\rho\sigma} = & -\delta^{\beta}{}_{\nu}\left(\delta^{\gamma}{}_{\rho}\delta^{\delta}{}_{\sigma} - \delta^{\gamma}{}_{\sigma}\delta^{\delta}{}_{\rho}\right) + \delta^{\beta}{}_{\rho}\left(\delta^{\gamma}{}_{\nu}\delta^{\delta}{}_{\sigma} - \delta^{\gamma}{}_{\sigma}\delta^{\delta}{}_{\nu}\right) \\ & -\delta^{\beta}{}_{\sigma}\left(\delta^{\gamma}{}_{\nu}\delta^{\delta}{}_{\rho} - \delta^{\gamma}{}_{\rho}\delta^{\delta}{}_{\nu}\right) \end{aligned} \tag{A.48}$$

A.5 Spinors

The spinors u (particles) and v (anti-particles) and their adjungated partners

$$\bar{u} = u^{\dagger}\gamma_0 \ , \quad \bar{v} = v^{\dagger}\gamma_0 \tag{A.49}$$

satisfy the Dirac equations

$$\begin{aligned} (\not{p} - m)\, u &= \bar{u}\,(\not{p} - m) = 0 \ , \\ (\not{p} + m)\, v &= \bar{v}\,(\not{p} + m) = 0 \ . \end{aligned} \tag{A.50}$$

A summation over the spins yields

$$\sum_{ss'} u(p,s')\bar{u}(p,s) = (\not{p} + m) \ , \tag{A.51}$$

$$\sum_{ss'} v(p,s')\bar{v}(p,s) = (\not{p} - m) \ . \tag{A.52}$$

Bouchiat-Michel-formulae

$$u(p,s')\bar{u}(p,s) = \frac{1}{2}\left(\delta_{ss'} + \gamma_5 \ \not{s}^a \sigma^a_{ss'}\right)(\not{p} + m) \tag{A.53}$$

$$v(p,s')\bar{v}(p,s) = \frac{1}{2}\left(\delta_{s's} + \gamma_5 \ \not{s}^a \sigma^a_{s's}\right)(\not{p} - m) \tag{A.54}$$

Appendix B

Feynman Rules

The propagators (section B.1), the vertices (section B.2) and the electroweak charges (section B.3) are adopted from [50]. The masses and physical constants summarized in section B.4 are listed in [51].

In this appendix the parameter Q is the electric charge in units of the elementary charge e, g_V and g_A are the vectorial and axial couplings and T_Z is the third component of the weak isospin. Further $\sin\theta_W = \frac{g}{e}$ is the weak mixing angle and ξ is the gauge parameter.

B.1 Propagators

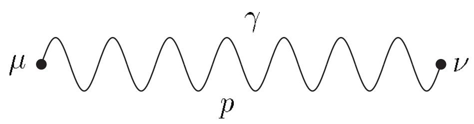

$$\frac{i}{p^2+i\epsilon}\left[-g_{\mu\nu}+(1-\xi)\,\frac{p_\mu p_\nu}{p^2}\right]$$

Figure B.1: γ-propagator

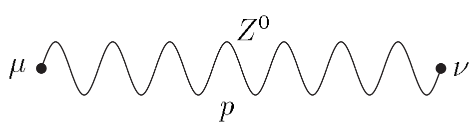

$$\frac{i}{p^2-m_Z^2+i\epsilon}\left[-g_{\mu\nu}+(1-\xi)\,\frac{p_\mu p_\nu}{\left(p^2-\xi m_Z^2\right)}\right]$$

Figure B.2: Z^0-propagator

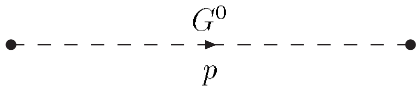

$$\frac{i}{p^2-\xi m_Z^2+i\epsilon}$$

Figure B.3: G^0-propagator

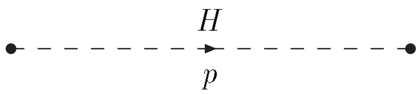

$$\frac{i}{p^2-m_H^2+i\epsilon}$$

Figure B.4: H-propagator

B.2 Vertices

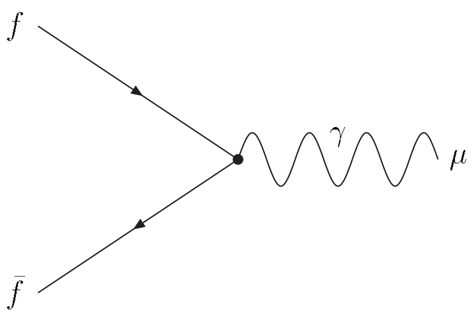

$$-ie\,\gamma_\mu\,Q_f$$

Figure B.5: $\gamma f\bar{f}$-vertex

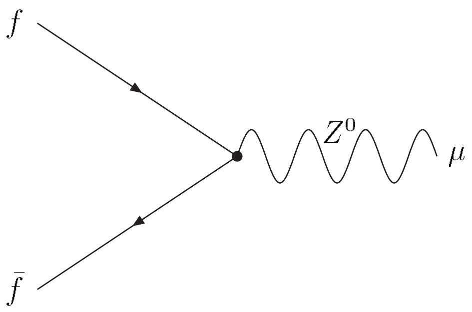

$$\frac{ig}{2\cos\theta_W}\,\gamma_\mu\left(g_V^f - g_A^f\,\gamma_5\right)$$

Figure B.6: $Z^0 f\bar{f}$-vertex

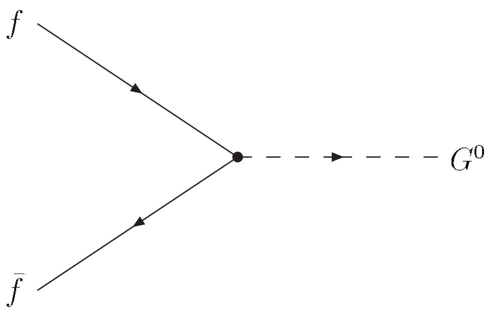

$$-g\,T_z^f\,\frac{m_f}{m_W}\,\gamma_5$$

Figure B.7: $G^0 f\bar{f}$-vertex

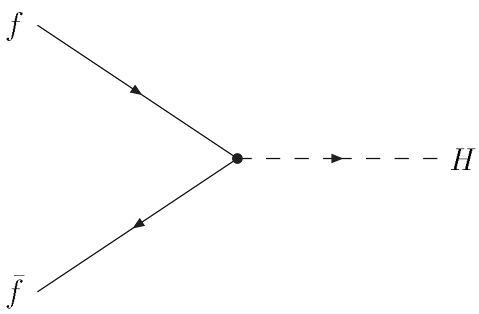

$$-\tfrac{1}{2}\,ig\,\frac{m_f}{m_W}$$

Figure B.8: $Hf\bar{f}$-vertex

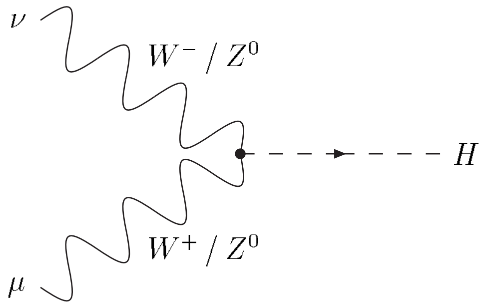

$$-ig\,\frac{m_V^2}{m_W}\,g_{\mu\nu}\ ,$$
where $V = \{W, Z\}$

Figure B.9: HVV-vertex

B.3 Electroweak Charges

Constant	$e,\ \mu,\ \tau$	u-, c-, t-quarks	d-, s-, b-quarks
Q_f	-1	$+\frac{2}{3}$	$-\frac{1}{3}$
T_z^f	$-\frac{1}{2}$	$+\frac{1}{2}$	$-\frac{1}{2}$
$g_V^f = -T_z^f + 2\,Q_f \sin^2\theta_W$	$+\frac{1}{2} - 2\sin^2\theta_W$	$-\frac{1}{2} + \frac{4}{3}\sin^2\theta_W$	$+\frac{1}{2} - \frac{2}{3}\sin^2\theta_W$
$g_A^f = -T_z^f$	$+\frac{1}{2}$	$-\frac{1}{2}$	$+\frac{1}{2}$

Table B.1: Electroweak charges of leptons and quarks

B.4 Constants

$$\begin{aligned}
\sin^2\theta_W &= 0.23117(16) && \text{(B.1)}\\
\alpha &= 1/128.9\,\left(\text{at } q^2 \approx m_W^2\right) && \text{(B.2)}\\
\\
m_Z &= 91.1882(22)\ \text{GeV} && \text{(B.3)}\\
m_W &= m_Z \cdot \cos\theta_W \ = \ 80.42\ \text{GeV} && \text{(B.4)}\\
\\
m_e &= 0.000511\ \text{GeV} && \text{(B.5)}\\
m_\mu &= 0.1057\ \text{GeV} && \text{(B.6)}\\
m_\tau &= 1.777\ \text{GeV} && \text{(B.7)}\\
\\
m_u &= 0.003\ \text{GeV} && \text{(B.8)}\\
m_d &= 0.006\ \text{GeV} && \text{(B.9)}\\
m_s &= 0.125\ \text{GeV} && \text{(B.10)}\\
m_c &= 1.25\ \text{GeV} && \text{(B.11)}\\
m_b &= 4.2\ \text{GeV} && \text{(B.12)}\\
m_t &= 174.3\ \text{GeV} && \text{(B.13)}
\end{aligned}$$

The u-, d- and s-quark masses are so-called “current-quark masses” in a mass-independent subtraction scheme such as $\overline{MS}$ at a scale $\mu \approx 2$ GeV. The c- and b-quark masses are estimated from charmonium, bottomonium, D and B masses. They are the “running” masses in the $\overline{MS}$ scheme. These can be different from the heavy quark masses obtained in potential models. The top-mass is derived from direct observations of top events [51].

Appendix C

The Scalar and Pseudoscalar Higgs-Couplings to Fermions

The scalar and pseudoscalar coupling constants of the neutral Higgs bosons to the down-type (to the leptons respectively) and to the up-type fermions in the scenarios described on page 52ff are plotted below. How such scenarios manifest themselves at a muon-collider is described in chapter 4. The decay widths are calculated for the LTS on page 57ff and for the HTS on page 59ff. The total and differential cross sections were presented on page 66ff (LTS) and on page 69ff (HTS).

Two properties of the coupling constants are significant:

- $(\mathbf{g^d})^2 \gg (\mathbf{g^u})^2$ is a result of (3.48) and (3.49):

$$\left(\frac{g^d_{S_i}}{g^u_{S_i}}\right)^2 = \frac{O^2_{1i}}{O^2_{2i}} \tan^2\beta \ , \tag{C.1}$$

$$\left(\frac{g^d_{P_i}}{g^u_{P_i}}\right)^2 = \tan^4\beta \tag{C.2}$$

  with $i = \{1, 2, 3\}$.

- The **"spikes"** that appear mainly in Fig. C.5 - Fig. C.8 are a manifestation of equation (3.64). This equation describes the relation between the elements $\mathcal{M}^2_{SP}$ of the mass matrix (3.34) with a not well-defined CP-quantum number and the CP-violating phase $\arg(\mathbf{a_t})$. The matrix elements $\mathcal{M}^2_{SP}$ themselves scale with the elements of the transformation matrix O (3.44) that determine the coupling constants.

C.1 Low-$\tan\beta$-Scenario

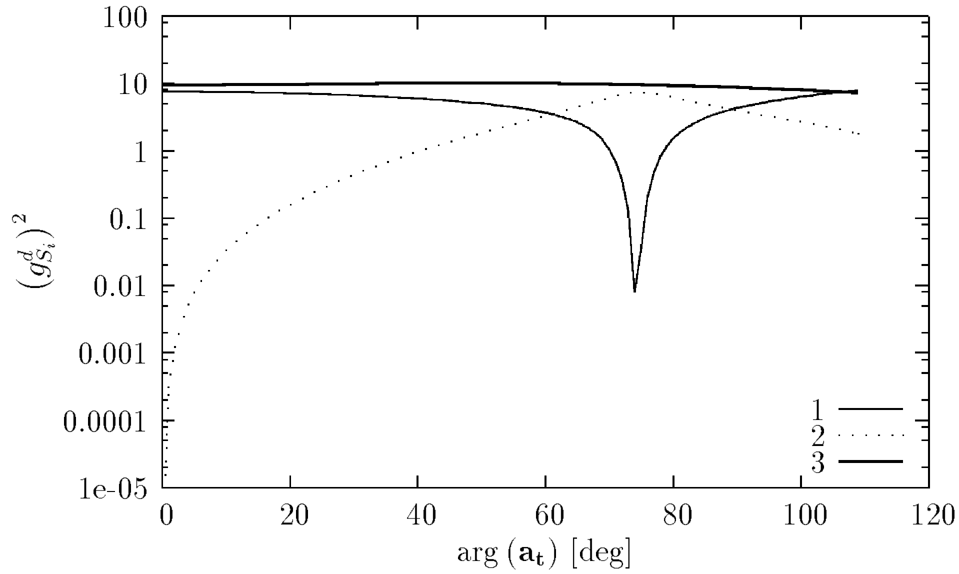

Figure C.1: $\left(g^d_{S_i}\right)^2$ versus $\arg\left(\mathbf{a_t}\right)$ in the LTS for $i = 1, 2, 3$

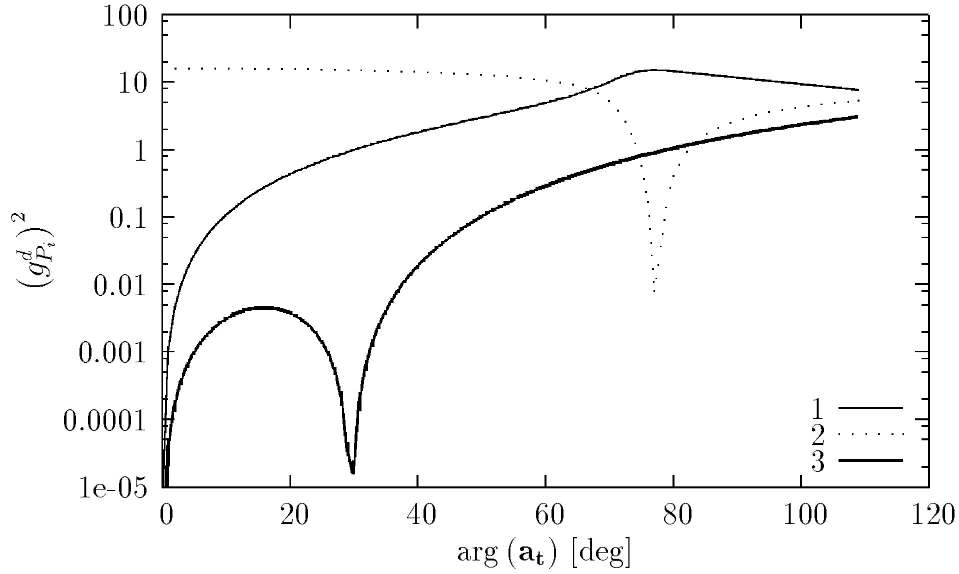

Figure C.2: $\left(g^d_{P_i}\right)^2$ versus $\arg\left(\mathbf{a_t}\right)$ in the LTS for $i = 1, 2, 3$

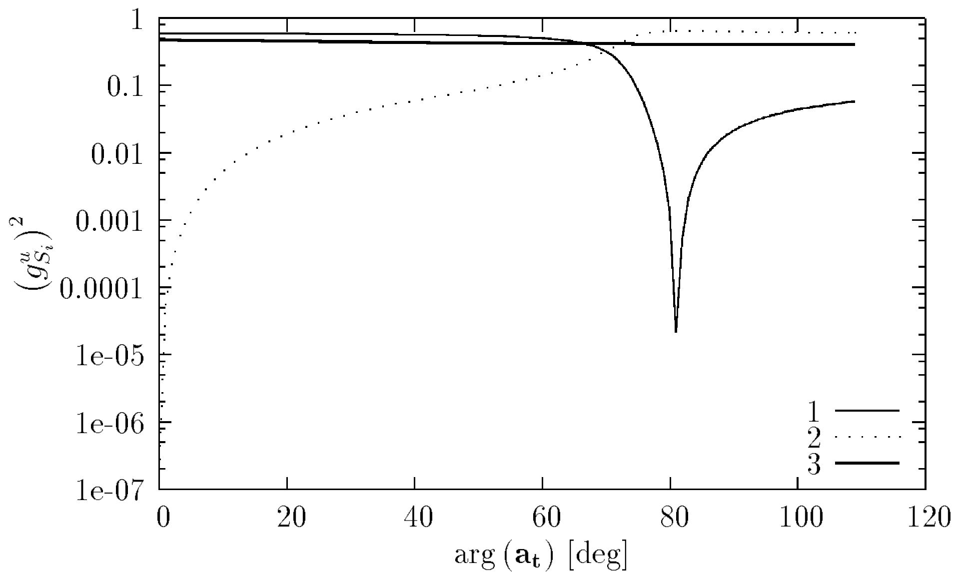

Figure C.3: $\left(g^u_{S_i}\right)^2$ versus $\arg\left(\mathbf{a_t}\right)$ in the LTS for $i = 1, 2, 3$

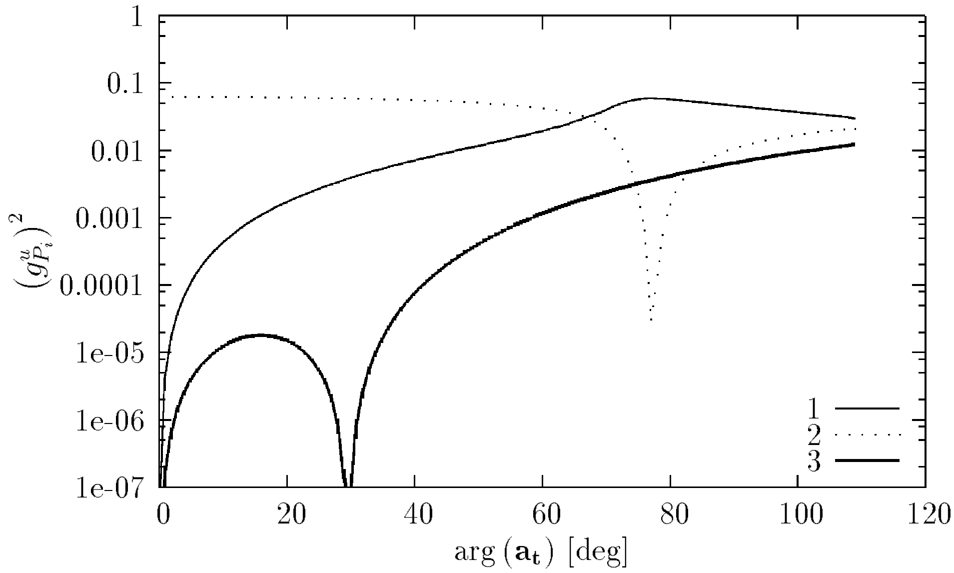

Figure C.4: $\left(g^u_{P_i}\right)^2$ versus $\arg\left(\mathbf{a_t}\right)$ in the LTS for $i = 1, 2, 3$

C.2 High-$\tan\beta$-Scenario

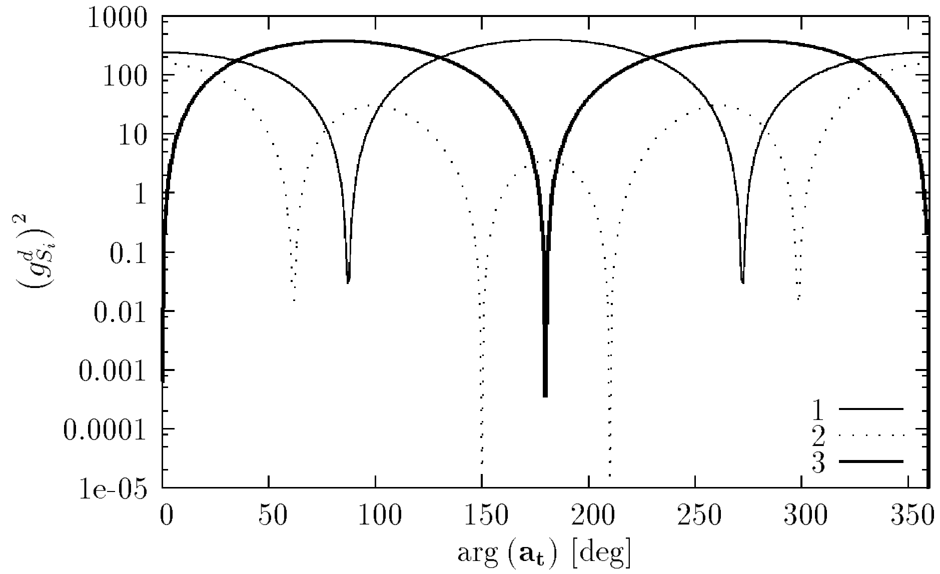

Figure C.5: $\left(g^d_{S_i}\right)^2$ versus $\arg(\mathbf{a_t})$ in the HTS for $i = 1, 2, 3$

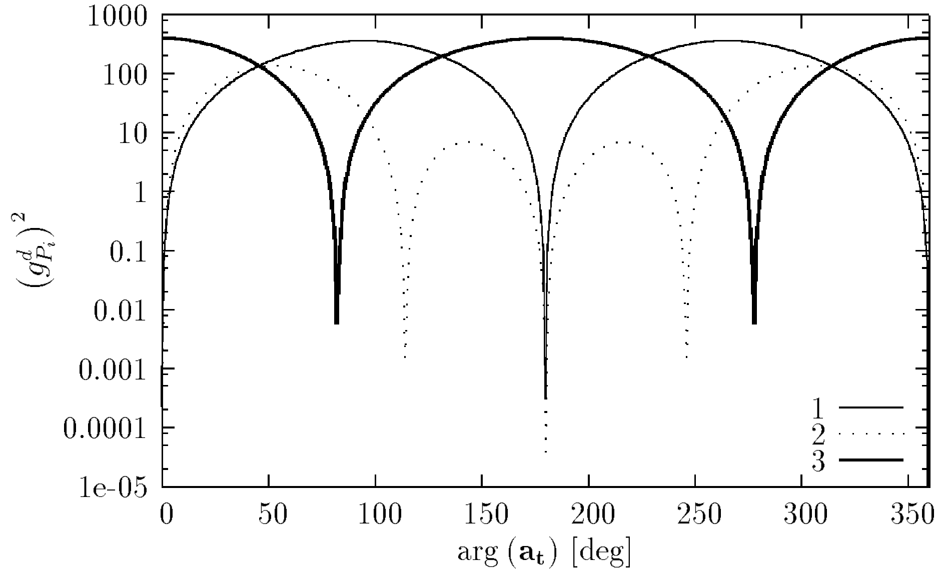

Figure C.6: $\left(g^d_{P_i}\right)^2$ versus $\arg(\mathbf{a_t})$ in the HTS for $i = 1, 2, 3$

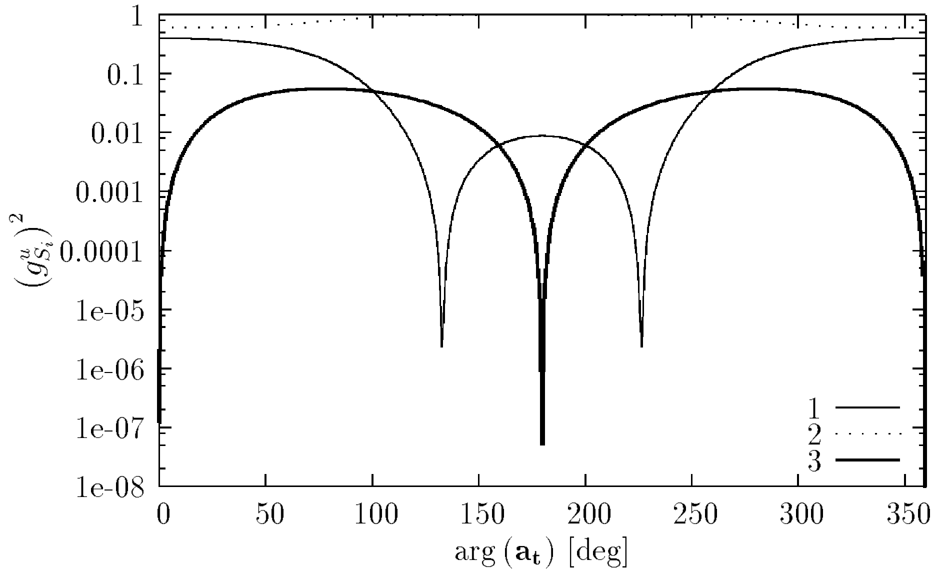

Figure C.7: $\left(g^u_{S_i}\right)^2$ versus $\arg\left(\mathbf{a_t}\right)$ in the HTS for $i = 1, 2, 3$

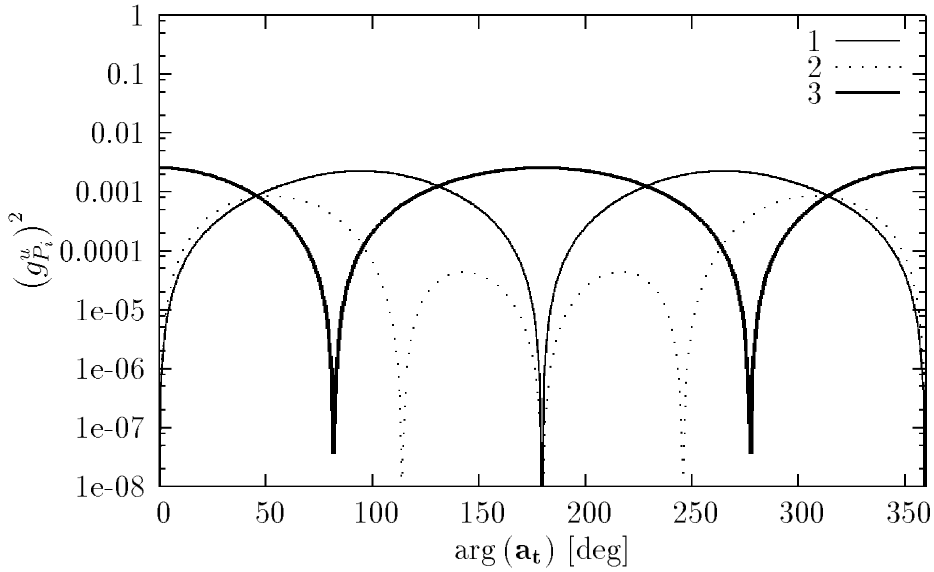

Figure C.8: $\left(g^u_{P_i}\right)^2$ versus $\arg\left(\mathbf{a_t}\right)$ in the HTS for $i = 1, 2, 3$

Bibliography

[1] S. L. Glashow. *Partial-Symmetries of Weak Interactions.* Nuclear Physics, 22, 1961. pages 579-588.

[2] Steven Weinberg. *A Model of Leptons.* Physical Review Letters, 19(21), 1967. pages 1264-1266.

[3] A. Salam. *Elementary Particle Theory.* In N. Svartholm, editor, *8th Nobel Symposium*, Stockholm, 1968. Almquist and Wiskell.

[4] Peter W. Higgs. *Broken Symmetries, Massless Particles and Gauge Fields.* Physics Letters, 12(2), 1964. pages 132-133.

[5] Peter W. Higgs. *Broken Symmetries and the Masses of Gauge Bosons.* Physical Review Letters, 13(16), 1964. pages 508-509.

[6] Peter W. Higgs. *Spontaneous Symmetry Breakdown without Massless Bosons.* Physical Review, 145(4), 1965. pages 1156-1163.

[7] F. Englert and R. Brout. *Broken Symmetry and the Mass of Gauge Vector Mesons.* Physical Review Letters, 13(9), 1964. pages 320-323.

[8] G. S. Guralnik, C. R. Hagen, and T. W. B. Kibble. *Gobal Conservation Laws and Massless Particles.* Physical Review Letters, 13(20), 1964. pages 585-587.

[9] F. Richard, J. R. Schneider, D. Trines, and A. Wagner, editors. *Executive Summary*, volume I of *TESLA - Technical Design Report.* Deutsches Elektronen-Synchrotron (DESY), Notkestr. 85, 22607 Hamburg, Germany, 2001. ISBN 3-935702-01-9.

[10] G. 't Hooft. *Renormalization of Massless Yang-Mills Fields.* Nuclear Physics, B(33), 1971. pages 173-199.

[11] G. 't Hooft. *Renormalizable Lagrangians for Massive Yang-Mills Fields.* Nuclear Physics, B(35), 1971. pages 167-188.

[12] G. Arnison et al. (UA1 Koll.). *Experimental Observation of Isolated Large Transverse Energy Electrons with Associated Missing Energy at* $\sqrt{s} = 540\ GeV$. Physics Letters B, 122, 1983. pages 103-116.

[13] G. Arnison et al. (UA1 Koll.). *Experimental Observation of Lepton Pairs of Invariant Mass Around* 95 GeV/c^2 *at the CERN SPS Collider.* Physics Letters B, 126, 1983. pages 398-410.

[14] P. Bagnaia et al. (UA2 Koll.). *Evidence for* $Z^0 \rightarrow e^+e^-$ *at the CERN* $p\bar{p}$ *Collider.* Physics Letters B, 129, 1983. pages 130-140.

[15] M. Banner et al. (UA2 Koll.). *Observation of Single Isolated Electrons of High Transverse Momentum in Events with Missing Trannsverse Energy at the CERN* $p\bar{p}$ *Collider.* Physics Letters B, 122, 1983. pages 476-485.

[16] P. Igo-Kemenes for the LEP Working Groups on Higgs Searches, November 2000. Talk at the LEPC Open Session.

[17] L3 Collaboration. *Higgs Candidates in* e^+e^- *Interactions at* $\sqrt{s} = 206.6$ *GeV.* hep-ex/0011043, November 2000.

[18] ALEPH Collaboration. *Observation of an Excess in the Search for the Standard Model Higgs Boson at ALEPH.* hep-ex/0011045, November 2000.

[19] DELPHI Collaboration (P. Abreu et al.). *Search for the Standard Model Higgs Boson at LEP in the Year 2000.* hep-ex/0102036, February 2001.

[20] I. Nakamura. *Search for the Standard Model Higgs Boson in OPAL.* hep-ex/0103029, March 2001.

[21] R.-D. Heuer, D. Miller, F. Richard, and P. Zerwas, editors. *Physics at an* e^+e^- *Linear Collider*, volume III of *TESLA - Technical Design Report.* Deutsches Elektronen-Synchrotron (DESY), Notkestr. 85, 22607 Hamburg, Germany, 2001. ISBN 3-935702-03-5.

[22] L3 ALEPH, DELPHI and OPAL Collaborations. *Searches for Higgs Bosons: Preliminary Combined Results Using LEP Data Collected at Energies up to 209 GeV.* ALEPH 2000-074 CONF 2000-051, July 2000.

[23] Stephen Martin. *A Supersymmetry Primer.* hep-ph/9709356v3, April 1999.

[24] G. I. Budker. *Accelerators and Colliding Beams (in Russian)*. In *Proc. 7th Int. Conference on High Energy Accelerators*, page 33, Yerevan, 1969. extract: AIP Conf. Proc. 352 (1996) 4.

[25] V. Barger, M. S. Berger, K. Fujii, J. F. Gunion, T. Han, C. Heusch, W. Hong, S. K. Oh, Z. Parsa, S. Rajpoot, R. Thun, and B. Willis. *Physics Goals of a $\mu^+\mu^-$ Collider*. hep-ph/9503258, March 1995.

[26] John F. Gunion. *Muon Colliders: The Machine and The Physics*. hep-ph/9707379v2, July 1997.

[27] V. Barger, M. S. Berger, J. F. Gunion, and T. Han. *Higgs Boson Physics in the s-Channel at $\mu^+\mu^-$ Colliders*. Physics Reports, 286, 1997. pages 1-51.

[28] Bohdan Grzadkowski, John F. Gunion, and Jacek Pliszka. *How Valuable is Polarization at a Muon Collider? A Test Case: Determining the CP Nature of a Higgs Boson*. hep-ph/0003091, March 2000.

[29] Marcel Demarteau and Tao Han. *Higgs Boson and Z Physics at the First Muon Collider*. hep-ph/9801407, Januar 1998.

[30] B. Autin. *Prospective Study of Muon Colliders and Muon Storage Rings at CERN*. CERN 99-02, ECFA 99-197, 1999.

[31] John F. Gunion. *Higgs Physics at a Muon Collider*. hep-ph/9703203, February 1997.

[32] Otto Nachtmann. *Phänomene und Konzepte der Elementarteilchenphysik*. Friedr. Vieweg & Sohn Verlagsgesellschaft mbH, Braunschweig, 1986. ISBN 3-528-08926-1, and the references therein.

[33] David Jeffrey Griffiths. *Intoduction to Elementary Particles*. John Wiley & Sons, Inc., New York, Chichester, Brisbane, Toronto, Singapore, 1987. ISBN 0-471-60386-4.

[34] Manfred Böhm, Ansgar Denner, and Hans Joos. *Gauge Theories of the Strong and Electroweak Interaction*. B. G. Teubner, Stuttgart, Leipzig, Wiesbaden, 2001. ISBN 3-519-02345-3.

[35] Michael E. Peskin and Daniel V. Schroeder. *An Introduction to Quantum Field Theory*. Advanced Book Program. Addison-Wesley Publishing Company, Reading (Massachusetts), Menlo Park (California), New York, Don Mills (Ontario), Wokingham (United Kingdom), Amsterdam,

Bonn, Sydney, Singapore, Tokyo, Madrid, San Juan, Paris, Seoul, Milan, Mexico City, Taipei, 1997. ISBN 0-201-50397-2.

[36] A. Blondel. *Overview of the Physics Capabilities.* In B. Autin, editor, *Prospective Study of Muon Colliders and Muon Storage Rings at CERN*, 1999. CERN 99-02, ECFA 99-197.

[37] R. Brinkmann, K. Flöttmann, J. Rossbach, P. Schmüser, N. Walker, and H. Weise, editors. *The Accelerator*, volume II of *TESLA - Technical Design Report.* Deutsches Elektronen-Synchrotron (DESY), Notkestr. 85, 22607 Hamburg, Germany, 2001. ISBN 3-935702-02-7.

[38] W. Murray. *Measurements of the Higgs-boson Properties.* In B. Autin, editor, *Prospective Study of Muon Colliders and Muon Storage Rings at CERN*, 1999. CERN 99-02, ECFA 99-197.

[39] Sally Dawson, John F. Gunion, Howard E. Haber, and Gordon Kane. *The Higgs Hunter's Guide*, volume 80 of *Frontiers in Physics.* Addison-Wesley Publishing Company, Redood City (California), Menlo Park (California), Reading (Massachusetts), New York, Don Mills (Ontario), Wokingham (United Kingdom), Amsterdam, Bonn, Sydney, Singapore, Tokyo, Madrid, San Juan, 1990. ISBN 0-201-50935-0.

[40] M. Carena, J. Ellis, Apostolos Pilaftsis, and Carlos E. M. Wagner. *Renormalization-Group-Improved Effective Potential for the MSSM Higgs Sector with Explicit CP Violation.* hep-ph/0003180v4, September 2000.

[41] A. Pilaftsis and C. E. M. Wagner. *Higgs Bosons in the Minimal Supersymmetric Standard Model with Explicit CP Violation.* hep-ph/9902371v4, August 1999.

[42] Apostolos Pilaftsis. *CP-odd Tadpole Renormalization of Higgs Scalar-Pseudoscalar Mixing.* Physical Review D, 58(096010), 1998.

[43] Sidney Coleman and Erick Weinberg. *Radiative Corrections as the Origin of Spontaneous Symmetry Breaking.* Physical Review D, 7(6), 1973. pages 1888-1910.

[44] Apostolos Pilaftsis. cph.f. The Fortran code is available from http://www.cern.ch/p/pilaftsi/www/.

[45] M. Carena, J. Ellis, A. Pilaftsis, and C. E. M. Wagner. *CP-Violating MSSM Higgs Bosons in the Light of LEP2.* hep-ph/0009212, September 2000.

[46] A. Pilaftsis and C. E. M. Wagner. *Probing CP-violation in the Higgs Sector of the MSSM*. In B. Autin, editor, *Prospective Study of Muon Colliders and Muon Storage Rings at CERN*, 1999. CERN 99-02, ECFA 99-197.

[47] A. Blondel. *Energy Calibration by Spin Presession*. In B. Autin, editor, *Prospective Study of Muon Colliders and Muon Storage Rings at CERN*, 1999. CERN 99-02, ECFA 99-197.

[48] James D. Bjorken and Sidney D. Drell. *Relativistische Quantenmechanik*, volume 98/98a of *Hochschultaschenbücher*. Bibliographisches Institut Mannheim, Hochschultaschenbücher-Verlag, Mannheim, 1966.

[49] Claus Blöchinger. *Produktion und Zerfall von Neutralinos und Selektronen in $e^-\gamma$-Stößen*. Diplomarbeit, Julius-Maximilians-Universität, Würzburg, September 1996.

[50] David Bailin and Alexander Love. *Introduction To Gauge Field Theory*. Graduate Student Series in Physics. Institute of Physics Publishing, Techno House, Redcliffe Way, Bristol BS1 6NX, UK, 1996. ISBN 0-7503-0281-X.

[51] D. E. Groom et al. *Review of Particle Physics*. The European Physical Journal, C15(1), 2000. http://pdg.lbl.gov/.

List of Figures

2.1 Definition of four-momenta and scattering angle θ 4
2.2 Higgs boson decay into fermions 7
2.3 Higgs boson decay into W bosons 8
2.4 Higgs boson decay into Z^0 bosons 9
2.5 Decay width Γ_H versus Higgs boson mass m_H 12
2.6 Main contributions of the decay width Γ_H^i versus Higgs boson mass m_H 12
2.7 Branching ratios in % of the different Higgs decay channels versus Higgs boson mass m_H 13
2.8 Feynman graph of the photon exchange 15
2.9 Feynman graph of the Z^0-boson exchange 16
2.10 Feynman graph of the Goldstone boson exchange 17
2.11 Feynman graph of the Higgs boson exchange 18
2.12 The Higgs resonance cross section σ_H for different Higgs boson masses m_H 25
2.13 The total cross section without the part caused by the Higgs boson (σ_{back}) 26
2.14 Total cross section for $\mu^+\mu^- \longrightarrow b\bar{b}$ in the presence of a Higgs boson with $m_H = 115$ GeV and $\Gamma_H = 4.5$ MeV. The dotted curve indicates the background cross section σ_{back} defined in section 2.4. 27
2.15 Same as Fig. 2.14 for a Higgs boson with $m_H = 165$ GeV and $\Gamma_H = 240$ MeV 28
2.16 Same as Fig. 2.14 for a Higgs boson with $m_H = 185$ GeV and $\Gamma_H = 820$ MeV 29
2.17 Angular distribution at $\sqrt{s} = 115$ GeV due to Higgs exchange (solid), continuum (dotted) and total (thin). 30
2.18 The forward-backward-asymmetry of the process $\mu^+\mu^- \longrightarrow b\bar{b}$ in the presence of a Higgs boson at $m_H = 115$ GeV. The continuum is indicated by the dotted line. 31
2.19 The Higgs resonance vs. $\sqrt{s}$ for different $\sigma_{\sqrt{s}}$ 32

2.20 Cross section peak vs. $\sigma_{\sqrt{s}}$ at $\sqrt{s} = 115$ GeV 32

3.1 Fermion loop correction to the Higgs field 34
3.2 Scalar particle loop correction to the Higgs field 35
3.3 The fermion contribution to the effective potential. 43
3.4 m_{H_i} versus m_{H^+} with $\tan\beta = 4$ and $\arg(\mathbf{a_t}) = 0°$ (dotted lines), $\arg(\mathbf{a_t}) = 90°$ (solid lines). 48
3.5 m_{H_i} versus m_{H^+} with $\tan\beta = 20$ and $\arg(\mathbf{a_t}) = 0°$ (dotted lines), $\arg(\mathbf{a_t}) = 90°$ (solid lines) 48
3.6 $g^2_{H_iVV}$ versus m_{H^+} with $\tan\beta = 4$ and $\arg(\mathbf{a_t}) = 90°$ 49
3.7 $(g^t_x)^2$ versus m_{H^+} for $i = S_2, S_3, P_2, P_3$ with $\tan\beta = 4$ and $\arg(\mathbf{a_t}) = 90°$ 50
3.8 $(g^\mu_x)^2$ versus m_{H^+} for $i = S_2, S_3, P_2, P_3$ with $\tan\beta = 4$ and $\arg(\mathbf{a_t}) = 90°$ 51
3.9 $g^2_{H_iVV}$ versus $\arg(\mathbf{a_t})$ with $\tan\beta = 4$ and $m_{H^+} = 150$ GeV . . 52
3.10 m_{H_i} versus $\arg(\mathbf{a_t})$ with $\tan\beta = 4$ and $m_{H^+} = 150$ GeV . . . 53
3.11 m_{H_i} versus $\arg(\mathbf{a_t})$ with $\tan\beta = 20$ and $m_{H^+} = 150$ GeV . . 53
3.12 $g^2_{H_iVV}$ versus $\arg(\mathbf{a_t})$ with $\tan\beta = 20$ and $m_{H^+} = 150$ GeV . . 54

4.1 Higgs boson decay into fermions 55
4.2 Higgs boson decay into gauge bosons 56
4.3 Decay width Γ_{H_i} for $i = 1, 2, 3$ versus $\arg(\mathbf{a_t})$ for $\tan\beta = 4$ and $m_{H^+} = 150$ GeV (LTS) 58
4.4 Decay width Γ_{H_i} for $i = 1, 2, 3$ versus $\arg(\mathbf{a_t})$ with $\tan\beta = 20$ and $m_{H^+} = 150$ GeV (HTS) 60
4.5 Total cross section due to γ and Z^0 exchange in the process $\mu^+\mu^- \longrightarrow b\bar{b}$ 65
4.6 The total cross section of $\mu^+\mu^- \longrightarrow b\bar{b}$ around the resonance of the lightest Higgs boson at $m_{H_1} = 91.534$ GeV (LTS). The γ-Z^0-background is dotted. 66
4.7 The total cross section of $\mu^+\mu^- \longrightarrow b\bar{b}$ around the resonance of the intermediate Higgs boson at $m_{H_2} = 104.741$ GeV (LTS). The γ-Z^0-background is dotted. 67
4.8 The total cross section of $\mu^+\mu^- \longrightarrow b\bar{b}$ around the resonance of the heaviest Higgs boson at $m_{H_3} = 152.747$ GeV (LTS). The γ-Z^0-background is dotted. 67
4.9 Angular distribution of the peak cross section σ_H, the background cross section σ_{back} and the total cross section $\sigma_{\text{back}} + \sigma_H$ at $\sqrt{s} = m_{H_2} = 104.741$ GeV (LTS). 68

4.10 The forward-backward-asymmetry of the process $\mu^+\mu^- \longrightarrow b\bar{b}$ in the presence of the intermediate Higgs boson at $m_{H_2} =$ 104.741 GeV (LTS). The asymmetry of the γ-Z^0-background is dotted. 68
4.11 The total cross section around the resonances of the Higgs bosons (HTS). The γ-Z^0-background is dotted. 69
4.12 The forward-backward-asymmetry of the process $\mu^+\mu^- \longrightarrow b\bar{b}$ (HTS). The asymmetry of the γ-Z^0-background is dotted. . . 70

5.1 The difference $\Delta\sigma = \sigma(m_\mu \neq 0) - \sigma(m_\mu = 0)$ around the resonance of the intermediate Higgs boson 76
5.2 Total cross section around the resonance of the intermediate Higgs boson (LTS) assuming $P_+ = P_- = \pm 0.0, \pm 0.2, \pm 0.4, \pm 1.0$ (from top to bottom). 77
5.3 Total cross section around the resonance of the intermediate Higgs boson (LTS). The polarization of the μ^+-beam is $P_+ = 0$, while the polarization of the μ^--beam varies. 77
5.4 Total cross section around the resonance of the intermediate Higgs boson (LTS). A longitudinal beam polarization of 20% with different signs is assumed. The unpolarized case is dotted. 78
5.5 Total cross section around the resonance of the intermediate Higgs boson (LTS). A longitudinal beam polarization of 40% with different signs is assumed. The unpolarized case is dotted. 79
5.6 Total cross section around the resonance of the intermediate Higgs boson (LTS). A longitudinal beam polarization of 100% with different signs is assumed. The unpolarized case is dotted. 80

B.1 γ-propagator 88
B.2 Z^0-propagator 88
B.3 G^0-propagator 89
B.4 H-propagator 89
B.5 $\gamma f\bar{f}$-vertex 89
B.6 $Z^0 f\bar{f}$-vertex 90
B.7 $G^0 f\bar{f}$-vertex 90
B.8 $Hf\bar{f}$-vertex 90
B.9 HVV-vertex 91

C.1 $\left(g^d_{S_i}\right)^2$ versus $\arg(\mathbf{a_t})$ in the LTS for $i = 1, 2, 3$ 94
C.2 $\left(g^d_{P_i}\right)^2$ versus $\arg(\mathbf{a_t})$ in the LTS for $i = 1, 2, 3$ 94
C.3 $\left(g^u_{S_i}\right)^2$ versus $\arg(\mathbf{a_t})$ in the LTS for $i = 1, 2, 3$ 95
C.4 $\left(g^u_{P_i}\right)^2$ versus $\arg(\mathbf{a_t})$ in the LTS for $i = 1, 2, 3$ 95

C.5 $\left(g^d_{S_i}\right)^2$ versus arg $(\mathbf{a_t})$ in the HTS for $i = 1, 2, 3$ 96
C.6 $\left(g^d_{P_i}\right)^2$ versus arg $(\mathbf{a_t})$ in the HTS for $i = 1, 2, 3$ 96
C.7 $\left(g^u_{S_i}\right)^2$ versus arg $(\mathbf{a_t})$ in the HTS for $i = 1, 2, 3$ 97
C.8 $\left(g^u_{P_i}\right)^2$ versus arg $(\mathbf{a_t})$ in the HTS for $i = 1, 2, 3$ 97

List of Tables

2.1 Coefficients in the differential cross section (2.86) predicted by the Standard Model 24

3.1 Matter supermultiplets of the MSSM 37
3.2 Gauge supermultiplets of the MSSM 38

4.1 Masses and coupling constants of the neutral Higgs bosons for $\arg(\mathbf{a_t}) = 80°$, $\tan\beta = 4$ and $m_{H^+} = 150$ GeV (LTS) 58
4.2 Branching Ratios of the neutral Higgs bosons for $\arg(\mathbf{a_t}) = 80°$, $\tan\beta = 4$ and $m_{H^+} = 150$ GeV (LTS) 59
4.3 Masses and coupling constants of the neutral Higgs bosons for $\arg(\mathbf{a_t}) = 80°$, $\tan\beta = 20$ and $m_{H^+} = 150$ GeV (HTS) 60
4.4 Branching Ratios of the neutral Higgs bosons for $\arg(\mathbf{a_t}) = 80°$, $\tan\beta = 20$ and $m_{H^+} = 150$ GeV (HTS) 61
4.5 Coefficients in the differential cross section (4.15) with scalar and pseudoscalar Higgs couplings 64

5.1 Coefficients in the differential cross section (5.9) with massless longitudinal polarized muons 74

B.1 Electroweak charges of leptons and quarks 91

Danksagung

Zum Schluß möchte ich all denjenigen danken, die mich bei meinem Studium und speziell dieser Diplomarbeit unterstützt haben.

Mein besonderer Dank geht an Herrn Prof. Dr. Rückl, der mir die Möglichkeit gegeben hat, an seinem Lehrstuhl diese Arbeit anzufertigen. Seine Hinweise und Anregungen haben wesentlich zu ihrem Gelingen beigetragen.

Herrn Dr. Apostolos Pilaftsis sei für die Überlassung seines Codes gedankt, mit dessen Hilfe ich meine Ausgangsdaten generieren konnte.

Meinem langjährigen Studienfreund Alexander Wagner danke ich für die konstruktive Zusammenarbeit und die vielen spannenden Diskussionen. Sein Computerwissen hat mir in vielen Situationen sehr geholfen. Ganz besonders danke ich ihm für die zeitweilige Überlassung seines Notebooks. Auch die stets gut gefüllte Kaffekanne soll hier nicht unerwähnt bleiben. Ich wünsche ihm weiterhin alles Gute und viel Erfolg.

Ferner bedanke ich mich bei Herrn Prof. Dr. Fraas, Claus Blöchinger, Frank Deppisch, Stefan Glück, Ilja Kaufmann, Olaf Kittel, Alexander Mück, Frederico von der Pahlen, Andreas Redelbach, Reimer Selle, Stefan Vidi, Brigitte Wehner und allen hier nicht namentlich genannten “stillen Helfern” für ihre Unterstützung.

Auch möchte ich nicht versäumen, meiner Familie und besonders meiner Mutter zu danken, ohne die mein Studium nicht möglich gewesen wäre.

Erklärung

Hiermit versichere ich, daß ich die vorliegende Arbeit selbstständig verfasst und keine anderen als die angegebenen Hilfsmittel und Quellen verwendet habe.

Würzburg, ...

6. August 2001 (Thorsten Ratzka)